ALONE IN THE DARK

Time-resolved fluorescence spectroscopy on single biomolecules

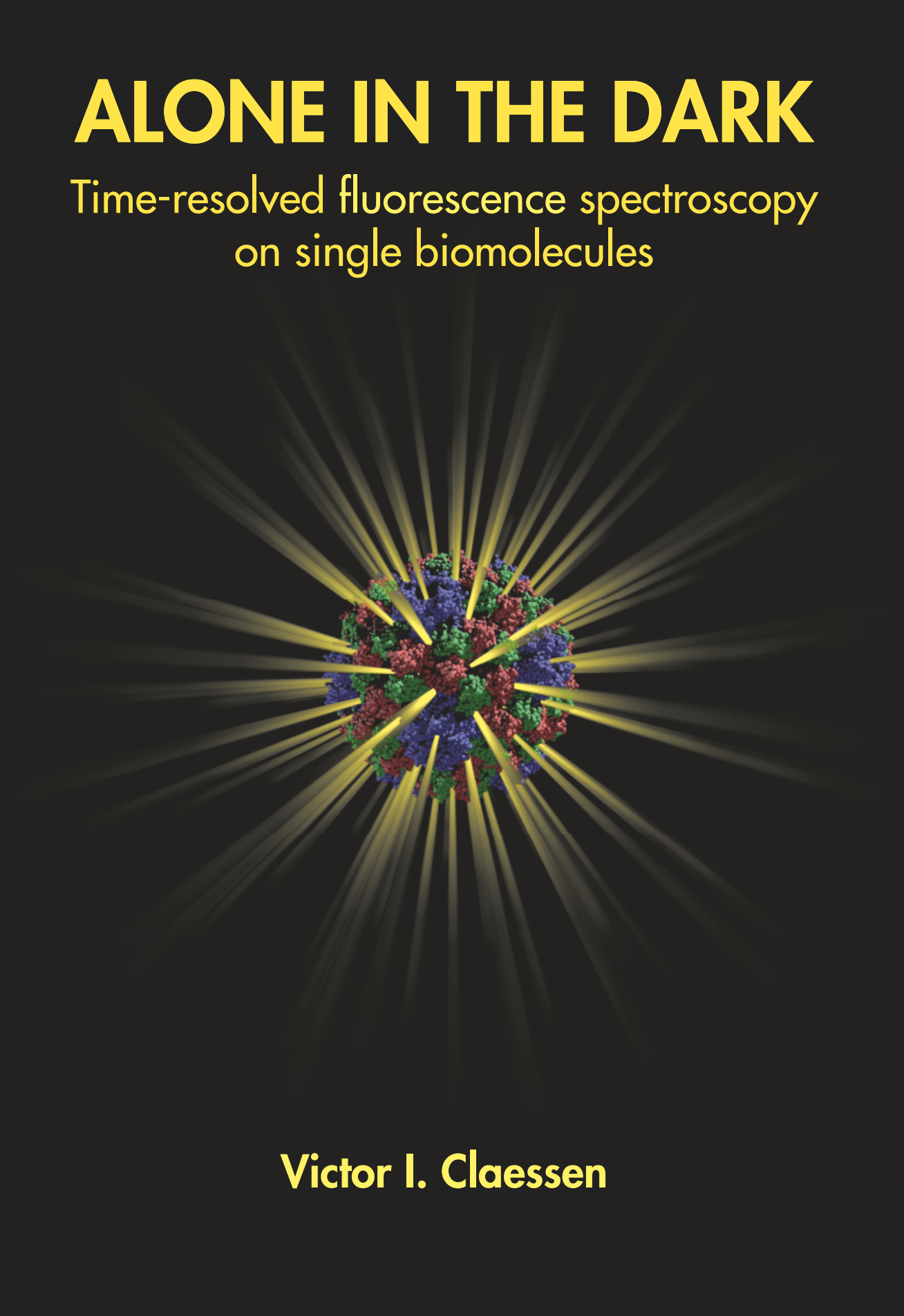

Victor I. Claessen

Alone in the dark

Time-resolved fluorescence spectroscopy on single biomolecules

Victor I. Claessen

Alone in the dark:
Time-resolved fluorescence spectroscopy on single biomolecules
Victor I. Claessen
Thesis Radboud University Nijmegen - Illustrated
With references - With summary in Dutch
ISBN: 978-90-9026687-9
NUR-code: 927

This thesis was printed on graphene-free paper

© 2012, Victor I. Claessen

Carril del Zorro Publishing
URL: www.aloneinthedark.nl

Cover: A model of the cowpea chlorotic mottle virus containing a horseradish peroxidase enzyme molecule, which has generated fluorescent rhodamine 6G product molecules that have accumulated on the inside of the virus capsid (Chapter 5).

Alone in the dark

Time-resolved fluorescence spectroscopy on single biomolecules

Proefschrift

ter verkrijging van de graad van doctor
aan de Radboud Universiteit Nijmegen
op gezag van de rector magnificus prof. mr. S.C.J.J. Kortmann,
volgens besluit van het college van decanen
in het openbaar te verdedigen
op donderdag 21 juni 2012
om 10.30 uur precies

door

Victor Ilja Claessen

geboren op 29 september 1981
te Amsterdam

Promotoren:	Prof. dr. R.J.M. Nolte Prof. dr. A.E. Rowan
Copromotor:	Dr. H. Engelkamp
Manuscriptcommissie:	Prof. dr. S.S. Wijmenga Prof. dr. J. Hofkens (KU Leuven) Dr. K. Blank

Paranimfen:	Drs. A.M. van Buul Ir. O. Lugten

Alone in the dark

Time-resolved fluorescence spectroscopy on single biomolecules

Doctoral Thesis

to obtain the degree of doctor
from Radboud Universiteit Nijmegen
on the authority of the rector magnificus prof. dr. S.C.J.J. Kortmann,
according to the decision of the council of deans
to be defended in public
on Thursday, June 21th 2012
at 10.30 hours

by

Victor Ilja Claessen

born on September 29th, 1981
in Amsterdam

Supervisors:	Prof. dr. R.J.M. Nolte Prof. dr. A.E. Rowan
Co-supervisor:	Dr. H. Engelkamp
Doctoral Thesis Committee:	Prof. dr. S.S. Wijmenga Prof. dr. J. Hofkens (KU Leuven) Dr. K. Blank

Paranymphs:	Drs. A.M. van Buul Ir. O. Lugten

Le véritable voyage de découverte ne consiste pas à chercher de nouveaux paysages,
mais à avoir de nouveaux yeux.

- Marcel Proust

Contents

Chapter 1

An introduction
to single-molecule enzymology

1.1 Enzymes as tiny biological tools

We need enzymes. Our cells require these little (~5–50 nm) protein molecules for everything. Without enzymes, cells could not build, repair and recycle their components, could not assimilate food, could not detect and react to changes in their environment, could not signal to other cells and could not multiply. Just as humans need tools, cells need enzymes. Luckily, there is an enzyme for every job. Enzymes work by catalysing reactions that would otherwise proceed very slowly. They do this by lowering the activation barrier, *i.e.* by decreasing the amount of free energy required for the reaction to proceed. Enzymes typically speed up reactions by as much as a millionfold or more. The purpose of this research is to obtain a better understanding of how enzymes work by studying them individually.

1.2 What do we already know about the way enzymes work?

We thought we knew enzymes pretty well. Since the formulation of Michaelis-Menten kinetics almost a century ago [1], investigators have felt that enzyme kinetics had been adequately described. And why not? If one doubles the amount of enzyme, the reaction rate will also double; if more substrate is added, the rate will increase until a saturation point is

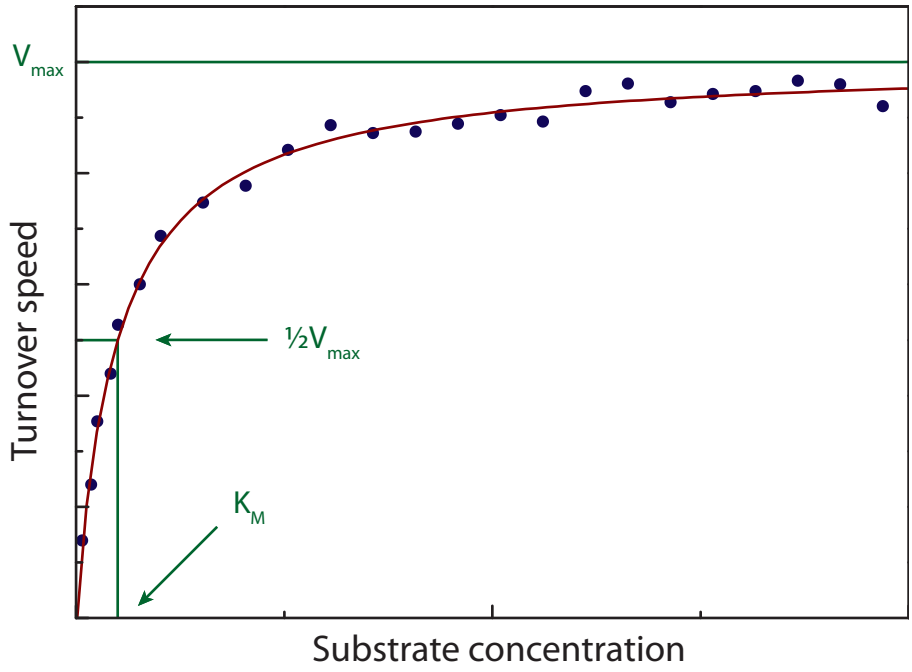

Figure 1.1: A typical Michaelis-Menten plot showing the relationship between substrate concentration and enzyme turnover rate. The substrate concentration at which V equals one half of V_{max} is referred to as K_M.

reached at which the enzyme cannot turn over any faster, as illustrated in Figure 1.1. The basic Michaelis-Menten reaction scheme is discussed at length in every biochemical textbook, but a brief recapitulation is appropriate: A substrate molecule (S) combines with an enzyme molecule (E) to yield an enzyme-substrate complex (ES), which then reacts to form the enzyme-product complex (EP). Thereafter, the enzyme rapidly releases the product molecule (P) (Equation 1.1):

$$E+S \underset{k_{-1}}{\overset{k_1}{\rightleftharpoons}} ES \xrightarrow{k_2} EP \rightarrow E+P \tag{1.1}$$

When enzyme and substrate are mixed ($[E] \ll [S]$), a steady state is attained after a very brief period, and the concentration of ES is proportional to the substrate concentration. The reaction velocity under these steady-state conditions can be described by the Michaelis-Menten equation (Equation 1.2):

$$V = \frac{v_{max}[S]}{K_M + [S]} \tag{1.2}$$

where $v_{max} = k_2[E]$ is the maximum reaction velocity of the enzyme and the Michaelis-Menten constant $KM = \frac{k_{-1}+k_2}{k_1}$ quantifies the affinity of the enzyme for its substrate (provided that $k_2 \ll k_{-1}$, which is a common assumption).

The Michaelis-Menten equation holds for most enzymatic reactions, even when the reaction scheme is more complex and involves intermediates along the reaction pathway. Without diminishing the achievements of Leonor Michaelis and Maud Menten, however, it has been recognised that K_M and k_{cat} simply provide a phenomenological description of the enzymatic reaction and that a detailed understanding of the molecular process requires different approaches. A number of methods—such as the measurement of pre-steady-state kinetics with stopped flow—has been developed to identify intermediates on the reaction pathway and to determine the corresponding rate constants. However, these measurements provide average rate constants for the whole ensemble of enzymes under study, thus providing only part of the picture.

1.3 Why now individually?

Traditional kinetics experiments require large amounts of enzyme. A typical experiment performed at an enzyme concentration of 1 μM in an Eppendorf tube of 1.6 mL contains the astonishing number of 10^{15} enzyme molecules. Any kinetic data collected is averaged over that number of molecules—and over time usually—and expressed as a single statement: an enzyme molecule performs *on average* x turnovers per second. This is akin to saying that the world's gross domestic product (GDP) per capita is € 6160 per year. The issue here is that the distribution of the data is also quite relevant. In the example, the mean cannot convey the significant gap between the incomes of an inhabitant of Burundi and one of Monaco (€ 102 and € 149000, respectively). Figure 1.2 shows that there are large

differences in GDPs between countries. To measure this, it is necessary to look not just at the world as a whole but at all countries individually, or ideally: at individual inhabitants. Single molecule experiments do just that: to measure not just the mean value of a property but also its distribution, by looking at single molecules.

1.4 What has been done before?

By the early 1960s, Boris Rotman [2] had realised that it is possible to measure the catalytic activity of individual enzyme molecules when they are compartmentalised in the droplets of a water-in-oil emulsion. Individual enzyme molecules were encapsulated—by using a *very* low concentration—together with a fluorogenic substrate in these emulsion droplets, and the amount of generated fluorescent product molecules was measured after several hours. Through the use of this innovative approach, the effect of a heat shock on the enzyme preparation was investigated, revealing that individual enzymes were either dead or alive with no intermediate state. Rather than exhibiting different levels of activity, the individual enzyme molecules either retained full activity or were completely inactivated. This result could only have been obtained through examination of individual enzymes, and this method promised to answer important questions about the functioning of enzyme molecules that ensemble measurements could not resolve. Yet for the next 35 years this newborn field of research remained dormant; Boris Rotman was three decades ahead of his time. Only in the past two decades or so sufficient improvements in sensitivity and time resolution were made to enable kinetic experiments on individual enzymes.

The second important step came with the 1998 paper by Sunney Xie *et al.* [3]. Xie and his colleagues managed to detect single turnover events from single cholesterol oxidase molecules using a confocal microscope and a highly sensitive photodetector. During the reaction cycle, a cofactor in the active site switches between a fluorescent and a non-fluorescent state, inducing in every reaction cycle a period of fluorescence followed by a dark period. The reaction rate of the enzyme could then be calculated from the frequency of switching. They found that the enzyme reaction rate was not constant in time, as the enzyme molecules showed periods of high activity followed by periods of low activity; they had discovered dynamic disorder.

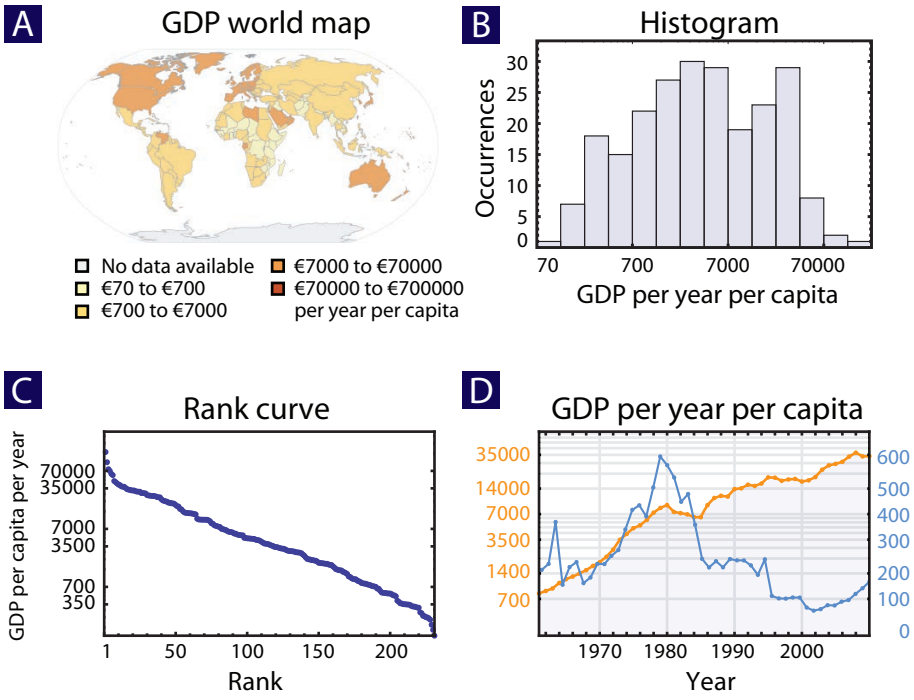

Figure 1.2: A) World map illustrating the relevance of the (geological) distribution of the gross domestic product (GDP) per year per capita. B) Histogram of the GDP per year per capita in euro showing static disorder. C) Rank curve of the GDP per year per capita in euro. D) GDP per year per capita in euro of the Netherlands (orange, left) and Democratic Republic of the Congo (blue, right) over time showing dynamic disorder. Data from Wolfram Alpha.

1.5 Aim and outline of this thesis

This thesis is organised as follows: Two introductory chapters introduce the reader to the field of single molecule studies. These chapters are followed by four chapters that describe the new experiments.

Chapter 1 has welcomed you into the thesis and has enticed you to read thus far. Chapter 2 presents a review of the history of the single enzyme molecule field, it identifies the key experiments that have lead to our current understanding and it acquaints the reader with the various optical techniques that are used. Chapter 3 deals with what can be learnt from single molecule experiments performed in solution. As it turns out, some form of immobilisation of enzyme molecules is often required in order to study molecules for a longer period of time, lest they diffuse away. Following the initial droplet experiment [2], most early research on single molecule enzymatics has involved surface immobilisation. We, too, have performed enzyme experiments on a surface, and the results are described in Chapter 4. However, it seems that lately the focus of attention in the field has shifted from surface immobilisation to entrapment in containers. In Chapter 5 we show the potential of a plant virus as a reaction container and as a tool to study single enzyme kinetics. And ultimately, Chapter 6 explores if sol-gels are a convenient matrix for immobilisation.

1.6 References and notes

[1] L. Michaelis, M. L. Menten, *Biochemische Zeitschrift* **1913**, 49, 333–369.

[2] B. Rotman, *Proceedings of the National Academy of Sciences of the United States of America* **1961**, 47, 1981–1991.

[3] P. Lu, L. Xun, S. Xie, *Science* **1998**, 282(5395), 1877–1882, doi: 10.1126/science.282.5395.1877.

Chapter 2

Techniques

for optical single molecule experiments

2.1 Introduction

This chapter introduces some of the important techniques that are used for single molecule detection. The first section focusses on the microscopy techniques, and the second section discusses some key experiments from the past and the techniques that are used to extract useful information from the processes that are perceived optically. The focus is on the review of the state of the art of fluorescence-based single-molecule approaches that directly monitor the catalytic reaction. Other versatile detection strategies based on single-molecule fluorescence resonance energy transfer that are designed to, for instance, monitor conformational changes have been summarised in recent reviews [2, 3].

How to detect the activity of a single enzyme

The activity of an enzyme is commonly monitored through the use of substrates that are converted to dye molecules as a result of the enzymatic reaction. These dye molecules, which absorb light of a certain wavelength, accumulate over time, and the absorbance of the solution increases. The absorbance of an amassed pool of product molecules is readily

Some of this work was published in Annual Reviews of Analytical Chemistry [1].

observed with a photodetector, and such enzyme-activity measurements are the standard assay of classical enzyme kinetics. Adaptation of this approach to perceive the absorbance of a single product molecule is possible [4, 5] but definitely impractical. Fortunately, there are better ways of detecting single molecules, *e.g.* by means of fluorescence. Fluorescence is the emission of a photon from an atom or a molecule that had previously absorbed a photon of a different wavelength. An important point is that fluorescence coming from an object is typically much weaker than the light source that is used to excite it. It is therefore necessary to eliminate the excitation light to get a high signal-to-noise ratio. This is usually done by exploiting either the anisotropic nature of the emitted fluorescent light, *i.e.* by simply detecting the fluorescence at a right angle to the incident light, or its energy loss, by filtering out the excitation light; either way, no light other than fluorescent light will reach the detector. Herein lies the power of fluorescence: where absorption by a single molecule merely causes a small decrease in a large signal, fluorescence introduces a small signal where previously there was none. In microscopy, the filtering approach is used. The sample is illuminated with a light source—usually either a lamp or a laser—and this light is reflected by a long-pass dichroic mirror onto the sample where it excites the fluorescent molecules. The fluorescent light emitted by these molecules passes through the same dichroic mirror and is detected either by a photomultiplier tube, a sensitive charge-coupled device (CCD) camera, or an avalanche photodiode (APD).

The increased sensitivity makes enzyme substrates that are converted into fluorescent dye molecules a powerful alternative to substrates that are converted into absorbing dyes. Detection methods based on fluorescence therefore usually provide better signal-to-noise ratios. Not only does state-of-the-art optical detector technology allow for the detection of picomolar concentrations of fluorescent dyes in a cuvette, it also permits the detection of individual fluorescent dye molecules, a prerequisite for single-molecule experiments. With modern detectors, tens of thousands of photons can be collected from a single fluorescent molecule every second, generating a large signal. However, this sensitivity is not without its disadvantages because many types of molecules fluoresce, and can also scatter light. Rayleigh scattering can send a photon towards a detector placed at an angle, and Raman scattering can induce photons of different wavelengths that pass through the filters. Photon noise originating from Raman scattering of the solvent—mostly water in enzyme

experiments—is an issue that is hard to avoid. At any rate, one must take care to eliminate contaminations. The number of different (contaminating) fluorophores that are detected can be limited by careful choice of the illumination source and the filter set, which restricts the excitation and emission wavelengths to the dye of interest. Also, the size and the geometry of the illuminated volume critically determine the number of contaminants that contribute to the detected signal. Several types of microscopy that were invented to address this issue (see Figure 2.1), are discussed in the following section. Once the contamination issue has been resolved, the only remaining requirement is to ensure sufficient spatial separation between the enzyme molecules so that they can be inspected independently. For in single-molecule studies, two is a crowd!

2.2 Microscopy for single-molecule fluorescence detection

Total Internal Reflection Fluorescence microscopy

The total internal reflection fluorescence (TIRF) microscope was developed in the 1980s to overcome the problem of background fluorescence and Raman scattering originating from molecules that were not bound to the surface of a sample glass slide. The principle is based on the fact that light is totally internally reflected from the glass-water interface when it strikes the interface at low angles. An evanescent wave of the light, however, penetrates into the water. The intensity of the evanescent wave decays exponentially with the distance from the surface. As a result, only molecules very close to the surface (<100 nm) are excited. Therefore, the reduction of the penetration depth of the light into the sample allows the number of excited fluorophores to be minimised, resulting in a lower background signal. TIRF microscopy was the first technique that showed single-fluorophore sensitivity applied to an enzymatic reaction [6]. Enzymatically active, dye(Cy5)-labelled fragments of the molecular motor protein myosin were immobilised and localised on the surface, and the association-(hydrolysis-)dissociation reaction of individual Cy3-ATP(ADP) molecules was recorded with a camera. In contrast to freely diffusing Cy3-ATP, myosin-bound fluorescent molecules remained immobilised for a certain time. This keystone experiment represented a significant breakthrough for monitoring individual reaction events for the study of single enzymes. It has, however, one major drawback. Both substrate and product are equally flu-

orescent; thus, enzymatic turnovers cannot be fully quantified. That every binding event indeed corresponded to one catalytic reaction event was proven only indirectly by comparing the dissociation rate in the single-molecule experiment with the turnover rate for Cy3-ATP determined by ensemble measurements. The power of this approach in the study of molecular motors has been demonstrated with a number of follow-up experiments. For example, the time between the hydrolysis of one ATP molecule and the generation of force by the myosin molecule could be determined by combining the TIRF microscope with optical tweezers (31). This knowledge filled a gap in our understanding of the molecular mechanism of myosin. Similarly, Cy3-ATP-based experiments have also been applied to dissect details of the mechanism of the rotary motor F1-ATPase [7, 8]. As in the above examples, TIRF excitation is coupled primarily with a CCD camera for detection. The advantage of this combination is that it allows a number of immobilised molecules to be monitored simultaneously. However, this benefit comes at the expense of a time resolution limited to the millisecond regime. Another limitation of TIRF, which is not shared by the techniques described below, is that—by design—a TIRF microscope can detect only molecules close to the surface.

Confocal microscopy

The key point to confocal microscopy [9] is that only a small volume (in the order of 10^{-19} m^3) in the sample is illuminated and observed, securing a very high signal-to-noise ratio. A confocal microscope uses two tricks in order to accomplish this. Firstly, the light source—usually a laser—is focused into a diffraction-limited spot to reduce the size of the illuminated volume. And secondly, a pinhole is inserted into the emission light path in front of the detector that blocks most of the light originating from areas that are out of the microscope objective's focus. This strategy prevents out-of-focus light from reaching the detector and improves both the contrast and the resolution. It is the combination of these two measures (illuminate only that which you wish to detect, and detect only what is illuminated) that gives confocal microscopy its excellent signal-to-noise ratio. It is possible to use the small surface area of the photodetector as a pinhole instead of a dedicated detection pinhole. Either way, one obtains a high resolution (~1 μm) in the z direction. Because

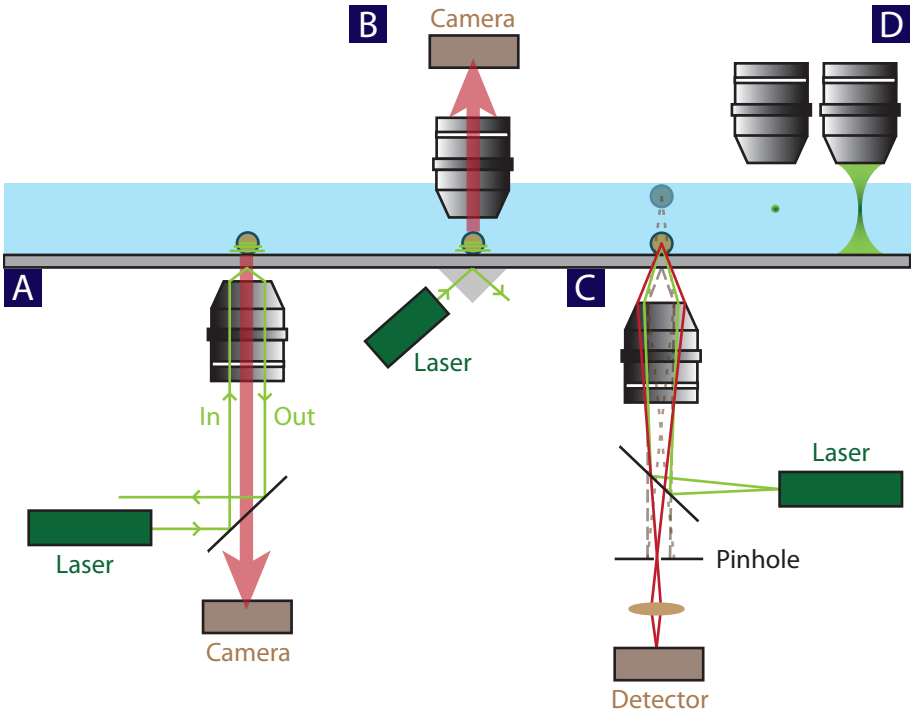

Figure 2.1: Principles of A) objective-type total internal reflection fluorescence (TIRF), B) prism-type TIRF, C) confocal microscopy, and D) a comparison of the illuminated areas in two-photon and single-photon excitation. In TIRF, only molecules close to the surface are illuminated and therefore detected. In confocal microscopy, a certain depth in the sample can be selected, and light from other layers is rejected by the pinhole.

the detection occurs in a single point, movement of the confocal volume over the sample is required to acquire an image. This can be achieved either by scanning the sample over a fixed beam [9] or by using mirrors to scan the beam across the sample. The latter approach vastly improves the speed at which an image can be produced. By moving the microscope objective up and down, one can image several planes in the sample (from tens to several hundreds of micrometers deep) in succession to generate a three-dimensional image with a vertical resolution in the (low) micrometer range. Therefore, it takes longer to obtain information about the position of molecules on a surface, and the time to scan two subsequent images is slower than the frame rate of a CCD camera. However, the time resolution of an APD detector—which is frequently used in confocal microscopes—is superior when the catalytic activity of an individual enzyme molecule is being measured at a defined position. Individual fluorescent dyes can be observed with a sustained sub-millisecond time resolution, which is better by at least a factor of ten than the best available CCD cameras. The first application of confocal microscopy to individual enzymatic turnover reactions is described in a seminal paper by Xie and colleagues [10], who studied the enzyme cholesterol oxidase immobilised in an agarose gel. The analysis method that was used for this experiment will be discussed later on in one of the next sections.

2.3 Data analysis techniques for single molecule experiments

To date, there are but a handful of articles that use experimental data for analysis of enzyme behaviour. The next sections will discuss the two single molecule techniques, fluorescence correlation spectroscopy (FCS) and single event timetrace analysis, introduced by Rigler and Xie, respectively, into the field of single molecule enzymology. In short, FCS averages single events from many individual molecules, while timetrace analysis samples single events from individual single molecules.

Both techniques start by capturing the photon stream in the experimental setup. A single photon detector generates electrical pulses—for each photon—that are recorded by a computer. Each pulse is tagged with its arrival time and placed in a queue. In order to express the data as a practical intensity over time for display in a graph, some method of integration is needed. Therefore, the photon pulse data stream is divided into segments

(bins), and all the pulses in each segment are binned. The number of pulses per segment of time is the intensity. The result is an intensity-time trace, similar to the one shown in Figure 2.3.

Fluorescence Correlation Spectroscopy

Fluorescence correlation spectroscopy (FCS), which was invented in the 1970s [11–14], uses autocorrelation analysis (*vide infra*) to detect events from a fluorescence intensity time trace. The autocorrelation function describes the fluctuations of the signal around the mean over a large range of time scales. It is defined as the average of the product of the variation around the mean and the variation around the mean some time τ later, divided by the mean squared (2.1):

$$G(\tau) = \frac{\langle \delta F(t) \delta F(t+\tau) \rangle}{\langle F(t) \rangle^2} \tag{2.1}$$

Using this temporal correlation, one can obtain information about the time scale of the fluctuations by fitting the autocorrelation function with a suitable physical model that describes the origin of the observed intensity fluctuation. In studies of, for instance, the diffusion of molecules through a detection volume of known size, fitting the autocorrelation function gives the average diffusion speed (from which the hydrodynamic radius can be calculated) of the molecules and the concentration of these molecules in the solution. Autocorrelation can be calculated in real time by the multiple τ algorithm [15], or by simply binning the photons and correlating the binned fluorescence time trace. Furthermore, one can correlate the photon-arrival times directly, which can greatly increase the time resolution [16, 17].

Although FCS is not generally applicable to experiments on single enzymes, autocorrelation analysis is useful for single-enzyme time traces. In FCS, the molecules under study are generally not surface immobilised; rather, they diffuse freely through the confocal volume. The concentration of the sample is chosen such that there is only a small number (typically 1–100) of fluorescent molecules in the focus at one point in time. Every gain or loss of a fluorescent molecule in the focus causes the signal intensity at the detector to change. This experimental setup causes the measured fluorescence time trace to contain transient contributions from a large number of different molecules diffusing through the

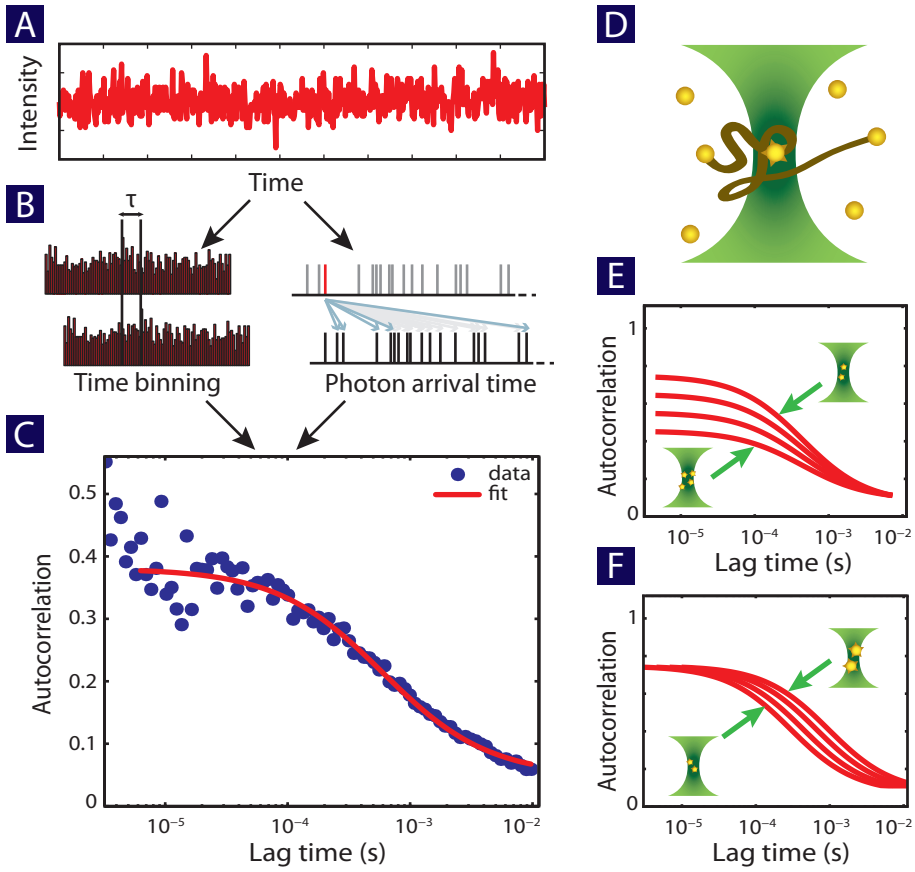

Figure 2.2: As molecules move in and out of the focus D) of a microscope objective, A) the recorded fluorescence intensity signal fluctuates. B) By autocorrelating this fluorescence intensity—either via correlation of the binned signal (left) or via direct correlation of the photon arrival times(right)—one can obtain the autocorrelation function C). Two parameters can be obtained from the fit: the correlation time, which is related to the diffusion constant, and the correlation coefficient, which is related to the concentration. E) An increase in concentration leads to a decrease in the correlation coefficient since the passing of an individual molecule contributes less to the total intensity and the fluctuation is therefore smaller. F) An increase in molecular size gives rise to longer correlation times since each molecule resides for a longer time in the confocal volume.

confocal volume. FCS, therefore, is not really a single-molecule technique, although the detection of individual molecules in the detection volume is certainly possible. FCS allows one to measure the properties of molecules when the ensemble is in (dynamic) equilibrium (Figure 2.2). Fluctuations in fluorescence intensity can be directly related to changes in molecular properties originating from, *e.g.* fluorescence blinking—*i.e.* random switching between dark and bright states under continuous excitation due to intersystem crossing to the triplet state [18–20]—intra- and intermolecular interactions, diffusion, and even enzymatic reactions.

Having worked in the area of FCS, Rigler and colleagues [21] performed a single-enzyme experiment with the enzyme horseradish peroxidase (HRP) and analysed the results with autocorrelation analysis. Biotinylated HRP was immobilised on the surface of a streptavidin-coated cover slip. After adding the fluorogenic substrate dihydrorhodamine 6G, which is converted by the enzyme to yield the fluorescent dye rhodamine 6G, the authors identified spots on the surface that had a higher fluorescence intensity than the rest of the surface. Also, the fluorescence signal fluctuated as a result of the enzymatic activity. Data measured at the position of these spots showed a different autocorrelation function than did data from the surface itself, where the autocorrelation function was flat. Time traces of more than one hundred enzyme molecules were recorded and analysed by autocorrelation. Within the duration of the experiment, the individual enzyme molecules showed a large distribution of rates for the formation of the enzyme-product complex (static disorder). Furthermore, like in the experiment with cholesterol oxidase, the autocorrelation functions could not be fitted with a single exponential function; rather, a stretched exponential function was introduced to obtain a good fit. A stretched exponential is thought to be characteristic of dynamic disorder, and seems to indicate that a large number of different rate constants contribute to the reaction of a single enzyme. This HRP experiment provides additional proof that autocorrelation analysis is a powerful way to characterise the behaviour of individual enzyme molecules [22].

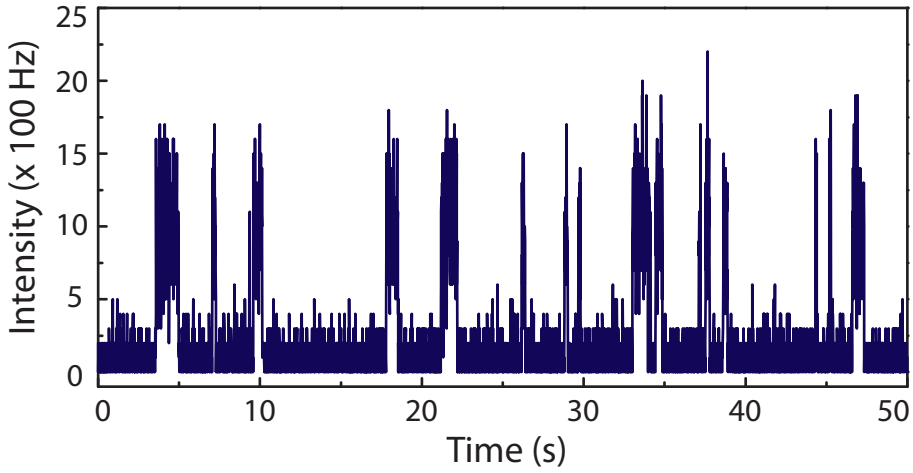

Figure 2.3: Simulated intensity-time trace for a system with two levels that are Poisson-distributed, the 'on' level having an average duration of 0.5 s and an intensity of 1000 s^{-1}, and the 'off' level having an average duration of 0.5 s and an intensity of 100 s^{-1}. The bin width is 10 ms.

Single event timetrace analysis

In most single enzyme experiments, fluorescent molecules appear as a result of a chemical reaction. The fluorescence signifies the presence of a fluorescent molecule that materialises somewhere in a reaction cycle. The début and departure of the fluorescence then indicates one turnover event in the reaction cycle. It is important to note that the chemical reaction itself is usually too fast to be resolved, but the apparent duration of the events is lengthened due to diffusion limitations on the molecules and thermal activation barriers in the reaction. In the experiment by Xie *et al.* [10], the active site of the enzyme that was used, *i.e.* cholesterol oxidase, contained a cofactor that is fluorescent in its oxidised form, but not in its reduced form. This cofactor is cycled between its oxidised and reduced forms in every reaction cycle; so every redox cycle was detected as an on/off cycle in the fluorescence measurement. Although this technique is certainly an elegant way of examining an enzyme—as it does not rely on artificial labelling, which might interfere with the enzyme's behaviour—it is not widely applicable because most enzymes do not have a fluorescent co-

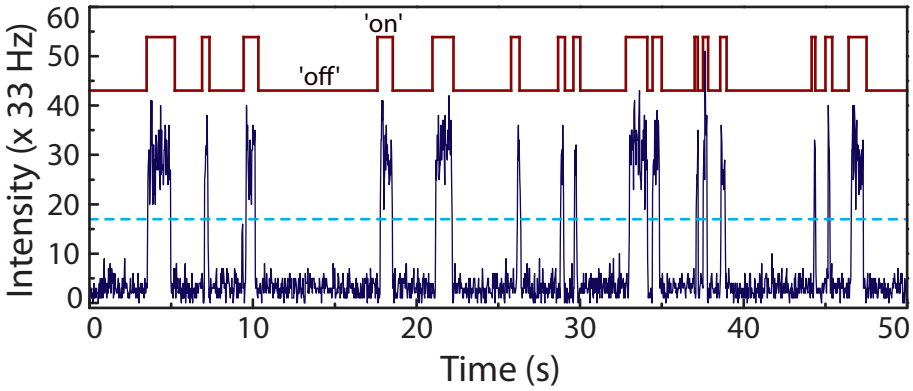

Figure 2.4: The same trace as was shown in Figure 2.3, now shown with 30 ms bins. A threshold (dashed line) has been set at the level 17 counts per 30 ms. The system is said to be in the 'on' state if the intensity level exceeds the threshold, and it is deemed to be 'off' when the intensity is below the threshold. The red line at the top indicates the binary trajectory.

factor. The unique advantage of using the cofactor as the fluorescent reporter system is that one can determine not only the time of one complete turnover cycle, but also the durations of the individual states in the turnover cycle, *i.e.* the oxidised, highly fluorescent state and the reduced, nonfluorescent state.

To obtain the desired kinetic information, the authors converted the fluorescence-intensity time trace into a binary on/off trajectory, which allowed for the determination of the durations of the oxidised (on) and reduced (off) states, respectively. An example conversion can be seen in Figure 2.4. The simplest method through which to perform such a conversion is to apply a threshold to the fluorescence time trace. Any level above the threshold is considered 'on', everything below is considered 'off'. The appropriate threshold level can be estimated from the photon-counting histogram. For traces with a high signal-to-noise ratio, like in the case of the cholesterol oxidase experiments, setting a threshold for separating the on and off levels can be trivial. For lower quality traces with a lot of Poisson photon counting noise a trade-off is required; the larger the bins, the better the two states can be separated, but at the same time any fast events which occur within the bin time are lost.

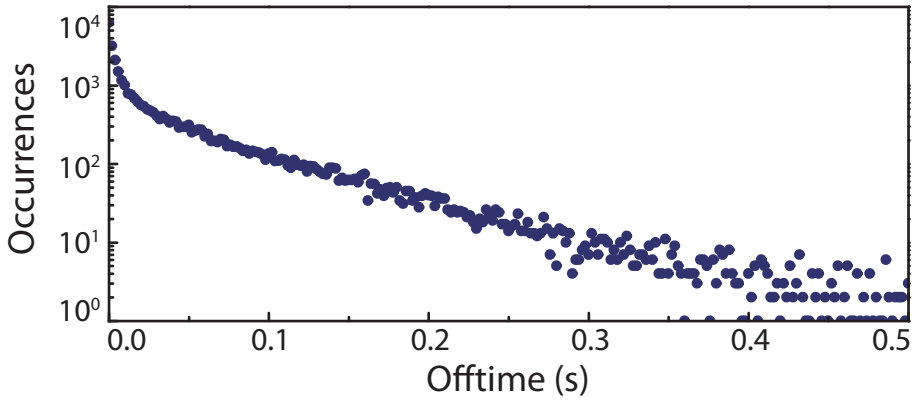

Figure 2.5: Histogram of 'off' times between turnovers of a single *Thermomyces lanuginosa* lipase (TLL) enzyme. [23]. For a purely stochastic process an exponential decay is expected. In this figure it is clear that the data does not follow an exponential function, *i.e.* there are too many short offtimes.

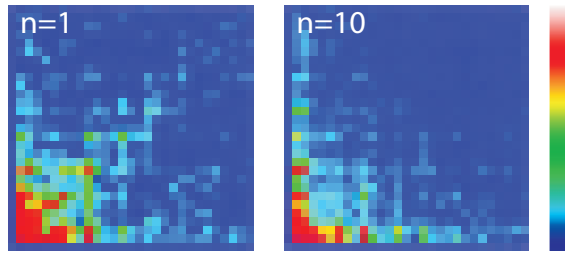

Figure 2.6: 2D correlation histograms of events separated by n events. The diagonal feature present at n=1 (subsequent events) disappears at a separation of ten turnovers. Reproduced from [10].

The determination of the threshold level is important. As the bin size shrinks, the Poisson noise increases and the levels start to overlap. Any threshold placement will necessarily introduce false positives and false negatives as bins are erroneously attributed to on and off periods. The minimum total number of errors is obtained if the threshold is placed exactly at the point where the curves for each level intersect in the photon counting histogram. Recently, another technique has been developed for obtaining binary trajectories, *viz.* change point analysis [24, 25], in which a generalised likelihood ratio test is used to find the intensity change points. Low frequency variations, *e.g.* background increase due to buildup of fluorescent molecules, are an issue when applying a threshold to a timetrace. Change point analysis circumvents this by determining the threshold locally rather than globally.

After the waiting times for the on and off levels have been determined, kinetic information can then be obtained from the times' respective probability distributions. The enzymatic turnover reaction may naïvely be considered as a stochastic process characterised by an exponential decay in the waiting-time (offtime) distribution. In this case, one expects the data points to follow a linear pattern when plotting the histogram of the waiting times semi-logarithmically. The waiting-time distribution in the Xie experiment [10], however, deviated from this exponential behaviour: More short waiting times were observed than would be expected from a purely stochastic process, meaning that the rate of reaction was apparently not constant in time. More importantly, there was a correlation between successive on waiting times. This correlation manifested itself in the observation that short waiting times were more frequently followed by short waiting times and that long waiting times were more frequently followed by long waiting times. This so-called memory effect was depicted by a two-dimensional plot in which each waiting time was plotted against its preceding waiting time or the n^{th} preceding waiting time (for illustrations, see Figures 2.5 and 2.6). Similarly, the autocorrelation function—explained in more detail in the previous section—of the waiting times showed a clear correlation over several waiting times. It is this observed memory effect that lead to the conclusion that the enzyme remembers its previous conformational state. This behaviour of the enzyme is described in the so-called fluctuating enzyme model, which will be explained in the next section. Autocorrelation analysis is applicable not only to the extracted waiting times. In the Xie experiment with cholesterol oxidase, it was also directly used on the intensity time trace. It provides

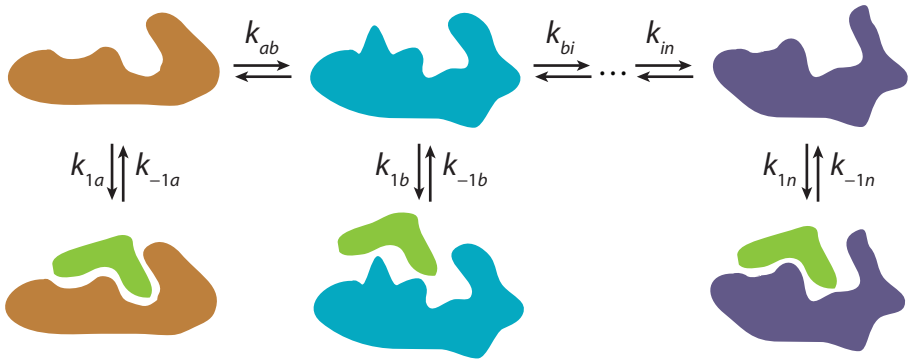

Figure 2.7: As an enzyme changes conformation its affinity for a substrate changes, as does its ability to catalyse the reaction of substrate to product. As a result the enzyme exhibits different rates over time.

an additional analysis method that does not require the use of a threshold. Similar to the waiting-time distribution, the intensity autocorrelation function could not be fitted to a single exponential, which would be expected for a first-order reaction. The intensity autocorrelation function thereby provided additional proof that more than one rate constant determines the catalytic reaction of cholesterol oxidase.

2.4 The fluctuating enzyme model

Generally, as molecules become more complex, they begin to exhibit *primo* static disorder, *i.e.* the distribution of distinct properties among the general population of molecules, and *secundo* dynamic disorder, *i.e.* the fluctuation of the properties of an individual molecule in time. In the case of enzymes, both static and dynamic disorder are directly related to the three-dimensional structure and the related dynamics of the amino acid polymer [26, 27]. State-of-the-art single-enzyme kinetics experiments aim to shed light on the structure-function-dynamics relationships that relate to this disorder. Aristotle might have agreed that a string of amino acids does not a functional protein make; the folding of the amino acid chain into a specific conformation is vital to the function of proteins. Even the so-called natively unfolded proteins fold into a defined structure upon binding to one of their lig-

ands [28, 29]. The requirement for a specific conformation is especially necessary for enzymes, which usually rely on a certain, very precise spatial coordination of specific amino acid residues to form an active site. Enzymes are a remarkable product of evolution because their specific conformation must be maintained in the presence of thermal motion, which constantly induces fluctuations in the amino acid chain. The fact that the reaction rate is not constant in time [10, 21, 30–34] is easily explained by these fluctuations in the three-dimensional structure of the enzyme: The enzyme can appear in different conformations, each with its own specific activity. In addition to the observation that conformations may differ in terms of catalytic activity, it is now well established that conformational changes are essential in many enzymatic reactions. They can even be the rate-limiting step in the catalytic turnover cycle [35, 36]. The number of thermodynamically and kinetically accessible conformations, their relative probabilities, and their interconversion rates are defined by the so-called 'energy landscape' of the enzyme. As a result, the enzyme sometimes finds itself in a conformation in which it turns over many times before converting to a state with a lower activity (Figure 2.7), which explains the memory effect that has been observed in single-molecule experiments [10, 22, 23, 32, 37, 38]. The energy landscape, therefore, crucially determines the time series of events observed in single-enzyme experiments, and investigators are attempting to reconstruct the energy landscape for an enzyme from single-molecule time traces [39, 40]. The energy landscape of an enzyme, however, is not static; every modification in the enzyme—in its interaction with the substrate or in the environmental conditions—affects the energy landscape by lowering or raising barriers. As a consequence, regulation of enzymatic activity, for example, may result from the (de)stabilisation of a conformation with high activity [41]. Evidence for this hypothesis has been obtained from nuclear magnetic resonance measurements and molecular dynamics simulations [27, 42]. Several studies show that a ligand-bound conformation is sampled in the conformational ensemble with a certain probability, even if the ligand is not present. In these cases, ligand binding merely shifts the equilibrium toward the bound conformation [41, 43]. Similar effects have been observed for the activation of proteins by phosphorylation [44, 45]. Shifts in a conformational equilibrium may further originate from changes in the micro environment, such as pH [46] and the presence of crowding agents [47]. Moreover, mutations might stabilise or destabilise certain conformations, and

evolution may proceed via the stabilisation of an alternative enzyme conformation with altered activity or specificity [48]. In addition to all these biochemical modulators of enzyme function, physical influences are attracting increasing interest. For example, stretching forces may be an important regulator of biological activity for proteins with structural and mechanical function. Although studying the influence of forces on enzymatic reactions is technically challenging, several experimental single-molecule approaches have been developed. Initial studies show that an applied force indeed influences enzymatic activity [33, 49–51]. On the basis of the limited data available to date, no general conclusions about the activating or deactivating effect of an applied force—which also greatly depends on the biological function of the enzyme under study—can yet be drawn. The application of forces at the single-molecule level has recently been combined with single-molecule fluorescence detection [33, 51]. This combination allows one to manipulate the enzyme landscape while simultaneously monitoring its activity, enabling one to study the effect of a force on an enzyme systematically.

2.5 Strategies for single-enzyme experiments

Following the breakthrough experiments described above, several other enzymes were analysed through the detection of either the turnover of a fluorogenic substrate or the redox state of a cofactor. Despite the many approaches used, all these systems exhibit static and/or dynamic disorder upon analysis, and each of the experiments has expanded our knowledge of single-enzyme behaviour. An issue that has been addressed in all these follow-up experiments is that of immobilizing and identifying the enzymes on a surface. Every immobilisation and labelling procedure may introduce disorder into the system due to interactions with the surface or the label. The following section discusses the different immobilisation methods that have been used on surfaces and describe the main differences between the experiments. The subsequent sections describe attempts to avoid direct contact of the enzyme with a surface, *e.g.* the encapsulation of individual enzyme molecules in microsized or nanosized containers. A pictorial overview of some of the surface attachment strategies is displayed in Figure 2.8.

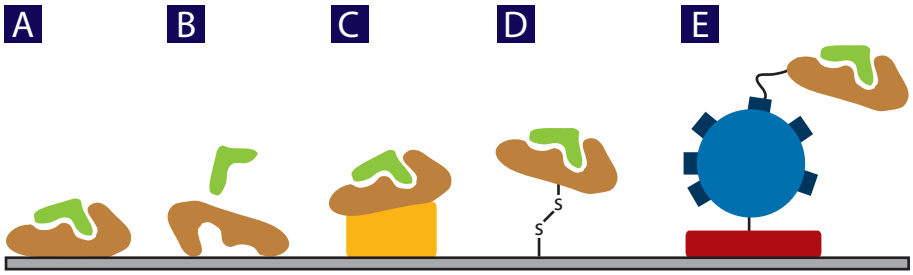

Figure 2.8: Schematic representation of surface immobilisation strategies. A) Non-specific adsorption. Note that B) some of the enzymes can adsorb in a way that leaves their active sites unreachable for substrate molecules. To overcome this, several strategies have been explored using C) a protein foot, D) a disulphide bond or E) a polymer bead coupled via a biotin-streptavidin interaction.

2.6 Surface immobilisation

2.6.1 Non-specific adsorption of the enzyme

Velonia *et al.* [31] deposited single molecules of Candida antarctica lipase B (CalB) on a glass surface that was made hydrophobic by functionalisation with dichlorodimethylsilane. The enzyme molecules adsorbed to the surface because of hydrophobic interactions. To achieve localisation of the enzymes, the authors labelled the enzyme with a fluorescent dye; CalB does not turn over substrate molecules fast enough to allow for its localisation from the accumulation of fluorescent product molecules in its proximity. After localizing an individual enzyme and placing it into the confocal volume, the authors [31] used the confocal laser to bleach the fluorescent label, and individual turnovers were subsequently detected. A significant fraction of the enzymes, however, were found to be inactive, possibly because the molecules were partly denatured, a result of the interaction with the hydrophobic surface. Alternatively, some of the lipase molecules, which naturally bind to hydrophobic surfaces, may have been oriented with the active site toward the surface, thereby preventing any substrate molecules from entering and reacting. Despite the problems encountered in this experiment, the active CalB molecules were measured for a much longer time than was possible in previous experiments (>20 min). As a result, by adding fresh substrate

solution with increasing concentration, the authors were able to study the same single enzyme at several substrate concentrations. Above a concentration of ~1 μM 2,7-bis-(2-carboxy-ethyl)-5-(and-6-)carboxyfluorescein, acetomethyl ester (BCECF, AM) the addition of substrate did not result in significantly higher enzyme activity. A Michaelis-Menten plot for an individual enzyme molecule showed typical saturation behaviour as predicted by Michaelis-Menten kinetics, suggesting that the Michaelis-Menten equation is also valid at the single-molecule level. The determination of the Michaelis-Menten plot was complicated by the solubility limit of BCECF, AM, which is a relatively hydrophobic substrate. The long time traces, however, did not only allow [31] to vary the substrate concentration, they also provided a high number of turnovers for the subsequent analysis of the waiting times between individual turnovers. CalB activity shows the typical fingerprint of dynamic disorder as well as a very pronounced memory effect: CalB activity is clearly separated in phases with very high activity and in phases where almost no enzymatic turnovers occur at all. Surprisingly, the enzyme was predominantly inactive; the active phases constituted only 3% of the overall measurement time [31, 33].

2.6.2 Site-directed enzyme adsorption via a "protein foot"

To overcome the previously encountered problems caused by non-specific adsorption of CalB to the hydrophobic surface, a strategy to allow site-directed adsorption of the lipase from Thermomyces lanuginosa (TLL) was developed [38]. The lipase was "clicked", *i.e.* coupled via 1,3-dipolar (3+2)-Huisgen cycloaddition, to bovine serum albumin (BSA). Well-defined positions—the single free solvent-accessible lysine on the TLL and the free solvent-accessible thiol of BSA—were chosen for this coupling reaction in both proteins, resulting in well-defined heterodimers. BSA is known to adsorb to hydrophobic surfaces, whereas TLL is less hydrophobic than CalB. The TLL–BSA heterodimer, therefore, prefers to orient itself with the BSA toward the hydrophobic glass when adsorbing to the surface. This strategy protected the enzyme from surface-induced denaturation and ensured that the enzyme was oriented with its active site toward the solution. The BSA also presented an anchor for the attachment of a fluorescent label without any further modification of the enzyme itself. The authors localised the labelled enzyme-BSA heterodimers by scanning

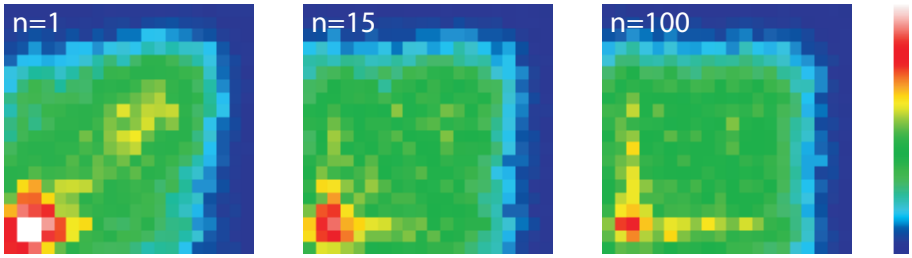

Figure 2.9: 2D correlation histograms of events separated by n events. The diagonal feature, which can be clearly seen in n=1 and is still present at n=15 but not at n=100, indicates the correlation between events. Short waiting times are more often followed by short waiting times, long waiting times are more often followed by long waiting times, which is indicative of a memory effect. Reproduced from [38].

the surface with the confocal microscope and then adding a 1 μM solution of the fluorogenic substrate 5(6)-carboxyfluorescein diacetate. Nearly all of the enzymes—which were identified with the help of the fluorescent label—were active, and the average turnover was 17 s^{-1}. Again, the analysis of the waiting times between turnovers revealed that the distribution of waiting times was not completely random (Figure 2.9). Short waiting times were more often followed by short waiting times, and long waiting times were most often followed by long waiting times. For TLL, this memory effect lasts for more than 15 turnovers, which corresponds to an extremely long time. This strong correlation provides a clear indication for the fluctuating enzyme model. As long as the enzyme is in the same conformation, it produces product molecules with a characteristic rate. Once it switches to another conformation, the rate changes. This TLL study was the first experiment in which the enzyme was immobilised to the surface in a site-specific way. It is therefore unlikely that any additional heterogeneities were introduced into the system by the experimental design. Fluctuations in the rate constants must be an intrinsic property of the enzyme itself.

2.6.3 Site-specific and covalent enzyme immobilisation

Site-specific immobilisation was also used for the single-molecule analysis of the enzyme nitrite reductase (NiR) from *Alcaligenes faecalis* [52]. NiR is a trimer with two copper cen-

tres per monomer, each involved in the catalytic reaction. An electron is accepted from a donor molecule by the type 1 copper centre, transferred to the type 2 copper centre, and subsequently used to reduce nitrite (NO_2^-) to nitric oxide (NO). In contrast to cholesterol oxidase, the copper cofactors are not fluorescent; neither are the substrate or product molecules. A different detection strategy was therefore necessary. This detection strategy was based on the broad absorption spectrum of the type 1 copper centre when it is in its oxidised state. The oxidised type 1 copper centre acted as a quencher for a fluorescent dye (ATTO655) that was coupled to the enzyme site-specifically in Förster distance to the copper centre. As a result, the ATTO655 dye was more fluorescent in the reduced state of the copper ion than in the oxidised state. Measuring the change in fluorescence emission of ATTO655 allowed the oxidation and reduction of the copper centre to be followed. To achieve immobilisation to the surface, a mutant of NiR containing a surface-accessible cysteine was prepared. This mutant was coupled to a mercapto-functionalised glass surface via a short homobifunctional polyethylene glycol spacer with thiol-reactive end groups. In this experiment [52], the ATTO655 label was used to identify enzymes on the surface. Autocorrelation analysis of the recorded single-molecule traces yielded $K_M = 31 \pm 17$ μM and $k_{cat} = 6.5 \pm 2$ s^{-1}. These values correspond well to the values measured at the ensemble level ($K_M = 50 \pm 20$ μM and $k_{cat} = 8 \pm 1$ s^{-1}). This agreement proves that in this system the surface immobilisation did not result in an altered enzymatic activity. As in the above-described experiments, the turnover rate of a single NiR enzyme varied over an order of magnitude, as indicated by the stretch parameter of the correlation fit. This result was intriguing because this enzyme is known from X-ray spectroscopy to have nearly superimposable conformations for the reduced and oxidised states as well as for the substrate- and product-bound states. The authors attributed the rate distribution to local variations in the coordination spheres of the copper centres. If they exist at all, the conformational fluctuations may be restricted to the close surroundings of the copper centres rather than to greater structural variations in the protein at large.

2.6.4 Enzyme immobilisation via receptor-ligand interactions

Agreement of the kinetic constants K_M and k_{cat} between single-molecule and ensemble experiments has also been found for the enzyme β-galactosidase [37]. Similar to the HRP experiment by Rigler *et al.* [21], biotinylated β-galactosidase was used for the immobilisation. In contrast to HRP, β-galactosidase was not immobilised to the surface directly but rather to a streptavidin-containing bead, which was subsequently deposited on a biotin-containing surface. The attachment to the bead provided another interesting strategy with which to localise enzyme molecules because the bead can easily be observed with differential interference contrast microscopy. Subsequent placement of the confocal volume at the position of the bead allowed the turnover of the fluorogenic substrate resorufin-β-D-galactopyranoside (RGP) to be recorded. RGP has a relatively high solubility in an aqueous buffer; therefore, much higher substrate concentrations (up to 380 μM) could be used. Use of these high-substrate concentrations required the autohydrolysis of the substrate to be considered. Product molecules originating from autohydrolysis diffuse through the confocal volume and are detected as product molecules generated by the enzyme. To account for this problem, a second strong, defocused laser beam was used to illuminate a 100 μm-diameter area around the bead to bleach any resorufin molecules in its proximity. After the data at different substrate concentrations were obtained, the corresponding waiting-time distributions of the off-times were analysed. At very low substrate concentrations, the off-times were fitted by a single exponential function, whereas they became increasingly multi-exponential at higher substrate concentrations. This discrepancy was explained by the fact that at low substrate concentrations the diffusion of the substrate to the enzyme is rate-limiting. Unfortunately, the substrate concentration could not be increased to K_M or higher because the enzymatic reaction proceeded so fast that individual turnovers could no longer be resolved. Despite the high solubility of RGP, the highest substrate concentration (100 μM) that could be used was approximately one-fourth of K_M (380 μM). On the basis of the available data points, an agreement of K_M and k_{cat} for single-molecule and ensemble measurements was obtained, and the validity of the Michaelis-Menten equation at the single-molecule level was confirmed. However, the shape of the waiting-time distribution at saturating substrate concentrations remains undiscovered and is difficult to determine

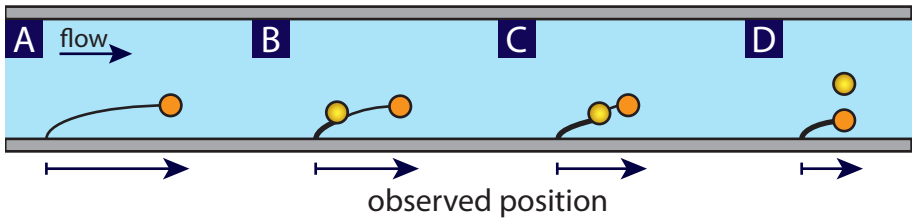

Figure 2.10: Illustration of a flow-stretch experiment [30]. A) A bead (orange) is attached via double strand DNA (thin line) to a glass surface. The flow stretches the DNA to its maximum length. B–C) The DNA contracts as the exonuclease converts an increasing fraction to single strand DNA (bold line), thus reeling in the bead. D) In the end only ssDNA remains and the enzyme is released. The change in position of the bead serves as a measure for the reaction rate.

with the currently available fluorogenic substrates because of solubility or autohydrolysis problems.

2.6.5 Immobilisation of the substrate

It is not necessary to limit an experiment to immobilisation of the enzyme; in some experiments, it is also possible—perhaps preferable—to immobilise the substrate. Especially for insoluble substrates such as lipid and phospholipid layers, as well as for high-molecular-weight substrates such as DNA, immobilisation of the substrate provides an important means of observing the catalytic reaction. For instance, the use of wide-field microscopy allows one to simultaneously observe and track a number of individual phospholipase molecules while they eat their way through a phospholipid bilayer [53]. In this study, both the enzymes and the phospholipid layer were fluorescently labelled so that the disappearance of the layer could be related to the presence of an enzyme. Although the experiment did not yield the precise rate of the catalytic reaction, it showed that the enzymes preferred the edge of the phospholipid layer, suggesting that these layers are cleaved starting from defects. More direct information about the rate of the catalytic reaction was obtained for the cleavage of DNA by the enzyme λ-exonuclease, which cleaves one strand of double-stranded DNA (dsDNA) successively from its 5' end, yielding single-stranded DNA (ss-

DNA). When DNA was stretched on the surface under flow conditions (as illustrated in Figure 2.10), ssDNA appeared shorter because it coiled up. Because an increasing fraction of the dsDNA was converted to ssDNA, the DNA shortened; this shortening was detected by the movement of a bead attached to the DNA [30]. This detection principle only works with DNA polymers that are long enough—16 μm in this case—to extend (well) beyond the diffraction limit of optical microscopy. Analysis of the bead movement allowed the authors to allocate the melting of the 5' base as the rate-limiting step of the reaction and furthermore the experiment again revealed dynamic disorder in the system. This experiment can be easily extended to fluorescence detection by labelling the DNA strand. This approach was recently used in a detailed analysis of DNA replication [54].

2.7 Spatial confinement

Individual enzyme molecules can also be encapsulated in micro- or nanosized containers such as vesicles, micelles, emulsion droplets, polymersomes, and virus capsids. These containers can then be fixed in space while the enzyme freely diffuses inside the container. This method of encapsulation may closely resemble biologically relevant conditions in which enzymes are frequently confined in small concentrations in subcellular compartments. Alternatively, small and sealable wells can be fabricated with micro- and nanofabrication techniques.

2.7.1 Encapsulation in droplets

Compartimentalisation in droplets is a good way to make sure that an enzyme and its substrate molecules can find one another. If the container is permeable neither for the substrate nor for the product, product molecules will accumulate as the enzymatic reaction proceeds, and the increasing product concentration can be determined as a function of time. This can be achieved for the droplets of a water-in-oil emulsion, for example, whose properties can be tuned such that all molecules in the water droplet are retained inside the droplet. This is the approach, followed by Rotman [55], that was briefly mentioned in the introduction. Rotman developed a method to study emulsified droplets made from an aqueous phase consisting of a very diluted solution of β-galactosidase and an appropriate fluorogenic sub-

strate. At that time (1961), approximately 1 million fluorescent product molecules were needed for the detection of the catalytic reaction in the droplets. Although Rotman tried to measure the same droplets repeatedly every few hours, any dynamic disorder in the activity of individual enzymes was well hidden by time-averaging. The water-in-oil emulsion method for single-molecule enzymology was later rediscovered [56] and expanded with more modern technology, such as a CCD camera. These improvements allowed for better time resolution and enabled the simultaneous analysis of many droplets. Despite these improvements, this approach suffers from an inherent limitation: The impact a single fluorophore has on the total signal intensity decreases dramatically already within the first few turnovers. The detection of the appearance of each new molecule gets increasingly hard. This rapid increase in bulk fluorescence quickly prohibits the detection of single enzymatic turnovers. Therefore, each measurement point will represent a time average over many turnovers. However, for β-galactosidase, fluctuations in the rate of product formation were still detectable on a minute time scale, proving that this approach has some value with the right choice of enzyme.

2.7.2 Femtoliter array

The main disadvantage of the emulsion approach is that the droplets are not monodisperse in size. The number of molecules caught in a droplet is related to the internal volume of the droplet and the concentration of the cargo. (The reader is referred to Chapter 5 for more on the statistics of encapsulation.) If there is a range of droplet sizes it is more difficult to select a useful cargo concentration. If the concentration is high enough to fill some of the small droplets, the large droplets will start to contain multiple molecules, which impedes their use in *single* molecule experiments. If the concentration is low enough to have mostly single molecules in the large droplets, then the small droplets will be mostly empty. This polydispersity problem can be overcome with arrays of microsized wells. These wells, whose volume is in the femtoliter range, can be prepared from various materials. They are filled by pipetting a diluted enzyme solution containing substrate on top of the array and then sealing the array with an appropriate lid. If the concentration is chosen correctly, one can deduce from Poisson statistics that approximately 90% of the chambers end up empty

and that most of the rest are filled with exactly one enzyme molecule. The first such experiment was performed with wells etched into quartz glass to analyse the catalytic activity of lactate dehydrogenase [57]. Later, soft lithography was used to prepare wells from polydimethylsiloxane for the analysis of β-galactosidase. Although these experiments represent primarily a first proof of principle, wells prepared in optical fibre bundles have been used for a more detailed analysis of the enzymes β-galactosidase [34, 58] and HRP [59]. The approach based on optical fibre bundles has the advantage that accumulated product molecules are excited by light travelling through the optical fibre. In the same way, the emitted fluorescence is recorded by a CCD camera after returning along the same optical path. Investigators have used experiments based on optical fibre bundles to visualise the buildup of product molecules inside the wells by repeatedly taking images for a period of time. The fluorescence intensity for each well was plotted in time to obtain the average turnover frequency for each entrapped enzyme molecule. In the β-galactosidase experiment [34], the average single-molecule K_M of 76 ± 23 μM was close to the value of 117 ± 23 μM found at the ensemble level. The average k_{cat} value of 916 ± 58 s^{-1} also compared well with the value of 888 ± 87 s^{-1} obtained from ensemble measurements. The distribution of velocities, however, was quite broad (coefficient of variation: 30%), indicating that not all enzymes in the population had the same activity. This static disorder is a good example of what can only be learnt from single molecule experiments. Furthermore, despite a low time resolution (seconds), fluctuations in the turnover rate were observed, indicating the presence of different enzyme conformations with interconversion rates on the second time scale [34]. In the HRP experiment [59], the apparent substrate turnover rates for the single-enzyme experiments were ten times lower than in ensemble measurements. These low rates were attributed to a more complex reaction of the substrate Amplex®Red, which requires a two-step reaction to form the fluorescent dye resorufin. Whereas the first step of the reaction is enzyme catalysed, the second step probably takes place outside the enzyme and is therefore susceptible to side reactions. The authors [59] point out that single-molecule data must be interpreted with care if the enzymatic reaction does not follow a one-step reaction with 1:1 stoichiometry for each reaction step to yield a fluorescent product molecule. For all these measurements in impermeable containers or chambers, the size of the chamber must be carefully adjusted to ensure that substrate molecules are not de-

pleted too quickly. Furthermore, depending on the choice of enzyme/substrate system, it is necessary to subtract a background caused by either photoxidation/autohydrolysis of the substrate to form the fluorescent product (positive background) or photobleaching of the fluorescent product (negative background). Photobleaching also defines the illumination intensity and the number of measurement points that can be taken. If the fluorescent dye bleaches faster than new product molecules are generated, no useful information can be obtained about the enzymatic reaction. In the HRP experiment [59], for example, the excitation intensity was chosen to be very low so that only very noisy single-enzyme time traces could be obtained. Despite these technical difficulties, the ability to perform highly parallel measurements of many individual enzymes at the same time makes the approach very powerful, and novel information about the observed enzymatic reactions has already been obtained.

2.8 Flow assay in a capillary

Another method that does not require immobilisation of the enzyme is based on capillary electrophoresis. When a capillary is filled with a very dilute (10^{-17} M dehydrogenase [60]) enzyme solution, the individual enzymes can be separated by centimetres. If this solution contains a fluorogenic substrate, fluorescent product molecules accumulate in proximity to the enzyme. After a certain incubation time, the enzyme and the generated product molecules are pulled through the capillary by electrophoresis. This means of course requires that both enzyme and product molecule are charged. Fluorescent product molecules are detected as they are swept past a photodetector, thereby making it possible to determine how active each individual enzyme has been. With this approach, differences in the rate of product formation during the incubation time were detected for the enzymes lactate dehydrogenase [60], alkaline phosphatase [61], and β-galactosidase [62]. Initially, the incubation was performed while stopping the flow in the capillary. In the meantime, the approach was further developed for use under continuous-flow conditions [63]. Exploiting the fact that the enzyme itself moves slower than the product molecules, investigators used the flow assay to vary the temperature along the capillary (Figure 2.11). With the product molecules running ahead of the enzyme, they are constantly separated from the enzyme and arrive

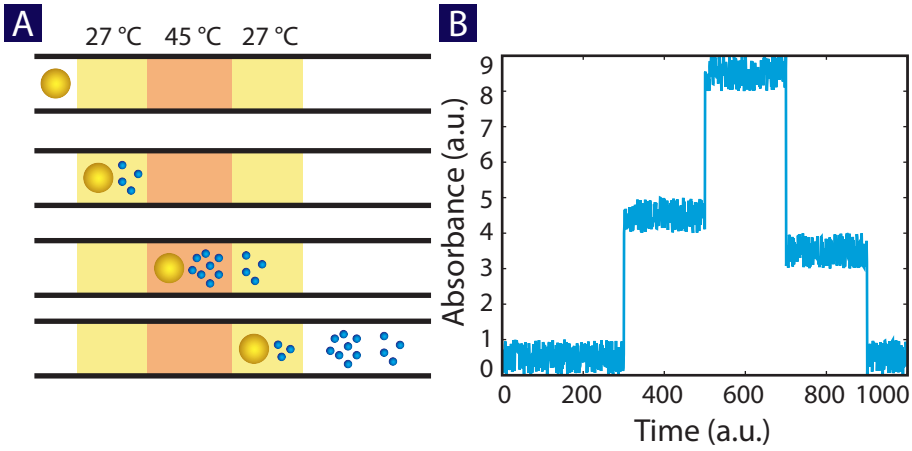

Figure 2.11: A) Schematic drawing of an enzyme (yellow) moving through a capillary. At different temperatures, it produces product molecules (blue) at different rates. The product molecules move faster than the enzyme. B) Simulated electropherogram arising from this bi-level temperature arrangement.

at the detector in the order in which they were generated. Using this assay, researchers recorded a profile of the activity of several enzymes as they moved along the capillary; the time resolution was on the order of seconds. As a result of the variations in the temperature along the capillary, the shape of the activity profile showed that enzymes work harder at elevated temperatures. However, they are also more likely to become denatured. A 20 s heat shock of 50 °C denatured 45 of 53 β-galactosidase molecules. The surviving enzymes showed a 56 ± 10% residual activity, probably caused by partial denaturing of the enzyme. β-galactosidase—from *E. coli* as used in this experiment—is a tetrameric enzyme. More specifically, it is actually a dimer of dimers, with two active sites at the interface of each dimer, and each active site comprising amino acid residues from two monomers [64, 65]. The observation that the activity always decreases by 50% (or 100%), and never by 25% or 75% indicates that a denaturation disturbs two active sites simultaneously. It is known that free dimers are inactive, so it can be concluded—from the observation that 50% of the activity can be retained—that the dimer-dimer interaction is apparently fairly well intact.

An important feature of this method is that it can be easily run unattended for large periods of time, allowing for the collection of numerous single-molecule profiles, which is vital for attaining proper statistics. In summary, the flow assay is another elegant way to perform single-enzyme experiments with increased throughput, although again at the cost of a dramatically decreased time resolution. An interesting option may arise from a combination of emulsion technology with a flow assay based on microfluidics. The preparation and manipulation of emulsion droplets in microfluidic channels is a fast-developing new field [66, 67]. Generated droplets are monodisperse and, if required, can even be kept stationary in the microfluidic system for a parallel kinetic observation [68]. The detection of a single fluorescent molecule in an optically trapped emulsion droplet has recently been demonstrated [69]. Through the use of high laser intensities, a product molecule can be bleached quickly, and the use of emulsion droplets may allow the detection of individual turnovers. In this context, new and exciting developments in single-molecule studies in droplet based microfluidic systems can be expected.

2.9 References and notes

[1] V. I. Claessen, H. Engelkamp, P. C. M. Christianen, J. C. Maan, R. J. M. Nolte, K. Blank, A. E. Rowan, *Annual Review of Analytical Chemistry* **2010**, 3(1), 319–340, doi: 10.1146/annurev.anchem.111808.073638.

[2] D. Smiley, G. Hammes, *Chemical Reviews* **2006**, 106(8), 3080–3094, doi: 10.1021/cr0502955.

[3] K. Blank, G. De Cremer, J. Hofkens, *Biotechnology Journal* **2009**, 4(4), 465–479, doi: 10.1002/biot.200800262.

[4] J. Ballard, E. Carmichael, D. Shi, J. Lyding, M. Gruebele, *Nano Letters* **2006**, 6(1), 45–49, doi: 10.1021/nl0519231.

[5] A. Gaiduk, M. Yorulmaz, P. V. Ruijgrok, M. Orrit, *Science* **2010**, 330(6002), 353–356, doi: 10.1126/science.1195475.

[6] T. Funatsu, Y. Harada, M. Tokunaga, K. Saito, T. Yanagida, *Nature* **1995**, 374(6522), 555–559, doi: 10.1038/374555a0.

[7] T. Nishizaka, K. Oiwa, H. Noji, S. Kimura, E. Muneyuki, M. Yoshida, K. Kinosita, *Nat Struct Mol Biol* **2004**, 11(2), 142–148, doi: 10.1038/nsmb721.

[8] K. Adachi, K. Oiwa, T. Nishizaka, S. Furuike, H. Noji, H. Itoh, M. Yoshida, J. Kinosita, *Cell* **2007**, 130(2), 309–321, doi: 10.1016/j.cell.2007.05.020.

[9] M. Minsky, *Scanning* **1988**, 10, 128–138.

[10] P. Lu, L. Xun, S. Xie, *Science* **1998**, 282(5395), 1877–1882, doi: 10.1126/science.282.5395.1877.

[11] D. Magde, E. Elson, W. W. Webb, *Physical Review Letters* **1972**, 29(11), 705–708, doi: 10.1103/PhysRevLett.29.705.

[12] D. Magde, E. Elson, W. W. Webb, *Biopolymers* **1974**, 13(1), 29–61, doi: 10.1002/bip.1974.360130103.

[13] M. Ehrenberg, R. Rigler, *Chemical Physics* **1974**, 4(3), 390–401, doi: 10.1016/0301-0104(74)85005-6.

[14] O. Krichevsky, G. Bonnet, *Reports on Progress in Physics* **2002**, 65(2), 251–297, doi: 10.1088/0034-4885/65/2/203.

[15] K. Schatzel, M. Drewel, S. Stimac, *Journal of Modern Optics* **1988**, 35, 711–718, doi: 10.1080/09500348814550731.

[16] M. Wahl, I. Gregor, M. Patting, J. Enderlein, *Optics Express* **2003**, 11(26), 3583–3591, doi: 10.1364/OE.11.003583.

[17] T. Laurence, S. Fore, T. Huser, *Optics Letters* **2006**, 31(6), 829–831, doi: 10.1364/OL.31.000829.

[18] W. E. Moerner, *Science* **1997**, 277(5329), 1059–1060, doi: 10.1126/science.277.5329.1059.

[19] D. A. V. Bout, W.-T. Yip, D. Hu, D.-K. Fu, T. M. Swager, P. F. Barbara, *Science* **1997**, 277(5329), 1074–1077, doi: 10.1126/science.277.5329.1074.

[20] J. Lakowicz, *Principles of Fluorescence Spectroscopy*, 2nd edition, Kluwer Academic/Plenum Publishers, **1999**, ISBN 0387312781.

[21] L. Edman, Z. Foldespapp, S. Wennmalm, R. Rigler, *Chemical Physics* **1999**, 247(1), 11–22, doi: 10.1016/S0301-0104(99)00098-1.

[22] L. Edman, R. Rigler, *Proceedings of the National Academy of Sciences of the United States of America* **2000**, 97(15), 8266–8271.

[23] H. Engelkamp, N. S. Hatzakis, J. Hofkens, F. C. De Schryver, R. J. M. Nolte, A. E. Rowan, *Chemical Communications* **2006**, (9), 935–940, doi: 10.1039/B516013H.

[24] L. Watkins, H. Yang, *The Journal of Physical Chemistry B* **2005**, 109(1), 617–628, doi: 10.1021/jp0467548.

[25] B. Kalafut, K. Visscher, *Computer Physics Communications* **2008**, 179(10), 716–723, doi: 10.1016/j.cpc.2008.06.008.

[26] H. Frauenfelder, *Cellular and Molecular Life Sciences* **1995**, 51(3), 200–203, doi: 10.1007/BF01931093.

[27] K. Henzler-Wildman, D. Kern, *Nature* **2007**, 450(7172), 964–972, doi: 10.1038/nature06522.

[28] J. Dyson, P. Wright, *Nature Reviews Molecular Cell Biology* **2005**, 6(3), 197–208, doi: 10.1038/nrm1589.

[29] K. Sugase, J. Dyson, P. Wright, *Nature* **2007**, 447(7147), 1021–1025, doi: 10.1038/nature05858.

[30] A. van Oijen, P. Blainey, D. Crampton, C. Richardson, T. Ellenberger, S. Xie, *Science* **2003**, 301(5637), 1235–1238, doi: 10.1126/science.1084387.

[31] K. Velonia, O. Flomenbom, D. Loos, S. Masuo, M. Cotlet, Y. Engelborghs, J. Hofkens, A. Rowan, J. Klafter, R. Nolte, F. de Schryver, *Angewandte Chemie International Edition* **2005**, 44(4), 560–564, doi: 10.1002/anie.200460625.

[32] O. Flomenbom, J. Hofkens, K. Velonia, F. Deschryver, A. Rowan, R. Nolte, J. Klafter, R. Silbey, *Chemical Physics Letters* **2006**, 432(1–3), 371–374, doi: 10.1002/prot.20893.

[33] H. Gumpp, E. Puchner, J. Zimmermann, U. Gerland, H. Gaub, K. Blank, *Nano Letters* **2009**, 9(9), 3290–3295, doi: 10.1021/nl9015705.

[34] D. M. Rissin, H. H. Gorris, D. R. Walt, *Journal of the American Chemical Society* **2008**, 130(15), 5349–5353, doi: 10.1021/ja711414f.

[35] E. Eisenmesser, D. Bosco, M. Akke, D. Kern, *Science* **2002**, 295(5559), 1520–1523, doi: 10.1126/science.1066176.

[36] E. Watt, H. Shimada, E. Kovrigin, P. Loria, *Proceedings of the National Academy of Sciences of the United States of America* **2007**, 104(29), 11981–11986, doi: 10.1073/pnas.0702551104.

[37] B. P. English, W. Min, A. M. van Oijen, K. T. Lee, G. Luo, H. Sun, B. J. Cherayil, S. C. Kou, X. S. Xie, *Nature Chemical Biology* **2006**, 2(2), 87–94, doi: 10.1038/nchembio759.

[38] N. S. Hatzakis, H. Engelkamp, K. Velonia, J. Hofkens, P. C. M. Christianen, A. Svendsen, S. A. Patkar, J. Vind, J. C. Maan, A. E. Rowan, R. J. M. Nolte, *Chemical Communications* **2006**, (19), 2012, doi: 10.1039/B516551B.

[39] A. Baba, T. Komatsuzaki, *Proceedings of the National Academy of Sciences of the United States of America* **2007**, 104(49), 19297–19302, doi: 10.1073/pnas.0704167104.

[40] C.-B. Li, H. Yang, T. Komatsuzaki, *Proceedings of the National Academy of Sciences of the United States of America* **2008**, 105(2), 536–541, doi: 10.1073/pnas.0707378105.

[41] K. Gunasekaran, B. Ma, R. Nussinov, *Proteins: Structure, Function, and Bioinformatics* **2004**, 57(3), 433–443, doi: 10.1002/prot.20232.

[42] D. Boehr, J. Dyson, P. Wright, *ChemInform* **2006**, 37(42), 3055–3079, doi: 10.1021/cr050312q.

[43] D. Boehr, P. Wright, *Science* **2008**, 320(5882), 1429–1430, doi: 10.1126/science.1158818.

[44] B. F. Volkman, D. Lipson, D. E. Wemmer, D. Kern, *Science* **2001**, 291(5512), 2429–2433, doi: 10.1126/science.291.5512.2429.

[45] M. Formaneck, L. Ma, Q. Cui, *Proteins: Structure, Function, and Bioinformatics* **2006**, 63(4), 846–867, doi: 10.1002/prot.20893.

[46] A. Fersht, *Journal of Molecular Biology* **1972**, 64(2), 497–509, doi: 10.1016/0022-2836(72)90513-X.

[47] H. Zhou, G. Rivas, A. Minton, *Annual Review of Biophysics* **2008**, 37(1), 375–397, doi: 10.1146/annurev.biophys.37.032807.125817.

[48] L. James, D. Tawfik, *Trends in Biochemical Sciences* **2003**, 28(7), 361–368, doi: 10.1016/S0968-0004(03)00135-X.

[49] H. Itoh, A. Takahashi, K. Adachi, H. Noji, R. Yasuda, M. Yoshida, K. Kinosita, *Nature* **2004**, 427(6973), 465–468, doi: 10.1038/nature02212.

[50] E. M. Puchner, A. Alexandrovich, A. L. Kho, U. Hensen, L. V. Schäfer, B. Brandmeier, F. Gräter, H. Grubmüller, H. E. Gaub, M. Gautel, *Proceedings of the National Academy of Sciences of the United States of America* **2008**, 105(36), 13385–13390, doi: 10.1073/pnas.0805034105.

[51] A. Ishijima, H. Kojima, T. Funatsu, M. Tokunaga, H. Higuchi, H. Tanaka, T. Yanagida, *Cell* **1998**, 92(2), 161–171, doi: 10.1016/S0092-8674(00)80911-3.

[52] S. Kuznetsova, G. Zauner, T. Aartsma, H. Engelkamp, N. Hatzakis, A. Rowan, R. Nolte, P. Christianen, G. Canters, *Proceedings of the National Academy of Sciences of the United States of America* **2008**, 105(9), 3250–3255, doi: 10.1073/pnas.0707736105.

[53] S. Rocha, J. Hutchison, K. Peneva, A. Herrmann, K. Müllen, M. Skjøt, C. Jørgensen, A. Svendsen, F. De Schryver, J. Hofkens, H. Uji-i, *ChemPhysChem* **2009**, 10(1), 151–161, doi: 10.1002/cphc.200800537.

[54] S. Hamdan, J. Loparo, M. Takahashi, C. Richardson, A. van Oijen, *Nature* **2008**, 457(7227), 336–339, doi: 10.1038/nature07512.

[55] B. Rotman, *Proceedings of the National Academy of Sciences of the United States of America* **1961**, 47, 1981–1991.

[56] A. Lee, *Biophysical Journal* **2005**, 88(6), 4303–4311, doi: 10.1529/biophysj.104.055053.

[57] W. Tan, E. S. Yeung, *Analytical Chemistry* **1997**, 69(20), 4242–4248,

doi: 10.1021/ac970631k.

[58] H. H. Gorris, D. M. Rissin, D. R. Walt, *Proceedings of the National Academy of Sciences of the United States of America* **2007**, 104(45), 17680–17685, doi: 10.1073/pnas.0705411104.

[59] H. Gorris, D. Walt, *Journal of the American Chemical Society* **2009**, 131(17), 6277–6282, doi: 10.1021/ja9008858.

[60] Q. Xue, E. S. Yeung, *Nature* **1995**, 373, 681–683, doi: 10.1038/373681a0.

[61] D. B. Craig, E. A. Arriaga, J. C. Y. Wong, H. Lu, N. J. Dovichi, *Journal of the American Chemical Society* **1996**, 118(22), 5245–5253, doi: 10.1021/ja9540839.

[62] G. K. Shoemaker, D. H. Juers, J. M. L. Coombs, B. W. Matthews, D. B. Craig, *Biochemistry* **2003**, 42(6), 1707–1710, doi: 10.1021/bi0204138.

[63] D. B. Craig, E. R. Nichols, *Electrophoresis* **2008**, 29(21), 4298–4303, doi: 10.1002/elps.200800482.

[64] B. W. Matthews, *Comptes Rendus Biologies* **2005**, 328(6), 549–556, doi: 10.1016/j.crvi.2005.03.006.

[65] A. Nichtl, J. Buchner, R. Jaenicke, R. Rudolph, T. Scheibel, *Journal of Molecular Biology* **1998**, 282(5), 1083–1091, doi: 10.1006/jmbi.1998.2075.

[66] Y. Schaerli, F. Hollfelder, *Molecular BioSystems* **2009**, 5, 1392–1404, doi: 10.1039/B907578J.

[67] B. T. Kelly, J. Baret, V. Taly, A. D. Griffiths, *Chem. Commun.* **2007**, pages 1773–1788, doi: 10.1039/B616252E.

[68] A. Huebner, D. Bratton, G. Whyte, M. Yang, A. J. deMello, C. Abell, F. Hollfelder, *Lab Chip* **2009**, 9, 692–698, doi: 10.1039/B813709A.

[69] J. Tang, A. M. Jofre, G. M. Lowman, R. B. Kishore, J. E. Reiner, K. Helmerson, L. S. Goldner, M. E. Greene, *Langmuir* **2008**, 24(9), 4975–4978, doi: 10.1021/la800329k.

Chapter 3

In solution

studies on freely diffusing enzyme molecules

3.1 Introduction

As mentioned in the introductory Chapters 1 and 2, we are interested in learning more about the catalytic activity of enzymes. We believe that it will broaden our understanding of the kinetics of enzymes if we were able to look at enzyme molecules individually. Pioneering experiments [2, 3] have hinted that there is both static and dynamic disorder among enzyme molecules, and we would like to investigate this further.

Most enzymes work in cells, which are crowded environments. But even in cells, many enzymes are not just floating around in the cytosol. Rather, they are present in specialised compartments, where optimal conditions for their functioning can be maintained and they can find protection from inhibiting molecules or proteases. Since the compartments usually are very small, the concentration of an enzyme can reach high values, and hence the reaction rates can be very high. Ideally, we would like to observe the activities of single enzymes *in vivo*. At the moment, this is technically too complicated, for instance because there is too much background noise for optical observation. To reduce background noise to an acceptable level, we have to simplify the environment of the enzyme.

Some of this work was published in Chemical Science [1].

Perhaps the simplest method to look at single enzyme molecules *in situ* is in solution. Diffusion ensures that the molecules are spread out over the solution—assuming that there are no or very weak intermolecular interactions—and thus dilution facilitates the observation of individual enzyme molecules. On the other hand, molecules are rapidly moving in solution, making it more difficult to observe them in the focal point of the microscope for any time larger than a few milliseconds. It is possible to track enzyme molecules in solution for longer periods of time by means of wide-field microscopy [4], but this approach requires a very high excitation laser intensity to gather enough fluorescence photons, which has the adverse effect of increasing the photobleaching rate of the enzymes and the fluorescence product molecules that they generate.

Since it is not yet possible to observe the activity of single enzymes freely diffusing in solution, as these are moving too fast, we have to consider other options. To slow the enzymes down, we can either increase the viscosity of the medium—which might change the dynamics of the enzyme reactions—or make the enzyme part of a larger complex of molecules, for instance by placing it in a container. While the latter does complicate the experiments, it provides us with an opportunity to more closely mimic the natural environment of an enzyme. In this way, like in a cell, the enzyme is present in a crowded environment and can experience some level of protection from harmful substances.

There are many possible choices for a container, *e.g.* a liposome and a polymersome, but these nanoparticles suffer from polydispersity, and therefore can cause substantial differences in reaction conditions. We decided to encapsulate an enzyme in an empty virus shell, because virus particles are monodisperse. The enzyme encapsulated in a virus shell diffuses slower due to an increased size—allowing for a longer examination time—and also the product molecules accumulate inside the shell, enhancing the intensity of the signal. The interior of the virus resembles somewhat the crowded inner environment of a cell, and also protects the enzymes from proteases. Furthermore, it should be possible to incorporate other enzyme molecules into the shell, which would allow for the study of interactions between enzymes in a confined environment; cascade reactions for instance. As a first step, we decided to include another protein together with the enzyme, with the aim of studying the effect of the total protein concentration inside the container on the kinetics of the enzyme. We have no evidence from bulk measurements that encapsulation in the capsid

changes the k_{cat} of our enzyme, so we assume that the capsid does not change the enzyme properties itself.

The capsid itself can freely diffuse in solution. We aim to observe the capsid by the fluorescence of the protein that is co-encapsulated with the enzyme, and the kinetics of the enzyme by the fluorescent product molecules that it generates. We extended our confocal microscope with an additional detection channel, such that we can observe both the protein and the enzyme simultaneously and independently at different wavelengths.

3.1.1 The container

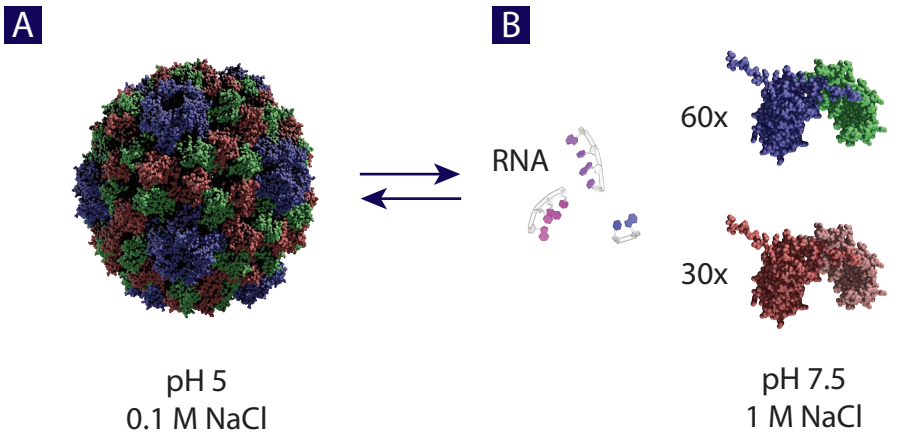

Figure 3.1: Reversible assembly and disassembly of A) CCMV into B) its components RNA and dimers of the coat protein. The 90 coat protein dimers are all chemically and structurally identical; The different colours indicate the different positions of the dimers in the virus shell.

For the container, we chose the Cowpea Chlorotic Mottle Virus (CCMV), since it is a plant virus, *ergo* harmless for humans, and it has the property of undergoing reversible assembly. The virus originates from the continental USA and it is transmitted by beetles. It causes a mosaic disease of cowpea plants (*Vigna unguiculata*), whose subspecies surprisingly enough comprise both black-eyed peas and yardlong beans. CCMV is a virus with

isometric particles with a diameter of 28 nm [5, 6] (see Figure 3.1A). The infectious particles—or virions—consist of an RNA strand that is wrapped in a protein shell. The shell is composed of 180 identical copies of the so-called coat protein. These coat proteins assemble into dimers, and these dimers in turn form a truncated icosahedron. An important feature of the CCMV is that its assembly is reversible. In fact, it was the first icosahedral virus that was reassembled *in vitro* from its components, the purified coat protein and its RNA, to yield a working—infectious—particle [7]. The disassembly and reassembly of CCMV are shown in Figure 3.1. Importantly, the protein shell of CCMV is stable in the absence of the genetic material, making it ideal for enzyme encapsulation. The RNA can be extracted by precipitation after the disassembly of the virus. The coat proteins can subsequently be reassembled into a hollow particle [8]. This empty particle, called capsid, can be used as a container for a range of cargoes.

There are multiple methods of encapsulation. In the experiments described in Chapter 5 for instance, we encapsulated enzyme molecules in the CCMV by statistical inclusion. To this end, the capsid was assembled in a solution containing the cargo, and some will become entrapped in the process. For the current experiment, we encapsulated the proteins PalB and EGFP (*vide infra*) by non-covalently linking them to the coat proteins with the help of a leucine zipper. The leucine zipper is a peptide motif that coils into a helix due to hydrophobic interactions [9]. When the heterodimeric polypeptide motif is divided in two, the two separate parts can be connected to different molecules. When solutions of the two peptide strands—with their cargoes—are combined, the strands self-assemble and tether the cargoes. In our experiment, one strand of the leucine zipper is expressed as a fusion protein with the coat protein, and the other strand is expressed as a fusion protein with each of the cargo proteins. When the coat protein-leucine zipper is subsequently mixed with the cargo-leucine zipper combination, the two leucine zippers dimerise and create a link between the coat protein and the cargo. This complex can then be mixed with wildtype capsid protein in the desired ratio and assembled to control the amount of cargo molecules inside the CCMV capsid.

3.1.2 The enzyme and protein molecules

PalB (*Pseudozyma antarctica* lipase B) is the second of two lipase enzymes extracted from *Pseudozyma antarctica* (formerly *Candida antarctica* [10] and therefore the enzyme is still habitually named CalB), a yeast found in the 1960s in Lake Vanda, Antarctica [11]. PalB is a 33 kDa enzyme consisting of 317 amino acids. Its structure was first determined in 1994 [12] and it has since become probably the most employed hydrolase in the biocatalysis field [13]. Its usefulness is evidenced by over a dozen patents that have been filed describing processes which make use of PalB, with applications ranging from the production of biodiesel [14] to the decomposing of soy sauce oil [15]. The enzyme retains most of its activity at pH 5.0 [16], which is the pH at which the capsid is stable.

GFP (Green Fluorescent Protein) is a 27 kDa protein of 238 amino acid residues originating from the jellyfish *Aequorea victoria*. This bioluminescent Medusozoa species is capable of producing flashes of light—usually for defense against predators—in a two-step process. The protein aequorin produces blue light that is absorbed by GFP, which in turn releases part of the energy as green light—hence the name green fluorescent protein. EGFP is an enhanced version of GFP created in 1995 which is more thermostable—it matures at 37 °C—and is easier to express as a correctly folded and functional protein in *E. coli* [17]. This stability, however, comes at the expense of a lower quantum yield—0.6 for EGFP vs 0.8 for GFP.

3.1.3 The technique

Dual-colour fluorescence cross-correlation spectroscopy ([DC]FCCS) is a recent extension to normal FCS [18–20] in which a second laser and detector pair is used, allowing not only the simultaneous use of two independent fluorophores in one experiment, but also more importantly the detection of interactions between molecules, for instance in binding studies. Usually, there is significant cross-correlation between two fluorophores if they are joined together, because they diffuse in and out of the focus simultaneously. In biomolecular chemistry, FRET pairs (Förster Resonance Energy Transfer) are often used to probe binding. In this case a photon is emitted from a chromophore when another molecule in close proximity (typically <10 nm) absorbs a photon of higher energy [21]. The advantage

of FCCS over FRET is that the fluorescent labels do not need to be as close to one another, which can facilitate the experimental design.

Cross-correlation is akin to autocorrelation, which was discussed in Chapter 2, in that, the information is extracted from the temporal fluctuations of a signal. In autocorrelation, a signal is correlated with itself at various lag times; in cross-correlation a signal is correlated with another signal, according to the formula: Cross-correlation is akin to autocorrelation, which was discussed in Chapter 2, in that, the information is extracted from the temporal fluctuations of a signal. In autocorrelation, a signal is correlated with itself at various lag times; in cross-correlation a signal is correlated with another signal, according to the formula:

$$G(\tau) = \frac{\langle \delta F(t) \delta G(t \pm \tau) \rangle}{\langle F(t) \rangle^2} \tag{3.1}$$

The cross-correlation function is indicative of the time scale at which the events in two signals are correlated. Other applications of cross-correlation analysis include cross-correlation laser scattering to measure rotational diffusion of asymmetric particles [22], and dual-focus fluorescence correlation spectroscopy. This dual-focus technique can accurately measure the flow speed and flow direction of a solution containing fluorescent molecules, by creating two focal volumes and then cross-correlating the fluorescence intensity fluctuations observed in these foci [23].

DCFCCS itself has been applied previously to studies on DNA, *e.g.* for recording DNA-DNA renaturation kinetics with two differently labelled complementary strands [19], for observing DNA-protein interactions [24], for monitoring PCR reactions using primers with different labels [25], and for high throughput screening of the activity of endonuclease enzymes [26, 27].

3.2 Results and discussion

3.2.1 Dual-colour fluorescence cross-correlation spectroscopy

A confocal microscope was equipped with two lasers, operating at 488 nm and 568 nm, and two avalanche photodiodes. On the excitation side, a dichroic mirror was installed that re-

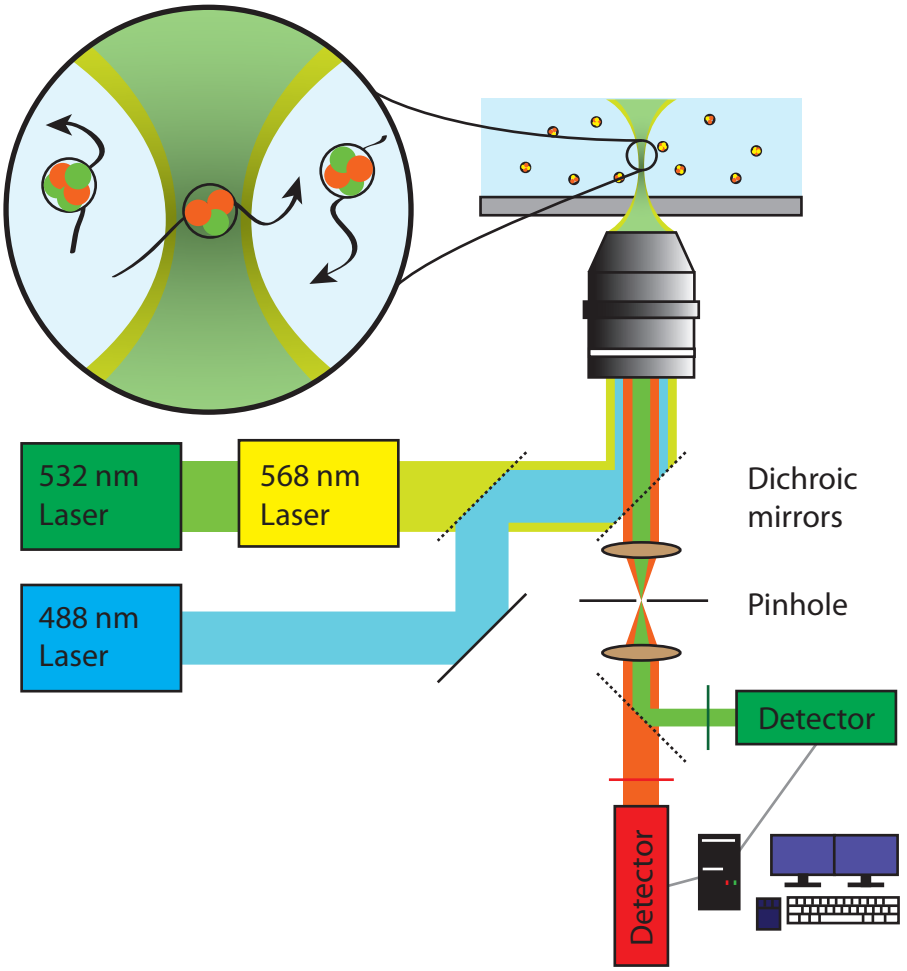

Figure 3.2: Dual colour fluorescence cross-correlation spectroscopy setup using a confocal microscope. Laser light of 488 nm excites a green fluorescent dye, while laser light of 568 nm excites a red fluorescent dye. The emitted green and red light are split by an additional dichroic mirror and filters, and subsequently sent to distinct detectors. In our setup, the laser light of 568 nm is generated by a dye laser pumped by light of 532 nm.

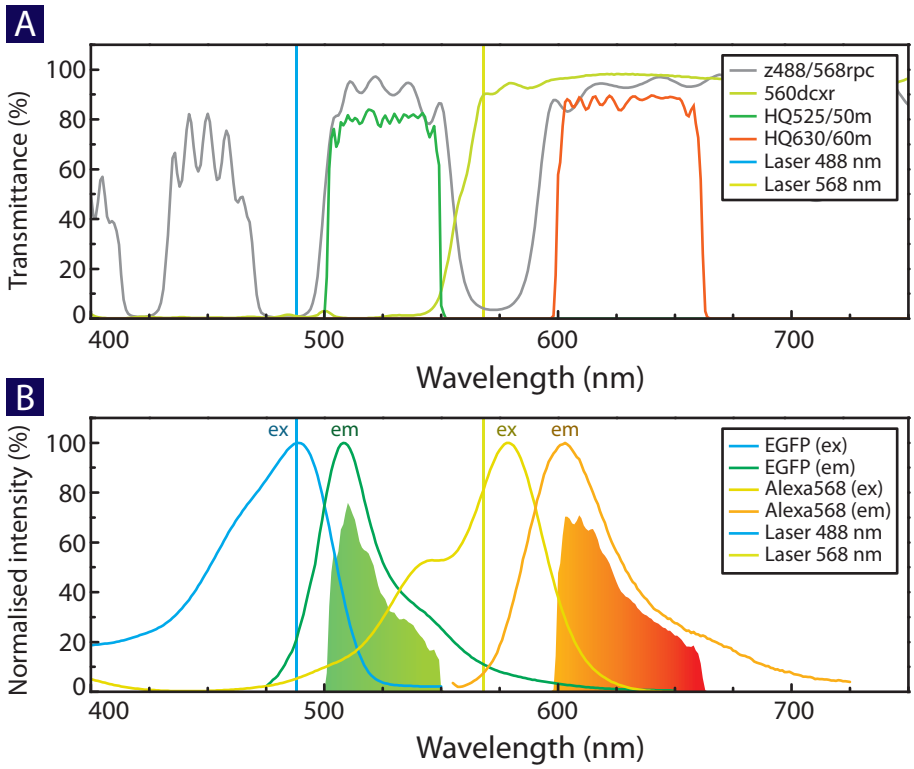

Figure 3.3: A) Transmittance spectra of the filter set components assembled for the two-colour fluorescence cross-correlation spectroscopy experiment. The confocal beam splitter (grey) transmits both laser lines (cyan and yellow-green). The collected fluorescent light is split by the detection beam splitter (green-yellow) and two filters (green and red) to attenuate any remaining laser light. B) Excitation (cyan) and emission (green) spectra of EGFP. Excitation (yellow) and emission (orange) spectra of Alexa Fluor® 568. The solid areas depict the spectral quantum efficiency of the detection—as determined by the filter set used—for each fluorophore. The excitation beam splitter that combines the laser lines is omitted for clarity.

flects light of 488 nm and transmits light of 568 nm. At the detection end, a second dichroic mirror was used to separate the fluorescent light from both fluorophores and sent each to its own detector. Each detector was fitted with an emission filter to attenuate any remaining laser light, as well as to block any light intended for the other channel. For an illustration of the beam paths see Figure 3.2 and for the spectra of the filter set see Figure 3.3A.

As a consequence of thermal motion, molecules in solution move randomly, colliding with one another. These small collisions occur frequently, but at any given moment the number of collisions a molecule—or larger particle—experiences from one side may deviate from the number of collisions from the other side. The net force results in the translation of that individual molecule. Since it was the botanist Robert Brown who for the first time described the above mentioned phenomenon for particles from pollen suspended in water, which he measured to be 7 μm [28], the term Brownian motion is most often used for larger particles, but Brownian motion effects particles of *any* size in liquids and gasses. The Brownian motion of many molecules together is called diffusion.

Since the diffusion of a molecule is akin to a random walk, the net displacement over time is proportional to the square root of the elapsed time, and it is more useful to express diffusion as the square of the distance moved in a given time t:

$$\langle x^2 \rangle = 2Dt \tag{3.2}$$

where $\langle x^2 \rangle$ is the average of the square of the distance, and D is the diffusion coefficient. The diffusion coefficient is a measure for the speed at which molecules translocate and depends on the temperature, the viscosity of the solution, and the hydrodynamic radius of the molecules. At a constant temperature and viscosity of the solution, the diffusion length of a molecule (of constant size) is determined only by the time. *Vice versa*, for a given observation volume—the focal volume of a microscope for instance—each molecule has a typical (average) time that it takes to diffuse through that volume. The diffusion time τ_D is a function of the diffusion coefficient and the size of the focus. The diffusion coefficient, of which some examples can be found in Figure 3.4, can be determined using the formula

$$D = \frac{s^2}{4\tau_D} \tag{3.3}$$

where s is the small radius of the observed prolate ellipsoid [29, p.803].

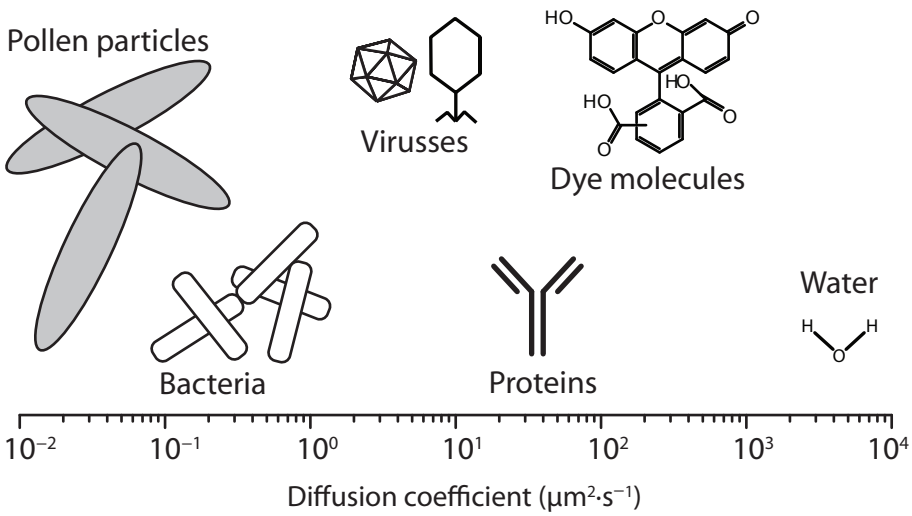

Figure 3.4: Length scale depicting objects ranging from pollen particles to small dye molecules. Fluorescence correlation spectroscopy (FCS) is often used for the determination of diffusion coefficients of particles like these.

To measure the diffusion time of a molecule, the autocorrelation function of a fluorescence intensity timetrace is calculated. The autocorrelation curve is then fitted with a model describing the diffusion. In a previous calibration of the focus of our confocal microscope, the ratio of axial to radial radii of the measurement volume was found to be 5:1 [30]. It has been previously found that for an elipsoid with a ratio of 4:1 (or more), the fit of the autocorrelation function with a 3D model is virtually indistinguishable [29, p.811] from that of a 2D model. In that case, the chance of a molecule diffusing out of the focal volume at the top or the bottom becomes so small as to be insignificant. It is therefore reasonable to fit our autocorrelation curves with the simple 2D model

$$G(t) = G(0)\frac{1}{(1+t/\tau)} \tag{3.4}$$

To calibrate our effective focal size, we measured the diffusion curve of EGFP at pH 7.5, which is plotted in Figure 3.5. Since the diffusion coefficient of the molecule is known

(95 $\mu m^2 \cdot s^{-1}$ at 25 °C [31]), the size of the effective focal volume could be directly calculated from the diffusion time of EGFP. The measured average diffusion time was found to be 505 µs. Using the Stokes-Einstein relationship $D = \frac{kT}{6\pi\eta R}$, we can correct for the fact that our experiment was conducted at 19 °C, which is a significant difference because the diffusion coefficient is dependent on the temperature—both in kT and in viscosity. At 19 °C, the diffusion coefficient for EGFP is then 80.7 $\mu m^2 \cdot s^{-1}$. Using this value we calculated our focus to be 404 nm wide, which is a realistic value, since it is only slightly larger than the 284 nm that can be expected for a focus that is determined by diffraction limited focussing of 568 nm laser light. It may be possible to approach the diffraction limit more closely by decreasing the size of the confocal pinhole or by fine-tuned filling of the back-aperture of the microscope objective.

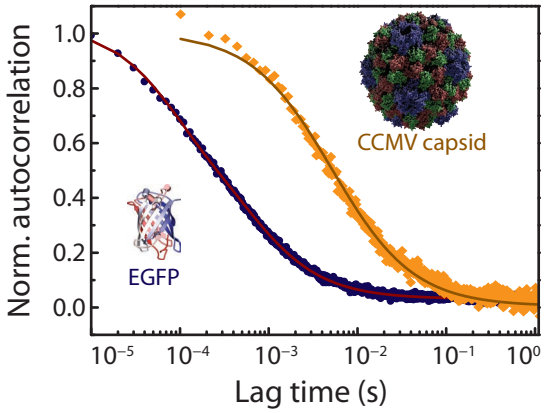

Figure 3.5: Diffusion curves of EGFP at pH 7.5 (left, blue) and of the CCMV capsid containing EGFP at pH 5.0 (right, orange).

The average diffusion time was also measured for the CCMV capsid and was found to be 6.0 ms. Using our previously calibrated radius of 404 nm, we obtain a diffusion coefficient of 6.8 $\mu m^2 \cdot s^{-1}$. According to the Stokes-Einstein relationship, this corresponds to a hydrodynamic radius of the capsid of 31.5 nm. This is in the size range of the capsid known from TEM images (28 nm).

In a similar fashion, we measured the diffusion constant of the free Alexa568 dye to which amounted to 113 $\mu m^2 \cdot s^{-1}$, corresponding to a hydrodynamic radius—or Stokes-Einstein radius—of 2 nm, which matches its molecular radius.

It should be noted that the Stokes-Einstein equation describes the diffusion of solid spherical objects that are much larger than the solvent molecules. For small molecules—such as Alexa568—the Stokes-Einstein radius is usually somewhat smaller than the molecular radius. The capsid is more than an order of magnitude larger and is also quite spherical, and as such its Stokes-Einstein radius matches its TEM radius quite closely.

3.2.2 Co-location of PalB and EGFP in the CCMV capsid

As a first test of the dual colour setup, it was used to look at the encapsulation of an enzyme (PalB) and a protein (EGFP) inside the empty capsid of CCMV. In this experiment, both PalB and EGFP were linked to the coat protein subunits via leucine zippers (see Section 3.1.1), and these subunits were assembled into the capsid. We wanted to know if both proteins would become entrapped together in individual capsids. EGFP was included in the capsid to measure the effect of crowding on the reaction rate of PalB in bulk experiments [32].

EGFP is naturally fluorescent but the second protein PalB is not. Therefore, PalB needed to be fluorescently labelled. The choice for this second fluorophore fell on Alexa Fluor® 568, because this dye has (i) the highest quantum yield (0.69) of all the readily available dyes in the 550–600 nm region [33], (ii) it is spectrally well separated from EGFP, and (iii) its excitation and emission wavelengths fit well with the used filter set. The fluorescence excitation and emission spectra for EGFP and Alexa568 are given in Figure 3.3B.

A buffered solution with capsids containing the EGFP and the PalB-Alexa568 complexes was put on the surface of a microscope cover slip's surface. As controls, different samples—containing capsids with only EGFP, capsids with only PalB-Alexa568, or a mixture of these two different capsids—were included. For each sample, the fluorescence intensity traces were cross-correlated to yield correlation curves, which were fitted with a simple diffusion model (see Figure 3.6). The curves are all normalized on the $G(0)$ parameter of the fit, and subsequently multiplied by the r-square of the fit for clarity. The capsids containing

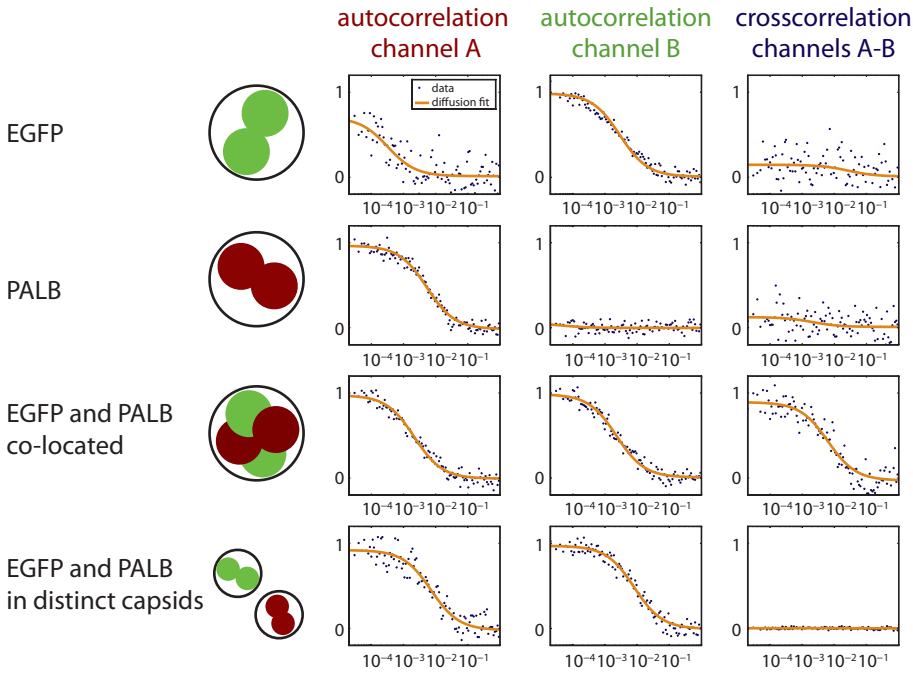

Figure 3.6: FCCS correlation curves of CCMV capsids containing EGFP (green circles), PalB (red circles) or both. When EGFP is encapsulated, there is correlation in the green channel B, when PalB is encapsulated there is correlation in the red channel A, but the cross-correlation arises only when both are present in the same capsid. Due to spectral overlap of EGFP and the Alexa Fluor® 568 dye at higher wavelengths, some of the emission of EGFP is recorded in the red channel, thereby causing some red channel autocorrelation even when the red dye Alexa568 is absent.

only PalB-Alexa568 emit in the region only visible to detector A (600–660 nm) and therefore only cause a signal in that detector. The sample with capsids containing EGFP emits mostly in the region visible to detector B (500–550 nm) and the diffusing capsids cause a correlation curve in channel B. Note (see Figure 3.3B) that there is a slight spectral overlap between the emission of EGFP and the detection region of detector A. There appears to be some photonic contamination, as there is a slight correlation visible in channel A, where—ideally—there should be none. In the sample where PalB and EGFP are encapsulated in the same capsid there is correlation in both channels, as well as in the cross channel, indicating that they are indeed co-located. As a control a mixture of the capsids containing only PalB-Alexa568 and capsids containing only EGFP was measured. In this control sample there is only autocorrelation in channel A (from the PalB-Alexa568 capsids) and autocorrelation in channel B (from the EGFP capsids), but no cross-correlation.

3.2.3 Activity of an enzyme in the CCMV capsid

For our experiment, we intended to study the conversion of the profluorescent substrate 5(6)-carboxyfluorescein diacetate, catalysed by PalB, as shown in Figures 3.7 and 3.8. The acetate groups are cleaved by the enzyme, and then the bonds in the rings rearrange to form a conjugated system. The resulting product molecule 5(6)-carboxyfluorescein is fluorescent. Since the enzyme itself is not fluorescent, the formation of the enzyme-product complex marks the only time in the reaction cycle that there is emission of fluorescence. Upon its release from the enzyme, the product molecule generally either photobleaches or diffuses into the bulk solution. A turnover cycle can therefore be identified by the appearance and vanishing of fluorescence.

After we had determined the diffusion coefficient of CCMV, we realised that in our setup, the diffusion time of virus capsids would probably be too short to see turnovers of PalB. The CCMV capsid takes on average 6 ms to diffuse through our focus. PalB has a k_{cat} of 4–16 s^{-1} for our substrate CFDA (see Chapters 4 and 6), meaning that—at saturated substrate condition—it takes 63–250 ms per turnover. The chance of seeing a turnover happening while a capsid with PalB is in our focus becomes quite small. In principle, it is possible to change the diffusion time by changing the viscosity of the solution or the size

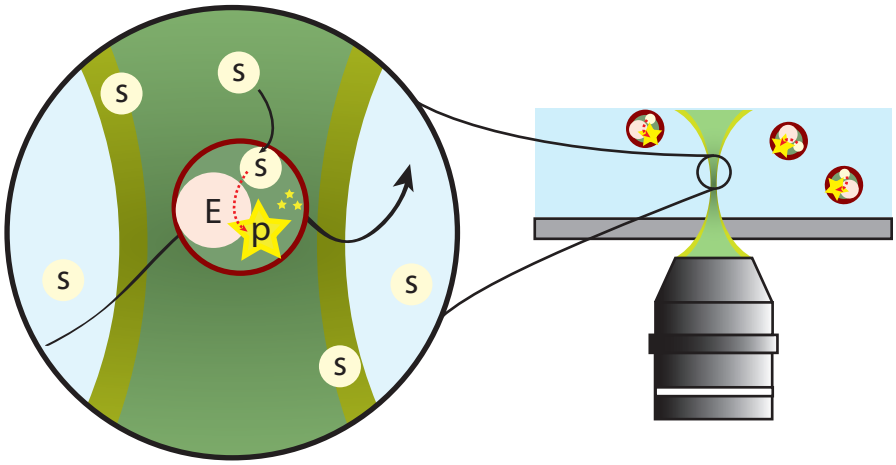

Figure 3.7: Alexa568-labelled CCMV capsids with enzyme inside diffuse through the focal volume. The enzyme (E) catalyses the reaction of a profluorescent substrate (s) to a fluorescent product (p).

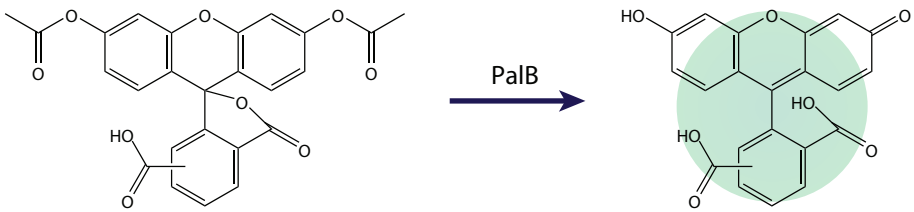

Figure 3.8: Conversion of 5(6)-carboxyfluorescein diacetate into the fluorescent carboxyfluorescein (ex. 492 nm, em. 517 nm) catalysed by PalB.

of the effective focal volume. The latter is done by increasing the size of the confocal pinhole, although the increased detection volume also brings proportionally more background noise from contaminations and from Raman scattering, rendering this approach virtually impractical. As it turned out, at that time, the dye laser became inoperative, regaining function only after the biological lifetime of our CCMV-PalB samples. It was therefore no longer possible to perform the planned experiments, since we could no longer excite the Alexa568 dye, and as a consequence we could not detect the passing of a CCMV capsid.

Since PalB turned out to be a suboptimal candidate, we switched to another enzyme-substrate combination that was available, *i.e.* horseradish peroxidase (HRP). The k_{cat} of HRP for the conversion of dihydrorhodamine by HRP was not precisely known in the literature; reported turnover numbers ranged from hundreds [34] to sixty million [35] molecules per second, depending on the substrate. Hence, we assumed that we would likely be able to record turnover numbers faster than the diffusion of the capsid.

We subsequently recorded fluorescence intensity timetraces of a mixture of the profluorescent substrate dihydrorhodamine 6G (D633) and Alexa568-labelled CCMV capsids containing HRP molecules. The autocorrelation data of the green channel—excited at 488 nm— fitted best to a diffusion model with an apparent diffusion time of 0.2 ms, corresponding to a diffusion coefficient of 200 $\mu m^2 \cdot s^{-1}$. It seems most likely that this number corresponds to the diffusion of free product molecules, as the diffusion coefficient of the virus is more than one order of magnitude slower. The literature reports that the lifetime of the enzyme-product complex, *i.e.* HRP-rhodamine 6G, is ~50 ms [36]. Hence, one turnover of the enzyme takes at the very least seven times longer than the diffusion of the CCMV capsid through the focus. We conclude, therefore, that PalB and HRP are too slow enzymes for observing their turnovers in a CCMV capsid freely diffusing in solution. In Chapter 5, we will show that it is possible to measure HRP enzyme activity in immobilised CCMV capsids.

3.2.4 Dissociation and assembly of the CCMV capsid influenced by pH

The CCMV capsid is known to reversibly dissociate into 180 protein subunits upon changing the pH of the solution from 5.0 to 7.5. An attempt was made to follow the disassembly

of the (large) capsid into (smaller) subunits with FCS. An excess of base was added to a weakly buffered solution containing fluorescently labelled CCMV capsids. The resulting timetrace was divided into two-second segments and the fluorescence intensity autocorrelation of each segment was calculated. The calculated diffusion time as a function of time is shown in Figure 3.9, together with the autocorrelation curves of two of the segments. There is a decrease in diffusion time, but this decrease is smaller than expected. Also, the diffusion time at the starting point is an order of magnitude smaller than was previously measured for the capsid. It is possible that the disassembly of the capsid occurs too rapidly for this technique to be accurately measured. The time resolution of this dataset could not be pushed beyond two-second intervals while maintaining satisfactory diffusion fits.

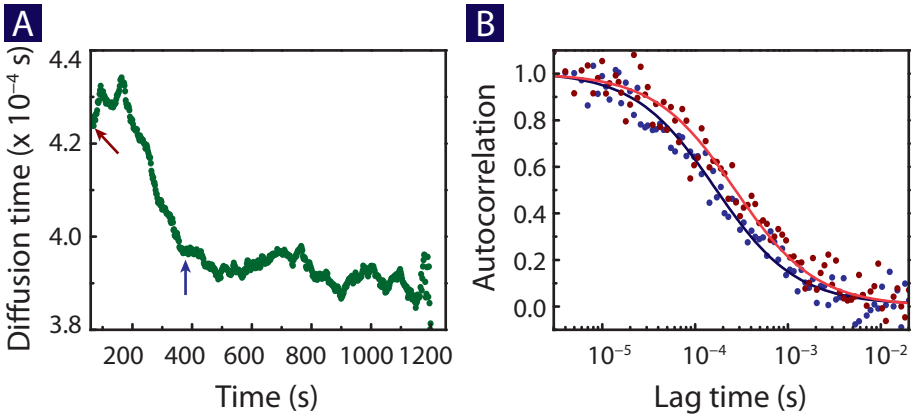

Figure 3.9: A) Evolution of the diffusion time during the dissociation experiment at two-second intervals (smoothed). The first minute is omitted while the solution settles from mixing and thermal convection. The arrows indicate the positions of the B) FCS curves at 82 s (red dots) and 384 s (blue dots) and their respective diffusion fits (red and blue lines).

An attempt to follow the reassembly of the coat proteins into the capsid was also undertaken. The pH of a solution containing the labelled coat protein dimers on the confocal microscope was lowered from 7.5 to 5.0 and subsequently the fluorescence intensity timetrace was recorded. The two-second segments were autocorrelated and the diffusion time was plotted over time. This plot can be found in Figure 3.10B. The diffusion time does

not seem to rise, apparently indicating that capsids did not form during the hour that the experiment ran. It is possible that the process takes longer. In fact, the standard protocol for reassembly of the capsid calls for the reaction to be left overnight. This is usually done because it is a convenient overnight break point in the (time-consuming) protocol, but perhaps the reaction may actually require such a long time to complete. In addition, we later realised that the negative results are probably caused by the difference in concentration. In the protocol for assembly in bulk solutions, the assembly is performed at concentrations in the order of 1 $mg \cdot ml^{-1}$, whereas in the confocal microscopy experiments the assembly was attempted at a concentration of 1 $ng \cdot ml^{-1}$. This ultralow concentration will make the rate of assembly very low. In retrospect, it would have been interesting to mix a low concentration—a concentration suitable for FCS—of fluorescently labelled coat proteins with the unlabelled coat protein at the concentration normally used for the assembly. In this way, most of the capsids would have been without a labelled protein, but the rate of assembly would not have been affected.

The long timetraces collected did, however, allow for a determination of the distribution of the diffusion coefficient of the coat protein dimers. The histogram of the fitted diffusion times is shown in Figure 3.10C. This histogram was fitted with a Gaussian function and from this curve, a diffusion time of 90 ± 17 μs and a diffusion coefficient of 451 $\mu m^2 \cdot s^{-1}$ were calculated. This is in excellent agreement with the diffusion time of 91 μs that was obtained from the autocorrelation curve of the entire trace. This autocorrelation curve is shown in Figure 3.10A.

The values for the diffusion time—obtained from fitting the autocorrelation curve of each 2 minute section—were autocorrelated themselves, yielding Figure 3.10D. As can be seen, there is no clear drop in the correlation function. However, there is some correlation up until circa the two minute lag time. This result may be explained by the occurrence of slow fluctuations in the laser power. Increased laser power—and hence increased excitation of the fluorescent molecules—increases the chance of the molecules being bleached while inside the focus of the microscope. A molecule that bleaches while diffusing through the focal volume is indistinguishable from a molecule that has just left that volume, and therefore its diffusion time will appear shorter.

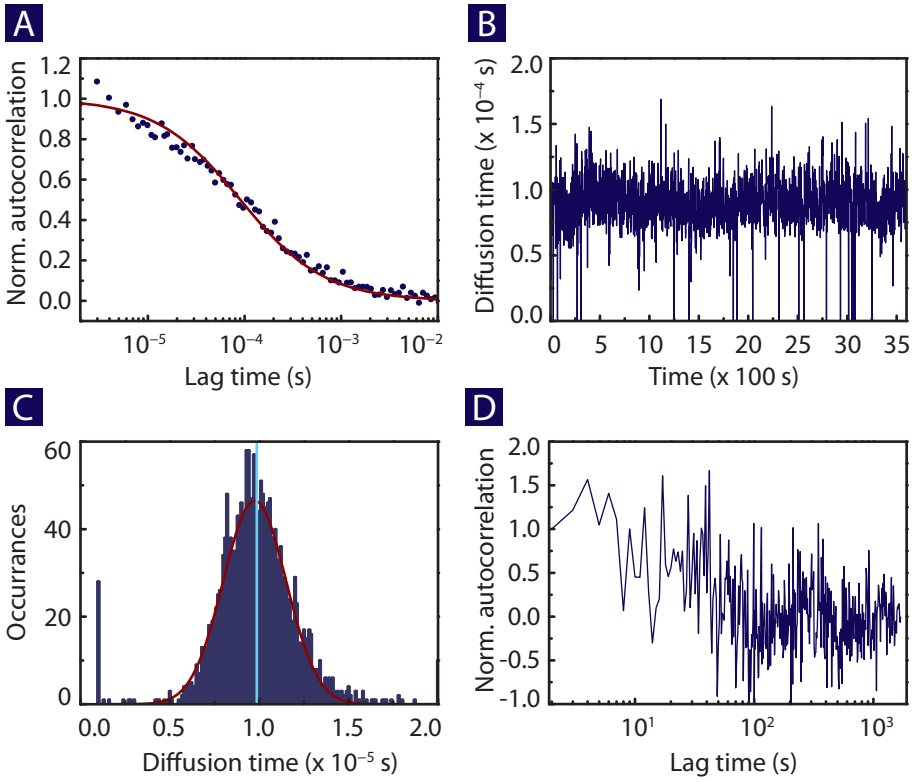

Figure 3.10: A) Normalised autocorrelation curve of the entire 1 hour trace for the assembly of the CCMV capsid. B) Evolution of the fitted diffusion time during the assembly of CCMV at two-second intervals. C) Histogram of the diffusion times, with Gaussian fit in red and the average value obtained by correlating the entire trace in cyan. D) Normalised autocorrelation of the diffusion times.

3.3 Conclusions

To observe single molecule activity of enzymes encapsulated in a virus capsid, our existing confocal microscope was extended with a second detection channel for dual-colour experiments. In the fluorescence correlation spectroscopy setup, the focal volume was calibrated with EGFP. With this calibration, the diffusion constant of the capsid was established to be

6.8 $\mu m^2 \cdot s^{-1}$. The calculated hydrodynamic radius of 31.5 nm is comparable to the 28 nm radius determined from TEM images. It would be interesting to measure the diffusion coefficient with different methods, for instance dynamic light scattering or gradient pulsed field NMR [37, 38], for comparison.

The successful co-location of an enzyme (PalB) and a protein (EGFP) in CCMV capsids was demonstrated by dual colour fluorescence cross-correlation spectroscopy. Individual turnovers of the enzymes PalB and HRP encapsulated in the capsid in solution could not be detected. Dissociation of CCMV capsid could not be followed by monitoring the diffusion time with FCS and we believe that this negative result is caused by the fact that the dissociation process is too fast for this technique. The (re)assembly of the capsid could not be seen, probably because the concentrations required for performing this experiments at the single capsid level make the reaction rate too slow. The disassembly and assembly experiments suggest that disassembly is fast and assembly is slow, and certainly seem to justify further experiments, which we have not been able to perform due to time constraints. For the disassembly experiment especially, a bulk technique such as NMR may be used as an alternative, as it can obtain a stronger signal with the same time resolution, so there is no need for the two-minute averaging.

3.4 Experimental

3.4.1 Two-colour fluorescence cross-correlation spectroscopy setup

Laser light of 488 nm (Spectra-Physics [Mountain View, CA, USA] 2080 argon ion laser) and 568 nm (Coherent [Santa Clara, CA, USA] CR-599 dye laser, by a 532 nm Spectra-Physics Millennia Nd:YAG laser), combined by means of a dichroic mirror (Chroma 530-DCLP), was coupled into a single-mode optical fibre (Thorlabs [Newton, NJ, USA] P1-460-FC-5), reflected by a dichroic beam splitter (Chroma [Bellows Falls, VT, USA] z488/568rpc) and focused onto the sample by an oil immersion 100x objective (Carl Zeiss [Jena, DE], NA = 1.30), which was mounted on a Carl Zeiss Axiovert 200 inverted microscope. Fluorescent light coming from the focal volume was collected by the same objective, passed through the dichroic beamsplitter, focused through a 100 mm pinhole, split by a second dichroic mirror (Chroma 560dcxr), filtered by either a 'red' (Chroma D630/50m) or 'green'

filter (Chroma HQ525/50m) and focused onto avalanche photodiodes (PerkinElmer [Waltham, MA, USA] SPCM-AQR-14). The photon count signals were recorded using a Picoquant [Berlin, DE] PicoHarp 300E TCSPC module or a general purpose data acquisition card (National Instruments [Austin, TX, USA] PCI-6036E). The autocorrelation and cross-correlation functions were calculated using Matlab (The MathWorks [Natick, MA, USA] 2010b) scripts developed in-house and fitted using the simplex search method from Lagarias *et al.* [39].

3.4.2 Timetrace recording and correlation

An avalanche photodiode generates electrical pulses that are recorded by a computer. Each pulse is tagged with its arrival time and put in a queue. In order to express the data as a practical intensity over time, some method of integration is needed. Therefore, the photon pulse data stream is divided into segments, and all the pulses in each segment are binned. The number of pulses per segment of time is the intensity.

Pulses—and therefore photons—are recorded via a data acquisition card (DAQ) by Labview software as counts against a 20 MHz clock, each count indicating a 50 ns increment of the interval between two pulses. The count is stored as a little-endian 32 bit unsigned integer in a data file. Simultaneously, a real-time monitor is implemented, displaying the number of each pulses that have arrived *per second* in an arbitrary interval, typically 2 ms. For the cross-correlation experiments, the DAQ could not keep up with the photon data streams from the two detectors, and therefore we recorded them by means of a time-correlated single photon counting (TCSPC) module.

Intensity timetraces are autocorrelated or cross-correlated offline, *i.e.* afterwards. The photon arrival times are binned (typically with a binsize of 1–10 μs) and the bins are then correlated at logarithmically increasing time lags to produce the correlation function.

3.4.3 Encapsulation of EGFP and PalB in the CCMV capsid

The encapsulation of EGFP and PalB in CCMV has been described extensively elsewhere [1] but to briefly illustrate the process: The leucine zipper coil was expressed in *E. coli* as a fusion protein with EGFP, PalB or the coat protein (CP). Since the proteins had an

N-terminal his-tag, purification could be performed with standard Ni^{2+}-NTA chromatography. The PalB-leucine zipper fusion protein was labelled with Alexa Fluor® 568-NHS ester. The different leucine-zipper-fusion proteins were subsequently brought together to form the heterodimeric EGFP-CP and PalB-CP complexes. These complexes were then mixed with the wild-type coat protein in pH 7.5 buffer. The pH was lowered to 5.0 with dialysis, upon which the coat proteins assemble into the capsid, encapsulating the fused proteins EGFP and PalB inside. Buffers used: Capsid buffer pH 5.0: 0.5 M NaCl, 0.05 M $NaCH_3COOH$, 0.01 M $MgCl_2$ and 0.001 M EDTA, the pH is set with HCl. Capsid buffer pH 7.5: 0.5 M NaCl, 0.05 M Tris-HCl, 0.01 M $MgCl_2$ and 0.001 M EDTA, the pH is set with HCl.

3.4.4 Activity of an enzyme in the CCMV capsid

The focus of the confocal microscope was positioned in 180 µl of a buffered solution of CCMV capsids containing PalB, labelled with Alexa568. To this solution, 20 µl of a 10 µM solution of 5(6)-carboxyfluorescein diacetate (CFDA) was added, giving a final concentration of 1 µM.

3.4.5 Co-location of PalB and EGFP in the CCMV capsid

The focal volume was positioned in 500 µl of a buffered solution of CCMV capsids containing EGFP, PalB or both. EGFP is autofluorescent and is excited at 488 nm, while the PalB was labelled with an Alexa568 dye which is excited at 568 nm. Emission of both fluorophores was filtered and recorded by separate photodetectors. Autocorrelation and cross-correlation curves were calculated using Matlab. The curves were normalised on the G(0) parameter and then multiplied by the r-square of the fit for clarity.

3.4.6 Dissociation and assembly of the CCMV capsid influenced by pH

For the dissociation experiment, 500 µl of capsid buffer pH 5.0 containing Alexa Fluor® 488-labelled capsids was placed onto the confocal microscope. The fluorophores were excited with a single laser light source at 488 nm. A single channel was used for detection of the

emitted light. At the start of the 1 hour measurement, 100 µl of an aqueous 1 M NaOH solution was added, and the solutions was vigorously mixed with a pipette. Autocorrelation curves were calculated and fitted using Matlab.

For assembly, 50 µl of capsid buffer pH 7.5 containing the coat protein dimers was mixed with 450 µl of capsid buffer pH 5.0 on the confocal microscope, after which a fluorescence trime trace was recorded for 1 h. Autocorrelation curves and histogram were calculated and fitted with the 2D diffusion model using Matlab.

3.5 References and notes

[1] I. J. Minten, V. I. Claessen, K. Blank, A. E. Rowan, R. J. M. Nolte, J. J. L. M. Cornelissen, *Chemical Science* **2011**, 2, 358–362, doi: 10.1039/C0SC00407C.

[2] P. Lu, L. Xun, S. Xie, *Science* **1998**, 282(5395), 1877–1882, doi: 10.1126/science.282.5395.1877.

[3] L. Edman, Z. Földes-Papp, S. Wennmalm, R. Rigler, *Chemical Physics* **1999**, 247(1), 11–22, doi: 10.1016/S0301-0104(99)00098-1.

[4] U. Kubitscheck, O. Kückmann, T. Kues, R. Peters, *Biophysical Journal* **2000**, 78(4), 2170–2179, doi: 10.1016/S0006-3495(00)76764-6.

[5] J. A. Speir, M. Sanjeev, G. Wang, T. S. Baker, J. E. Johnson, *Structure* **1995**, 3(1), 63–78, doi: 10.1016/S0969-2126(01)00135-6.

[6] L. Lavelle, J.-P. Michel, M. Gingery, *Journal of Virological Methods* **2007**, 146(1-2), 311–316, doi: 10.1016/j.jviromet.2007.07.020.

[7] J. B. Bancroft, E. Hiebert, *Virology* **1967**, 32(2), 354–356, doi: 10.1016/0042-6822(67)90284-X.

[8] B. J. M. Verduin, *FEBS Letters* **1974**, 45(1-2), 50–54, doi: 10.1016/0014-5793(74)80808-2.

[9] D. L. McClain, H. L. Woods, M. G. Oakley, *Journal of the American Chemical Society* **2001**, 123(13), 3151–3152, doi: 10.1021/ja004099l.

[10] T. Boekhout, *Journal of General and Applied Microbiology* **1995**, 41(4), 359–366, doi: 10.2323/jgam.41.359.

[11] S. Goto, J. Sugiyama, H. Iizuka, *Mycologia* **1969**, 61(4), 748–774.

[12] J. Uppenberg, M. T. Hansen, S. Patkar, T. A. Jones, *Structure* **1994**, 2(4), 293–308, doi: 10.1016/S0969-2126(00)00031-9.

[13] P. Domínguez de María, C. Carboni-Oerlemans, B. Tuin, G. Bargeman, A. van der Meer, R. van Gemert, *Journal of Molecular Catalysis B: Enzymatic* **2005**, 37(1–6),

36–46, doi: 10.1016/j.molcatb.2005.09.001.

[14] US7473791, **2009**.

[15] JP2002101847, **2002**.

[16] N. Miletić, V. Abetz, K. Ebert, K. Loos, *Macromolecular Rapid Communications* **2010**, 31(1), 71–74, doi: 10.1002/marc.200900497.

[17] K. R. Siemering, R. Golbik, R. Sever, J. Haseloff, *Current Biology* **1996**, 6(12), 1653–1663, doi: 10.1016/S0960-9822(02)70789-6.

[18] M. Eigen, R. Rigler, *Proceedings of The National Academy of Sciences* **1994**, 91, 5740–5747, doi: 10.1073/pnas.91.13.5740.

[19] P. Schwille, F. Meyer-Almes, R. Rigler, *Biophysical Journal* **1997**, 72(4), 1878–1886, doi: 10.1016/S0006-3495(97)78833-7.

[20] Z. Földes-Papp, *Experimental and Molecular Pathology* **2007**, 82(2), 147–155, doi: 10.1016/j.yexmp.2006.12.002.

[21] T. Förster, *Annalen der Physik* **1948**, 437(1-2), 55–75, doi: 10.1002/andp.19484370105.

[22] Z. Kam, R. Rigler, *Biophysical Journal* **1982**, 39(1), 7–13.

[23] T. J. Arbour, J. Enderlein, *Lab Chip* **2010**, 10, 1286–1292, doi: 10.1039/B924594D.

[24] K. Rippe, *Biochemistry* **2000**, 39(9), 2131–2139, doi: 10.1021/bi9922190.

[25] R. Rigler, Z. Földes-Papp, F.-J. Meyer-Almes, C. Sammet, M. Völcker, A. Schnetz, *Journal of Biotechnology* **1998**, 63(2), 97–109, doi: 10.1016/S0168-1656(98)00079-0.

[26] U. Kettling, A. Koltermann, P. Schwille, M. Eigen, *Proceedings of the National Academy of Sciences* **1998**, 95(4), 1416–1420.

[27] A. Koltermann, U. Kettling, J. Bieschke, T. Winkler, M. Eigen, *Proceedings of the National Academy of Sciences* **1998**, 95(4), 1421–1426.

[28] R. Brown, *Philosophical Magazine* **1928**, 4, 161–173.

[29] J. Lakowicz, *Principles of Fluorescence Spectroscopy*, 2nd edition, Kluwer Academic/Plenum Publishers, **1999**, ISBN 0387312781.

[30] H. Engelkamp: unpublished data.

[31] Z. Petrásek, P. Schwille, *Biophysical Journal* **2008**, 94(4), 1437–1448, doi: 10.1529/biophysj.107.108811.

[32] I. J. Minten, Ph.D. thesis, Radboud Universiteit Nijmegen, **2010**, ISBN 9789090259260.

[33] I. Johnson, M. T. Spence (editors), *Molecular Probes Handbook, A Guide to Fluorescent Probes and Labeling Technologies*, 11th edition, Invitrogen Life Science, **2010**,

ISBN 9780982927915.

[34] N. Mogharrab, H. Ghourchian, M. Amininasab, *Biophysical Journal* **2007**, 92(4), 1192–1203, doi: 10.1529/biophysj.106.092858.

[35] R. K. Sharma, S. Das, A. Maitra, *Journal of Colloid and Interface Science* **2005**, 284(1), 358–361, doi: 10.1016/j.jcis.2004.10.006.

[36] L. Edman, R. Rigler, *Proceedings of the National Academy of Sciences of the United States of America* **2000**, 97(15), 8266–8271.

[37] W. S. Price, *Gradient NMR*, volume 32 of *Annual Reports on NMR Spectroscopy*, Academic Press, **1996**, doi: 10.1016/S0066-4103(08)60078-2.

[38] P. Stilbs, *Analytical Chemistry* **1981**, 53(13), 2135–2137, doi: 10.1021/ac00236a044.

[39] J. C. Lagarias, J. A. Reeds, M. H. Wright, P. E. Wright, *SIAM Journal on Optimization* **1998**, 9(1), 112–147, doi: 10.1137/S1052623496303470.

Chapter 4

Bound to work

single PalB molecules on a surface

4.1 Introduction

In the previous chapter, we concluded that we could not measure the kinetics of the enzyme PalB in solution at the single molecule level, mainly because it diffuses too fast to observe it for the amount of time it takes to complete one reaction cycle, even if the rate of diffusion was decreased by making the enzyme bigger. As discussed in Chapter 2, many early experiments were carried out successfully on a surface. Since our ultimate aim is to study the effects of parameters such as pH and temperature on the enzyme kinetics of a single enzyme, we therefore decided to return to the immobilisation of PalB enzymes on a glass surface. Active enzymes were not found in earlier experiments [1] in which PalB was immobilised in agarose and polyacrylamide gels. But when PalB was deposited on a hydrophobised glass surface, a few molecules were found to be active in catalysing the reaction of the prefluorescent substrate 2N,7N-bis-(2-carboxyethyl)-5-(and-6)-carboxyfluorescein acetoxymethyl (BCECF-AM) ester to the fluorescent product BCECF. In the previous chapter, the substrate carboxyfluorescein diacetate (CFDA) was introduced. CFDA has several advantages over BCECF. Both dyes are pH sensitive at near-neutral pH, but BCECF much more so than carboxyfluorescein—the product of CFDA conversion by PalB. Eventually, we would like to investigate the effect of environmental parameters, such as pH, on

the activity of single enzyme molecules. Such experiments are, of course, facilitated by pH stable dyes. Additionally, carboxyfluorescein has a slightly higher quantum yield (0.93 vs 0.84) as well as a higher molar extinction coefficient (71000 vs 55000 $M^{-1} \cdot cm^{-1}$) [2, 3], making it the more efficient fluorescent dye of the two. The k_{cat} of PalB for BCECF has been reported to be as low as 0.001 s^{-1} [4], and it was also hoped that the conversion of CFDA would be faster. As mentioned before, PalB catalyses the reaction that is shown

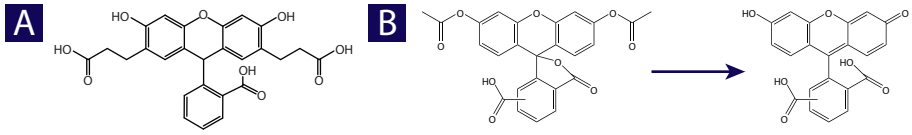

Figure 4.1: A) The pH-sensitive fluorescent dye 2'-7'-bis(carboxyethyl)-5(6)-carboxyfluorescein (BCECF) that was previously used as a substrate for PalB. B) The reaction of the non-fluorescent 5(6)-carboxyfluorescein diacetate (CFDA) to the fluorescent dye 5(6)-carboxyfluorescein.

in Figure 4.1. The reaction can be followed because of the carefully chosen substrate that is converted into a fluorescent product. Under illumination, the reaction cycle therefore produces alternating periods of fluorescence and caliginosity. The fluorescence emanating from a single enzyme molecule is therefore 'on' or 'off', depending on the position in the reaction cycle (see Equation 4.1).

$$\underbrace{E+S \rightarrow ES}_{\text{'off'}} \rightarrow \underbrace{EP \rightarrow E+P}_{\text{'on'}} \tag{4.1}$$

The time that the complex spends in the 'off' state—the off-time—is related to the time it takes the enzyme molecule to bind a substrate molecule and convert it into a product molecule. The time that the emission is 'on'—the on-time—corresponds to the time that the fluorescent product molecule is bound to the enzyme and, additionally, the time it takes to diffuse out of the focus of the microscope. The sum of off-times and on-times is inversely proportional to the turnover rate of the enzyme [5].

In this chapter, PalB was immobilized on a microscope glass by means of two different methods (see Figure 4.2), firstly directly onto a hydrophobic glass surface and secondly via

the leucine zipper that was introduced in Chapter 3. In the experimental section, at the end of the chapter, improvements on the image quality of our microscope are discussed.

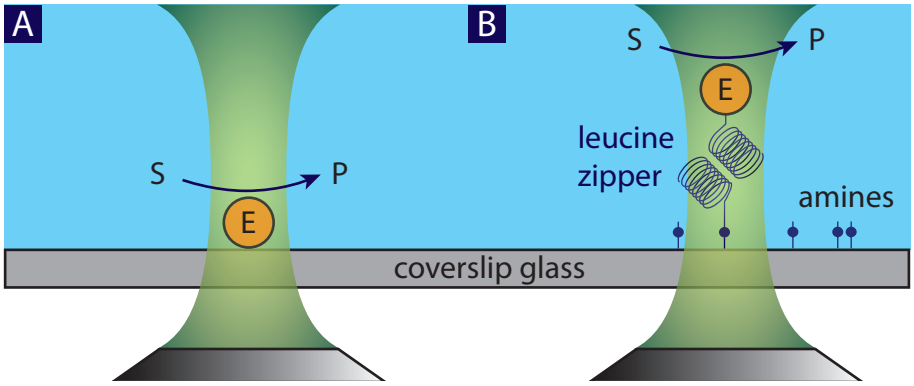

Figure 4.2: A) Enzyme molecule E immobilised directly on a glass cover slip, where it catalyses the reaction of substrate S to product P. B) Enzyme molecule co-expressed with a leucine zipper coil and immobilised via the complimentary leucine zipper coil that is attached via a linker molecule to an amine-functionalised glass surface.

4.2 Results and discussion

4.2.1 Glass preparation

In single molecule–experiments it is of the utmost importance to ensure that fluorescent contaminations are avoided. That being said, for experiments in which the focus is in the solution, a few fluorescent molecules on the surface of the sample need not be an insurmountable obstacle, provided that they stick well and do not diffuse through the focus. However, those molecules are exactly the ones one wants to avoid when scanning the surface in search of fluorescent enzyme molecules. The importance of clean glass, therefore, cannot be overstated. The amount of fluorescent molecules on each glass coverslip varies greatly between batches, but fluorescent contaminations are observed without exception. Therefore, to make sure that all fluorescent molecules are photobleached, the surface of our

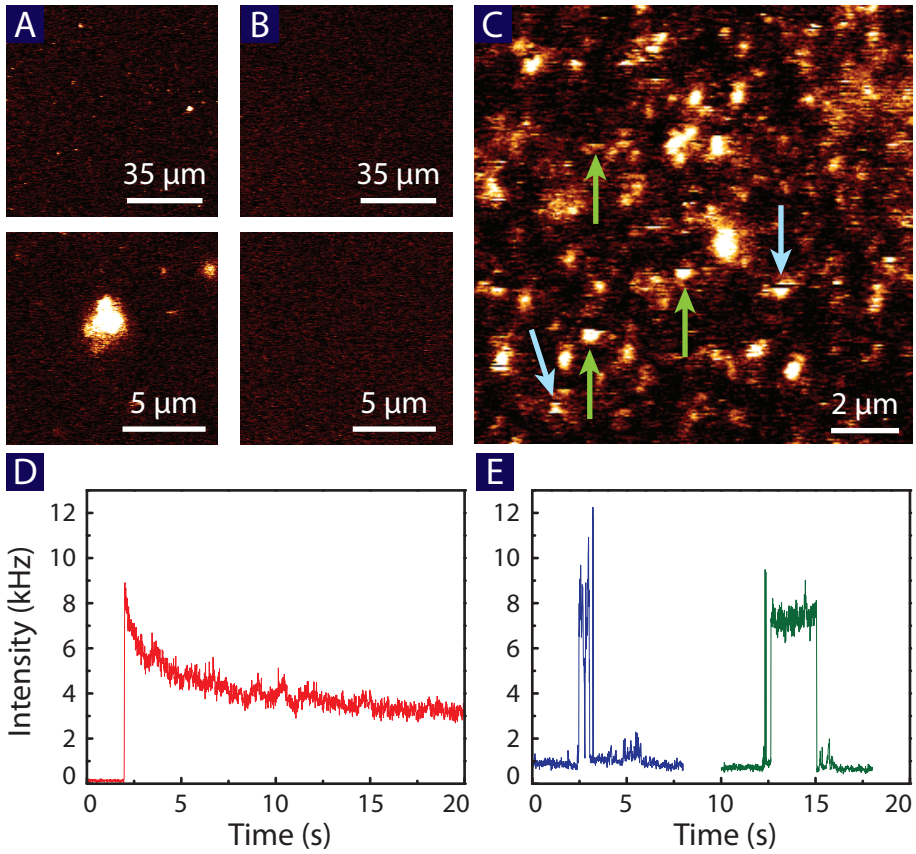

Figure 4.3: Confocal microscopy images of A) untreated glass 100×100 µm^2 (top) and 12.8×12.8 µm^2 (bottom) B) cleaned glass. The laser power in B is significantly higher than in A, and yet there is a complete lack of fluorescence in B. C) Cleaned glass with a sample of rhodamine 6G molecules. The upwards pointing green arrows show examples of molecules that bleached during the scanning of the image. The downwards pointing blue arrows show molecules that blinked during the scanning of the image. D) Fluorescence intensity timetrace of the big spot in A. Its exponential decay is evident, and indicates that there are many fluorescent molecules in this spot. E) Timetraces of spots in C, taken at significantly higher laser power than the timetrace in D. The background signal shown in the first few seconds of the trace is higher than in D and, after the laser is repositioned onto a spot, distinct single steps are apparent in the intensity as a result of single molecule bleaching.

coverslip glass was exposed to a combination of intense ultraviolet radiation and ozone in a UV-photocleaner. Figure 4.3 shows a comparison between cleaned and untreated glass.

4.2.2 Detecting the activity of single PalB molecules on a surface

In previous experiments [1], fluorescent spots appeared on the surface after the addition of BCECF, revealing the location of the individual enzyme molecules. However, after the addition of CFDA as a substrate, no fluorescent spots were observed, and thus the PalB molecules could not be located in this way.

In a typical experiment, with a timetrace binned with a bin size of 2 ms, the background intensity would be 2 counts per bin (1 kHz), whereas a spike would contain 20 counts per bin (10 kHz). If we assume that an enzyme performs 4 turnovers·s^{-1} with an average on-time of 10 ms, one will observe a signal of 4×5×20+480×2=1360 photons·s^{-1} at the site of an enzyme molecule, and a signal of 2×500=1000 photons·s^{-1} where there is none. The difference between 1000 and 1360 photons·s^{-1} is not large enough to provide sufficient contrast between enzyme and background during the scanning of an image. In another attempt to distinguish background fluorescence from fluorescence originating from enzymatic activity, one may try to use the fact that for the background fluorescence the variance of the intensity is equal to its mean due to its stochastic nature, whereas for a fluctuating signal the variance is always larger. This, however, requires long measurement times to attain a statistically significant dataset for each point in the sample, which conflicts with the concept of rapid survey of a sample.

The current thoughts on the previous success are that the fluorescent product BCECF may non-specifically absorb to PalB, possibly due to the highly (−4–5) negatively charged nature of the product around pH 7–8 [6] and the existence of positively charged amino acid residues on the surface of PalB [7]. The enzymes subsequently become visible in confocal microscopy scans by the emission of the lingering product molecules. Carboxyfluorescein (the hydrolysis product of CFDA) is only weakly charged at pH 7 (−0–1) and apparently does not absorb to PalB molecules, and therefore the enzymes could not be localised in this way.

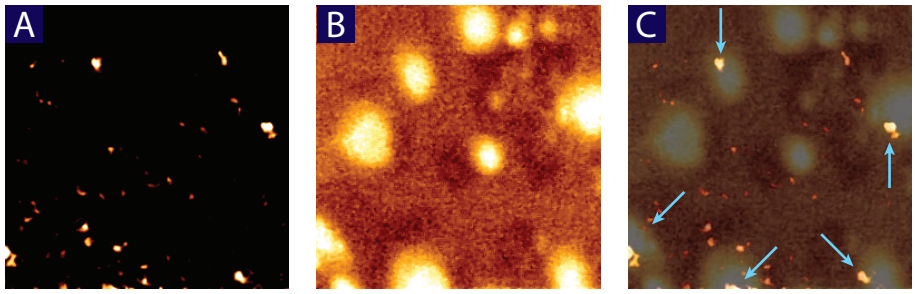

Figure 4.4: $25.6 \times 25.6\ \mu m^2$ Confocal fluorescence images of Alexa488-labelled PalB enzyme molecules adsorbed on a hydrophobic surface. A) Labelled enzyme molecules at the start of the experiment. B) Product accumulation after six hours. C) The two images have been superimposed showing that product accumulation is localised near the position of the enzyme molecules.

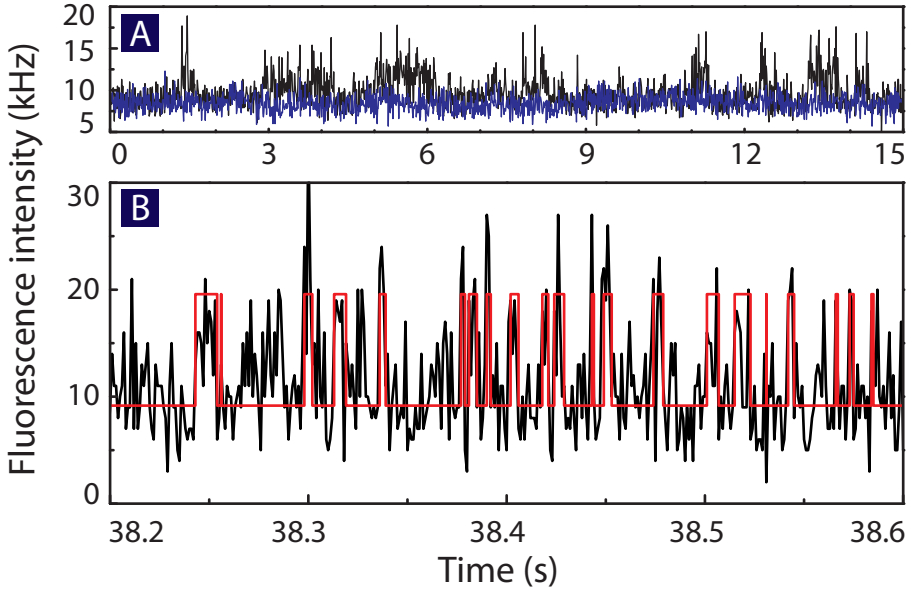

Figure 4.5: A) Comparison of fluorescence intensity traces taken in the background (blue line) and on a spot (black line). B) Comparison of the timetrace binned at 1 ms (black line) with the binary levels generated with the change point algorithm from [8] (red line).

Since we cannot increase the reaction rate of the enzyme in order for it to generate product molecules faster, PalB was labelled with the fluorescent label Alexa Fluor® 488. In this way, we were able to locate the enzyme molecules on the glass surface by the fluorescence of their labels (See Figure 4.4). When the focus was subsequently placed on the fluorescent spots, we observed for several of them fluctuations in the fluorescence intensity over time (see Figure 4.5). Similar fluctuations were not observed at non-fluorescent locations on the surface.

After waiting six hours, big fluorescent spots had appeared, and the background fluorescence had increased as well. Figure 4.4C shows that these larger spots often correlate with the location of the fluorescent labels that were observed earlier, and that some spots appeared where there was no label before. Since these large spots were not observed in a control sample without enzyme molecules, we attributed the large spots to enzyme activity. There is probably a significant amount of enzyme molecules that are unlabelled and therefore invisible, and those enzymes may have also been present on the surface. Alternatively, enzyme molecules may have adsorbed on the locations of the large spots after the initial scan at the start of the experiment.

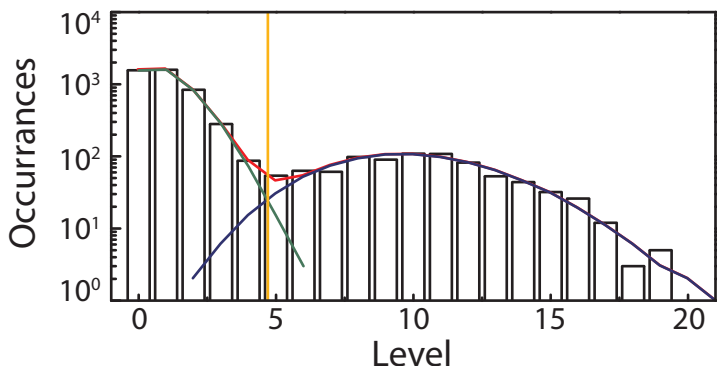

Figure 4.6: Histogram of the simulated intensity timetrace shown before in Figure 2.3 (black bars) fitted with two Poisson distributions (green line for the background or 'off' level, blue line for the spikes or 'on' level, red line is the sum of the two levels). The orange line indicates the statistically best value for placement of the threshold level.

The simplest method of converting fluorescence intensity timetraces to binary trajectories is by binning the data and subsequently introducing a threshold level to the trace. Points below the threshold are declared to be 'off' and points above the threshold to be 'on', the change points occurring where the intensity crosses the threshold level. This is adequate for traces with high signal-to-noise ratios, where the levels are well separated. However, in the case of traces with suboptimal signal-to-noise ratios, the levels are not well separated and the choice of a bin size starts to become more important. A larger bin sizes leads to increased separation between the levels at the cost of decreased time resolution. However, at the time resolution desired in typical single molecule experiments, the levels are not easily separated by means of a threshold. Theoretically, the best position for a threshold level is at the intersection between the levels. The most accurate position is easily obtained by fitting the levels with Poisson distributions (see Figure 4.6). However, the Poisson noise in the traces introduces many false positives and false negatives, as fast true transitions are overlooked because they are shorter than the bin size—and hence, averaged out—and random fluctuations are mistaken for false transitions. Furthermore, any increase in background fluorescence in time—such as originating from the accumulation of fluorescent product molecules in the sample—intensifies the amalgamation of the levels. It should be noted that the contribution of the fluorescence of free product molecules cannot be attenuated by means of spectral filters, unlike the broader background contributions from *e.g.* the Raman scattering of water.

Figure 4.7 shows plots of typical segments of an enzymatic timetrace at several bin sizes, on a long and a shorter time scale. For the longer trace, the corresponding histograms at each bin size are shown in Figure 4.8. In the histogram for a bin size of 50 ms, the two levels appear completely separated, however from the timetrace itself (see Figure 4.7) it is clear that the loss in time resolution is prodigious. At the same time, the probability that such a large bin contains only one specific level is very low. As the bin size decreases, the levels become increasingly overlapping, while the time resolution improves concurrently. There exists, therefore, an inevitable trade-off between bin size—time resolution—and the separation of the levels and it seems that the choice of the bin size is therefore rather arbitrary. Threshold analysis, however, is not the only method of extracting the desired data from the photon stream. There is another *viz.* change point analysis, which has been tailored by

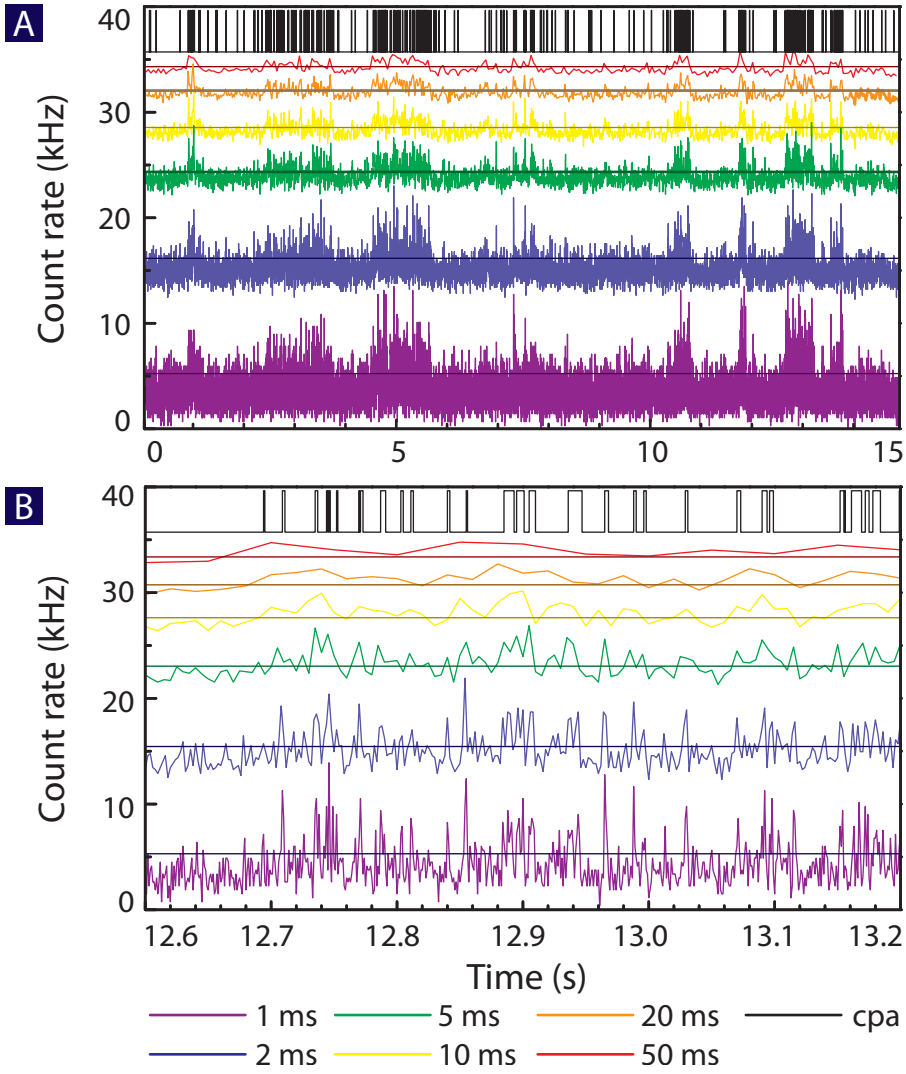

Figure 4.7: Comparison of methods of conversion of time traces to binary trajectories for A) long and B) shorter time scales. Time traces are shown stacked and binned at different bin sizes. The optimal threshold for separating two Poisson levels is indicated for each trace. The binary trace from the change point algorithm (cpa) is shown in black at the top of the figure.

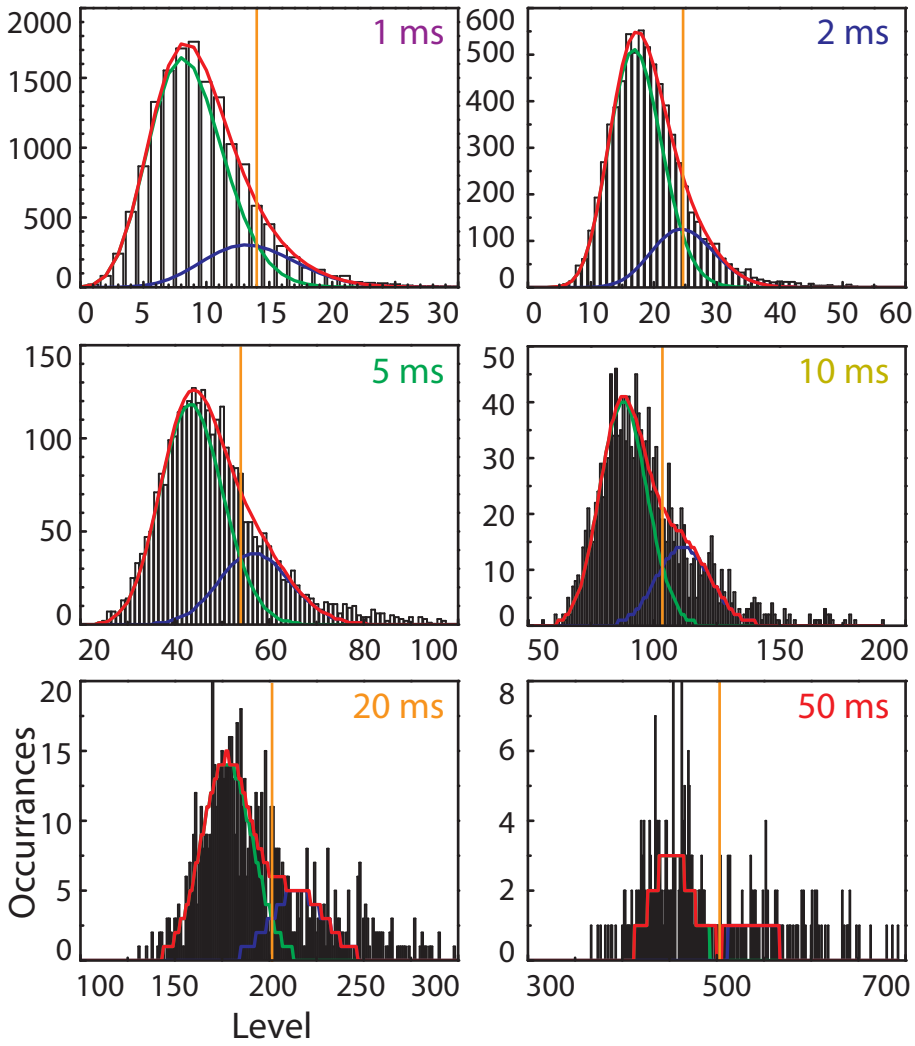

Figure 4.8: Histograms of the binned traces shown in Figure 4.7. The best fits for two Poisson levels (green and blue lines) are given, as well as the sum of the two (red lines) and the intercept of both levels, *i.e.* the threshold level (orange line).

the Haw Yang group at Berkeley (currently Princeton) for use in single molecule experiments [8]. In this method, change points between on and off periods are not determined by the crossing of the intensity with a predetermined threshold, but rather by determining where the change points are statistically most likely to occur. Since the algorithm is based directly on the inter-photon times, no binning is required. The algorithm recursively searches for the photon points where the trace switches from high to low levels and *vice versa*, which in our system corresponds directly with the 'on' and 'off' levels.

Using the Haw Yang implementation of the change point analysis algorithm, a representative fluorescence intensity timetrace, taken of a single PalB molecule, was found to contain 24749 events in 25 minutes, as indicated by the change points that were found. The following analysis and the corresponding Figures 4.9–4.11 relate to these events. The enzyme was found to work at an average turnover rate of 16 s^{-1}. No values have been reported for the reaction rate of PalB for this substrate, but PalB converts the somewhat similar dye BCECF at a rate of 4 s^{-1}, therefore this new rate does not seem to be implausible. With the levels determined, the offtimes and the ontimes were subsequently extracted (see Figure 4.9AB). Upon examination of the offtimes, it becomes apparent that they are clustered. Long offtimes and short offtimes occur in—separate—groups. The histogram of the ontimes and offtimes in Figure 4.9C shows an plethora of short offtimes, and since the histogram cannot, therefore, be fitted with a single exponential function, we conclude that the enzyme does not have a single reaction rate. The autocorrelation analysis of the offtimes in Figure 4.10 reveals that there is correlation up to ca. 20 events.

The overabundance of short offtimes brings to mind the memory effect that was used to explain similar results originally by Lu *et al.* [9] for cholesterol oxidase and more recently by Flomenbom *et al.* for PalB [2, 10].

To see if there are trends in the turnover times, 2D histograms were constructed of the time between n turnovers (see Figure 4.11). These histograms plot, on logarithmic time scales, the probability distribution $P(t(i),t(i+n))$ for the correlation between events spaced n turnovers apart, corrected by subtraction of the chance $P(t(i))P(t(i+n))$, yielding the difference distribution of turnover times [11, 12]. The diagonal feature, present in the figure showing the data for $n=1$, indicates that short turnover times are more often followed by short waiting times than would be expected. Similarly, long turnovers are more often fol-

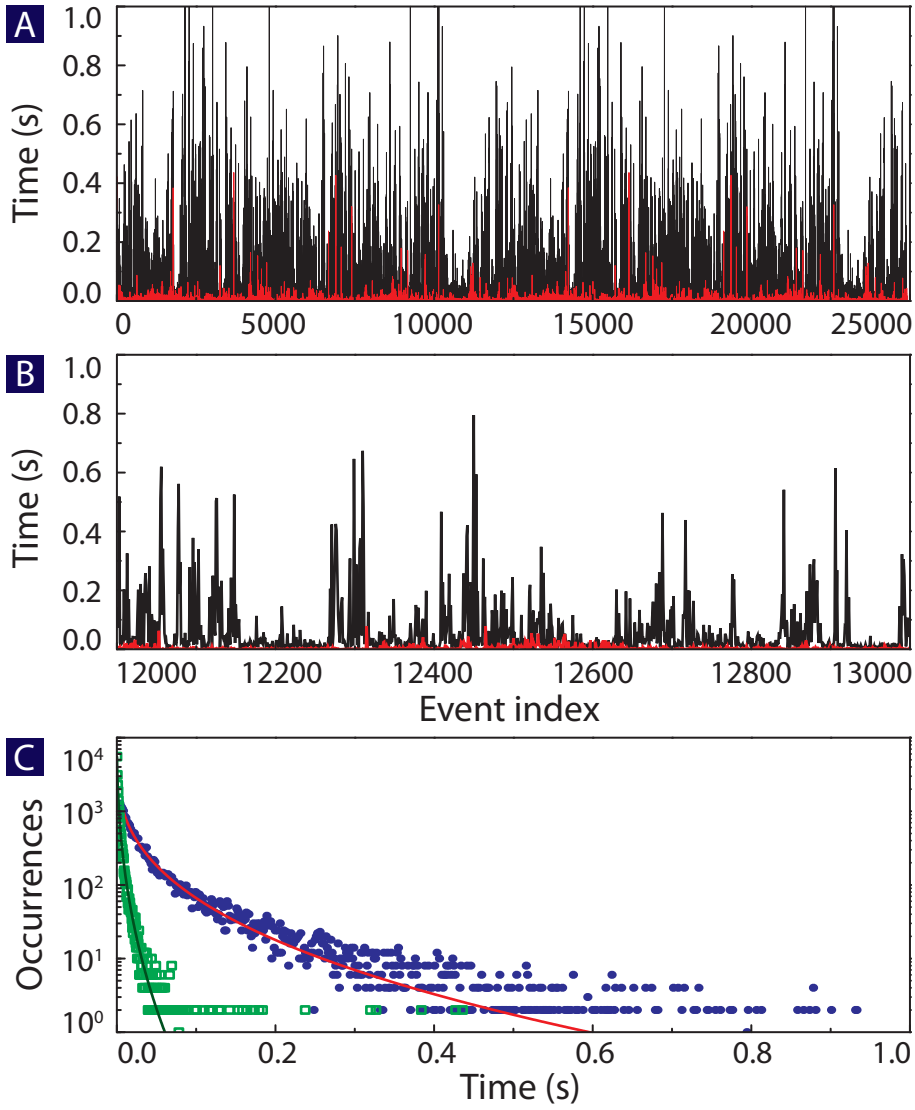

Figure 4.9: A) and B) Offtimes (black) and ontimes (red) for a single PalB enzyme molecule generated using the change point algorithm. C) Histogram of the offtimes (blue dots) and ontimes (green squares). Both histograms are fitted with a stretched exponential (solid red line for the offtimes, solid green line for the ontimes).

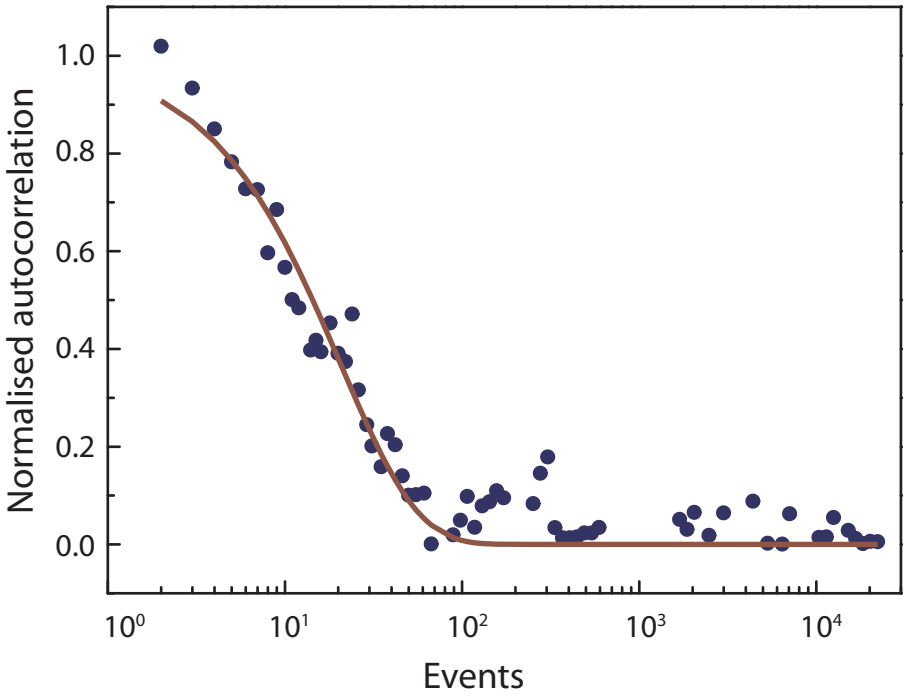

Figure 4.10: Normalised autocorrelation of 24749 offtimes for a single PalB molecule. The correlation persists up to 21 events, according to a single exponential fit.

lowed by long turnovers. This 'memory effect' disappears as the interval separating the turnovers increases. It is interesting to note that the turnovers appear in two clusters, *i.e.* there appear to be relatively few turnovers in the centre of the diagonal, which in turn suggests that there are predominantly two types of turnovers: short-wait-short-duration ones, and long-wait-long-duration ones. At the moment, the biological significance of this phenomenon remains uncertain. *Very* recently, new evidence has indicated that the stretched exponential function of the 'off' times that is often thought to be indicative of dynamic disorder may be an artefact introduced by the data analysis procedure [13], which firmly establishes the need for further future research on this matter.

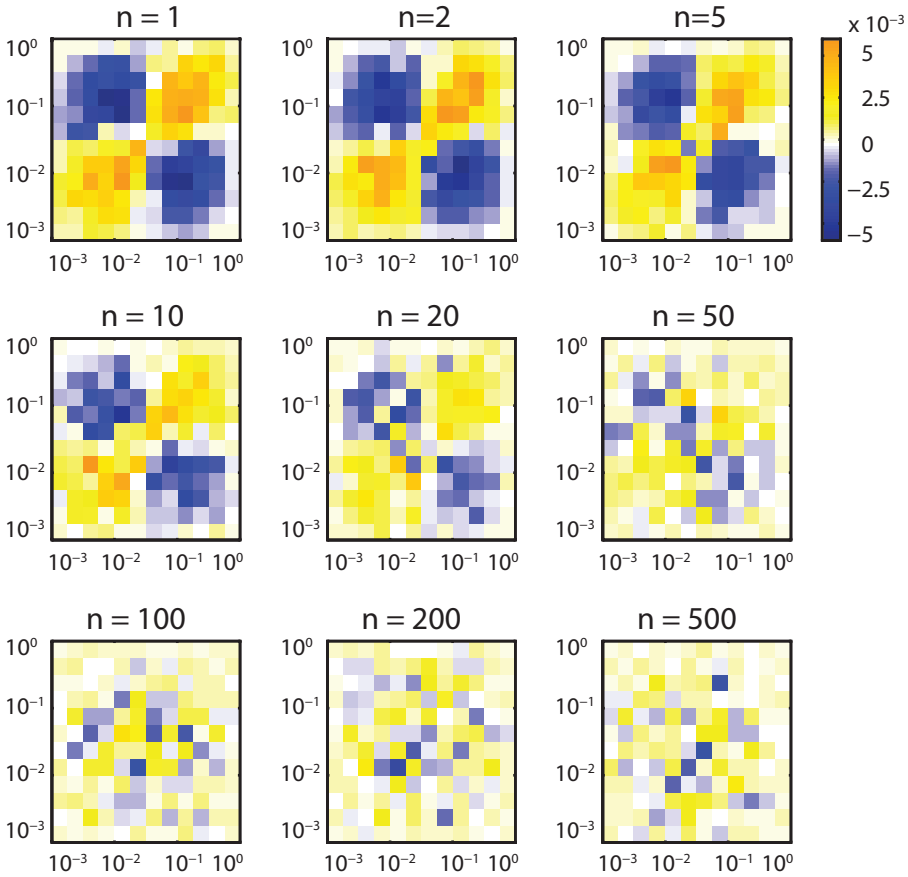

Figure 4.11: 2D histograms of turnovers spaced *n* events apart. The time between turnover events is plotted in seconds on a logarithmic scale. The diagonal feature indicative of the memory effect that is prominent at n=1 disappears as the event lag is increased.

The bulk rates of CFDA to CFMA and CFMA to CDFA are 1.1×10^{-5} and 2.7×10^{-5}, respectively [14]. Obviously the bulk reaction proceeds very slow; on average it takes PalB in bulk over 10 hours to produce one carboxyfluorescein molecule from its substrate CFDA. On the other hand on our hydrophobic surface we found a rate of 16 s^{-1} for a single enzyme molecule. It is known that PalB performs better on a hydrophobic surface (see, for instance [15], and also Chapter 6). Interfacial activation is known for many lipases, and this is usually attributed to the opening of a 'lid'-like section of the enzyme molecule [16]. PalB, however, does not have a lid, but has apparently still been evolutionarily optimised for functioning at a lipid/water interface, *i.e.* it has distinct surface areas of a hydrophobic or a hydrophilic nature [17]. There is a hydrophobic patch near its active site, which is unsurprising as its natural substrates are lipids.

It should also be noted that there is the open issue of the substrate–product intermediate. The carboxyfluorescein (CF) dye is doubly acetylated to turn it into a non-fluorescent substrate. Therefore, two bonds need to be broken for the highly fluorescent product to reappear [18]. The intermediate molecule carboxyfluorescein monoacetate (CFMA) is itself slightly fluorescent (about 2% of CF [14]) and has significant emission spectrum overlap with the product. It has been a matter of some internal discussion, and it has even been suggested that while we assume that we are observing fluorescence of the product molecules we are actually observing the intermediate in the reaction. If this is true then there is room for a fiftyfold improvement in the signal-to-background ratio; the future development of monosubstituted substrate molecules would ensure that the product molecule is made in a single step by the enzyme.

4.2.3 PalB immobilised by a leucine zipper

Since we noticed that the enzyme molecules were moving when physically adsorbed to a the hydrophobic surface, we also tried to immobilise PalB using the leucine zipper approach [19], which was introduced in Chapter 3, resulting in a stronger bond between PalB and the surface. One of the coils of the leucine zipper, *i.e.* the Kg-coil, was coexpressed as a fusion protein with PalB, and this compound was subsequently fluorescently labelled (see Figure 4.2). The other leucine zipper Eg-coil was immobilised via its C-terminal cysteine

to a linker molecule (see Figure 4.12) containing a maleimide group that was previously immobilised on an amine-functionalised glass surface via its NHS ester group. The surface containing the immobilised Eg-coil of the leucine zipper was subsequently incubated with low concentrations (0.1–10 nM) of the enzyme–Kg-coil fusion protein.

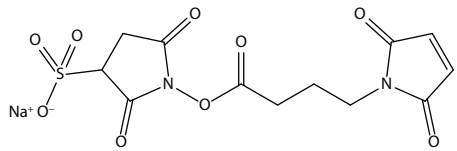

Figure 4.12: N-[γ-Maleimidobutyryloxy]sulfosuccinimide ester (sulfo-GMBS), which is the linker used to couple the Kg-coil of the leucine zipper to the aminated surface. The maleimide moiety reacts with the C-terminal cysteine on the peptide coil, while the NHS ester reacts with the amine groups on the surface.

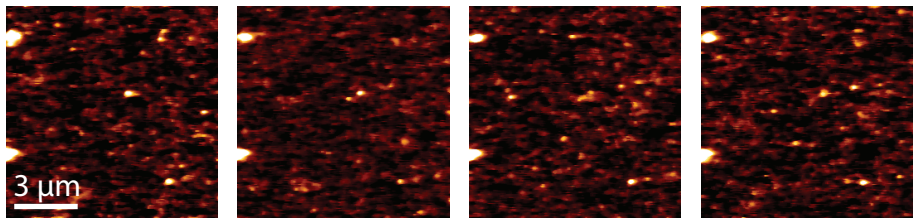

Figure 4.13: Consecutive confocal microscopy images, taken at an interval in the order of minutes, of PalB immobilized via leucine zippers to the glass surface ($10 \times 10\ \mu m^2$). Several single enzyme molecules are present in every image, indicating that they are immobilised. Some floating molecules are also visible, for instance in the bottom right corner of the second image, as well as two clusters of several molecules at the left hand side of the image. None of the molecules displayed enzymatic activity.

An example is given in in Figure 4.13 where a 1 nM solution of the enzyme was used for incubation. The surface is covered with lots of spots and the images show that most enzyme molecules are stationary. Some spots appear to be clusters of several molecules.

Unfortunately, while we did observe bleaching of the fluorescent labels, there was a dearth of enzymatic activity at all of the spots after addition of the substrate CFDA.

4.3 Conclusions

The improvement of the image quality of our confocal microscope (*vide infra*) allowed us to observe of active PalB enzyme molecules. The fluorescently labelled PalB molecules absorbed physically onto a hydrophobic glass surface seem to move, as we found them diffusing even after thorough washing of the samples. Several of the enzyme molecules appeared to be both immobilised and active, and we were able to follow their reaction up to several hours by observing the generation of fluorescent product molecules. Application of the so-called change point algorithm yielded the distributions of 'off' and 'on' times of the fluorescence emissions, and hence the reaction rates of the enzyme molecules. We observed a memory effect similar to the one that was found earlier for PalB, as well as for cholesterol oxidase. The direct physical absorption to the surface turned out to be a too unreliable method of immobilisation to study the effect of parameters like pH and temperature on the kinetics of PalB. Attempts to couple PalB via a leucine zipper linker to the surface in order to eliminate floating of the enzyme molecules was successful, yet none of the immobilised enzyme molecules was found to be active.

4.4 Experimental

4.4.1 Improving the confocal microscope image quality

For confocal imaging of surfaces we cannot simply use a camera as in wide-field microscopy. Only one position in the sample can be observed at a time, and furthermore our avalanche photon detector does not output an intensity signal but instead a single electrical pulse for each photon that it detects. In order to build up an image, we need to scan the sample in the XY plane and collect the electrical pulses—that are generated whenever a photon is detected—and tag them with their location. Previously, we accomplished this by guiding the photon stream, *i.e.* the electrical pulse stream, into a computer running a custom Labview program implementing a counter and a digital-to-analogue converter. The program counted the number of photons that arrived in a certain time interval, and converted this number to an output voltage that represented the light intensity. This voltage was subsequently used as an input for the XY-sample scanner which records the intensity as a func-

tion of position, in this way building up the image. This methods produces errors both in accuracy and in precision of the image.

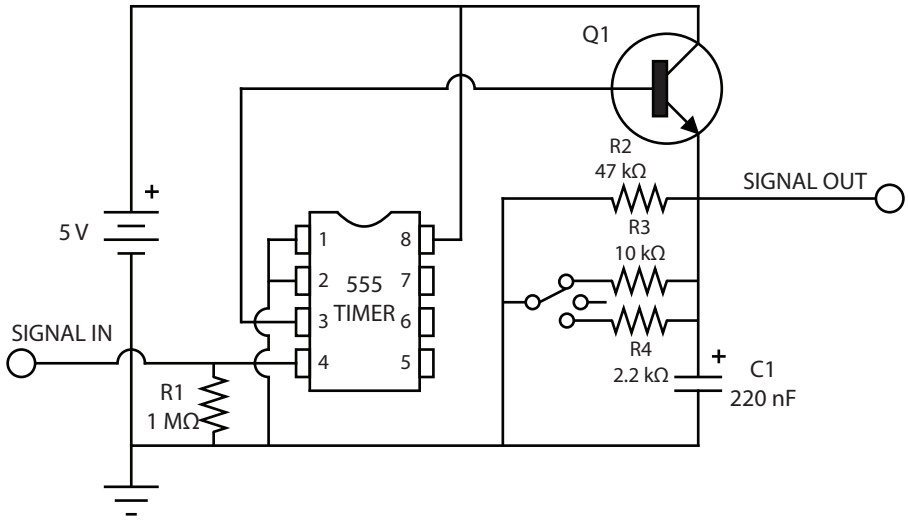

Figure 4.14: Circuit design diagram for the photodiode pulse integrator. The incoming TTL pulses from the photodiodes are made into a longer and more square wave by means of a 555 timer IC and pulldown resistor R1. The clean pulse subsequently triggers NPN transistor Q1 to partially charge capacitor C1. The charge on capacitor C1 is the output voltage sent to the XY scanner. The charge of capacitor C1 is constantly drained off by resistor R2 and optionally by R3 or R4, providing three settings for the overall sensitivity.

The time it takes the computer program to process the data introduces an offset between the actual position of the scanner and the perceived intensity, resulting in reduced accuracy. As a result, any features in the image are shifted with respect to their real position on the sample. This is a problem, because we are looking at very small objects, *i.e.* single molecules. If, after scanning an image, an object—a molecule—is to be observed for a long period of time, the confocal volume needs to be positioned exactly in the right place. With an XY-diameter in the order of half a micron, one easily gets suboptimal positioning in the focus, meaning a loss in signal and hence a reduced signal-to-noise ratio. Thus far, we have been able to estimate the correct position of a molecule by taking two images from opposite scan

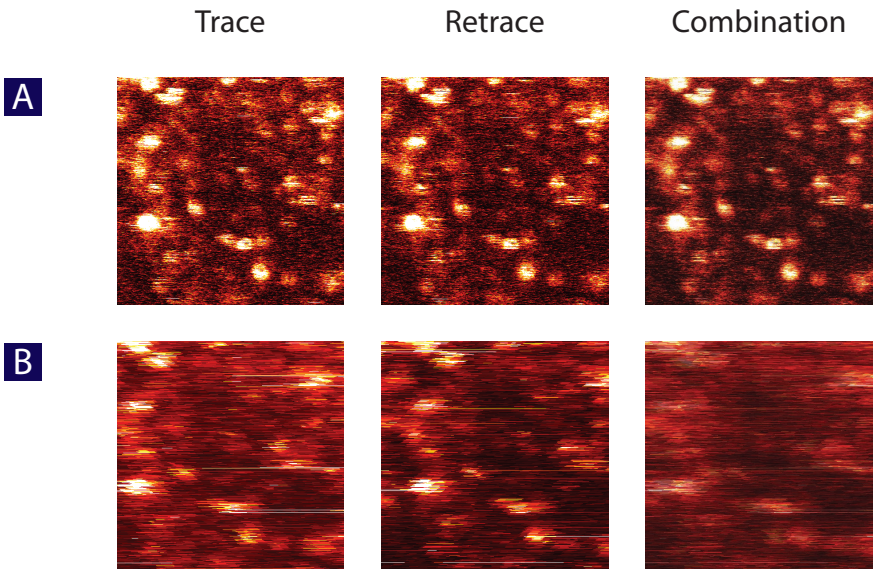

Figure 4.15: Comparison of confocal microscopy images of a single molecule sample of rhodamine 6G taken simultaneously using A) the pulse integrator described in this chapter, and with B) in-house–developed Labview software, using a line scan rate of 5 Hz. Note that the trace and retrace images of A are a virtually perfect match, resulting in reduced noise when the images are combined according to $Combination = \sqrt{Trace \times Retrace}$. The mismatch in the position of the spots in B results in a loss of image quality.

directions; every line is scanned a first time—trace—and a second time—retrace—as the laser is travelling back to its starting position. The two spots in the two scanned images will have the same offset but with a reversed sign, meaning that if the focus is aimed half way between the spots, it is approximately in the right place. Furthermore, the output of the computer has a significant capacitance, meaning that there is some smoothing of the output signal; the outputted voltage drops too slowly to keep up with a sudden decrease in light intensity. This in turn causes the scanned images to contain streaks, resulting in reduced precision.

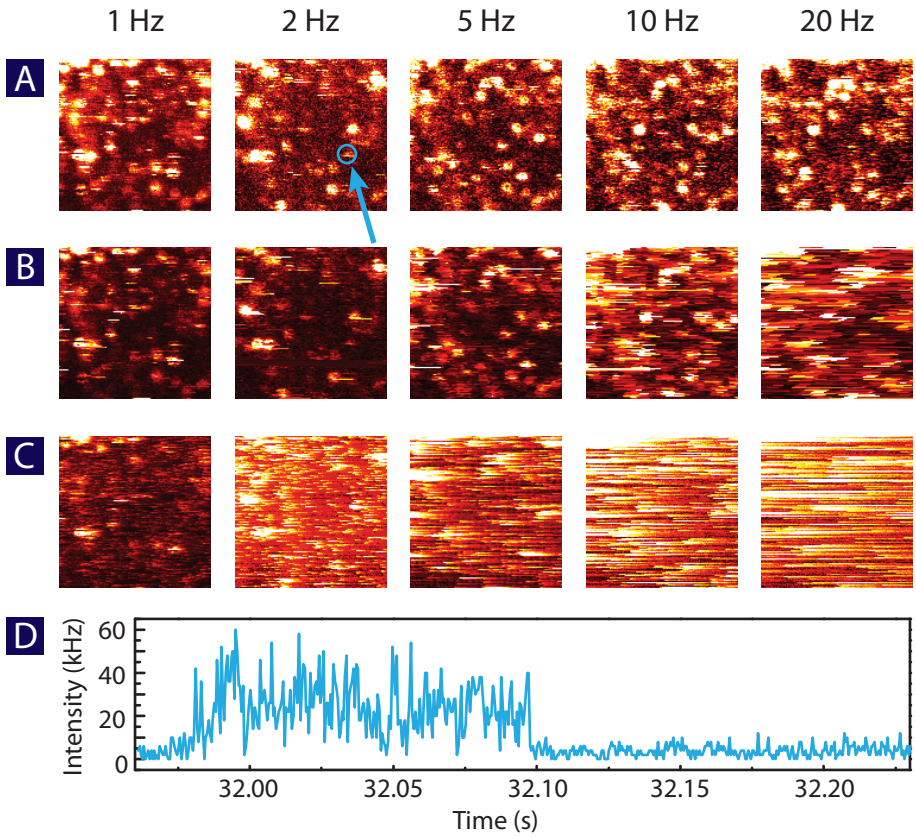

Figure 4.16: Comparison of confocal microscopy images of a single molecule sample of rhodamine 6G taken simultaneously with A) the pulse integrator described in this chapter, B) in-house–developed Labview software, and C) general pulse converter hardware, at different scan speeds. Note that the precision of the images generated in B and C but not in A deteriorates as the scan speed increases, as evidenced by the streaking. D) The fluorescent dot indicated by the blue arrow in A bleached in a single step (at 32.1 s), indicating that it was a single molecule.

To overcome both these limitations, we have designed and built the simple electronic circuit that is shown in Figure 4.14. Our photodiode pulse integrator keeps a moving average of the light intensity by buffering the number of electric pulses as charge in a constantly drained capacitor. Figures 4.15 and 4.16 show comparisons of accuracy and precision between images taken simultaneously of a single molecule sample of rhodamine 6G. Our new photodiode pulse converter is superior in both accuracy and precision. Additionally, it allows for higher line scan rates up to 50 Hz, meaning that a 128×128 pixel image can be scanned in little over 2 s. This not only helps improve workflow and reduce the time in which a large number of images can be scanned, but it also reduces photo-oxidative stress on the molecules, *i.e.* since they are excited for a shorter period of time, they are less prone to bleaching during the scanning of an image.

4.4.2 Standard glass surface preparation

Glass cover slips of 24 mm diameter (Gerhard Menzel [Braunschweig, DE] #1.5) were cleaned according to the following procedure: they were rinsed with acetone, sonicated (Branson [Danbury, CT, USA] B-1210-MT) for 5 minutes in an aqueous 1 M NaOH solution, rinsed to pH 7 with MilliQ water, and then stored in methanol. Prior to use, the cover slips were put in a UV ozone cleaner (UVP [Upland, CA, USA] PR-100 Photoreactor) for 30 minutes.

Rhodamine 6G–test samples were made by taking a saturated solution of rhodamine 6G in methanol (~400 $g \cdot L^{-1}$) and diluting this 10^{-10} times in MilliQ water (to a final concentration of 90 pM). A drop of this solution was put on a cotton bud, which was subsequently swiped over the glass surface.

4.4.3 PalB activity on a hydrophobic surface

Cleaned glass cover slips were mildly hydrophobized with a solution of 10% trimethoxymethylsilane in toluene, followed by repeated washing with toluene and water, and drying under nitrogen flow. PalB molecules were fluorescently labelled with on average one molecule of Alexa Fluor® 488, using the procedure prescribed by the manufacturer. A 1 pM solution of PalB-488 was incubated on the hydrophobic glass surface for 30 min-

utes and the glass coverslip was subsequently rinsed with MilliQ water. The coverslip was mounted onto the confocal microscope, and 100 µl of a 50 mM phosphate-buffered solution (pH 7.0) containing 150 mM NaCl, 10% acetonitrile, and 5.3 nM of the substrate 5,6-carboxyfluoresceindiacetate (CFDA) was added.

The fluorescence intensity timetraces were cut into 10 s segments and processed with a change point algorithm as implemented in C by the Haw Yang group [8] [version 1.11, parameters: type-I error 5%, 95% selection confidence interval]. The change points of all the segments thus obtained were recombined by sequential stitching to obtain complete binary traces; periods with high and low levels of fluorescence were designated as 'on' and 'off' periods, respectively. The binary traces were processed using Labview (National Instruments [Austin, TX, USA] 7.1), Matlab (The MathWorks [Natick, MA, USA] 2010b) scripts or GNU C scripts developed in-house and fitted with Matlab using the simplex search method from Lagarias *et al.* [20] to extract correlation times, 'on' times and 'off' times.

4.4.4 PalB immobilised by leucine zippers

The preparation of the leucine zipper–system was developed in-house [21], and can be summarised as follows. Glass cover slips cleaned using the method described above were additionally washed with a Piraña solution (7 H_2SO_4 : 3 H_2O_2) for 1 hour, rinsed well with water and dried in an oven at 120 °C for 10 minutes. The cover slips were immersed for 15 minutes in 10 mL of a 1% solution of N-(2-aminoethyl)-3-aminopropylmethyldimethoxysilane (AEAPS) in acetone with 5% water, rinsed with acetone, and then dried for 40 minutes. The cover slip surface was covered with a 10 mM phosphate buffered solution (pH 7.5) containing 10 mM N-[γ-maleimidobutyryloxy]sulfosuccinimide ester (sulfo-GMBS) and left in a wet chamber for 2 hours, after which it was rinsed with phosphate buffer. The cover slips were subsequently incubated overnight upside down on top of 60 µl of a phosphate buffered peptide solution containing 1 mg·ml^{-1} of the leucine zipper Kg-coil, after which they were rinsed with water.

The leucine zipper–Eg-coil was coexpressed with PalB as a fusion protein [21], and 500 µl of a 0.8 mg·ml^{-1} solution of this peptide was labelled with Alexa Fluor® 488 according to the procedure in the labelling kit (Molecular Probes [Eugene, OR, USA] A-10235).

Cover slips activated with the Kg-coil were washed with water, immersed in 10 ml 1M β-mercaptoethanol for 30 minutes at room temperature and then washed again with water. The cover slips were subsequently incubated with 0.1, 1, or 10 nM of the enzyme–Eg-coil conjugate in phosphate buffer for 1 hour and rinsed with phosphate buffer afterwards.

4.4.5 Confocal microscope setup

Laser light of 532 nm (Spectra-Physics [Mountain View, CA, USA] Millennia®) or laser light of 488 nm (Spectra-Physics [Mountain View, CA, USA] 2080 argon ion laser) was coupled into a single-mode optical fibre (Thorlabs [Newton, NJ, USA] P1-460-FC-5), reflected by a dichroic beam splitter (Chroma [Bellows Falls, VT, USA] 530dcxr or 505dcxr) and focused onto the sample by an oil immersion 100x objective (Carl Zeiss [Jena, DE], NA=1.30), which was mounted on an inverted microscope (Carl Zeiss Axiovert 200). Fluorescent light coming from the focal volume was collected by the same objective, passed through the dichroic beam splitter, focused through a 50–100 μm pinhole and subsequently focused onto an avalanche photodiode (PerkinElmer [Waltham, MA, USA] SPCM-AQR-14). The photon count signals were integrated simultaneously on three devices for comparison. Primo: using a data acquisition card (National Instruments [Austin, TX, USA] PCI-6036E) and LabView (National Instruments [Austin, TX, USA] 7.1) software. Secondo: using in-house–developed general purpose pulse counter hardware (Radboud University Werkplaats [Nijmegen, NL]). Tertio: using the pulse integrator described in this chapter (*vide supra*). All three signals were routed into an TAO (tip-assisted optics) module (JPK [Berlin, DE] Nanowizard I) with a 100×100 μm XY scanner and JPK software to create the images.

4.5 References and notes

[1] K. Velonia, O. Flomenbom, D. Loos, S. Masuo, M. Cotlet, Y. Engelborghs, J. Hofkens, A. Rowan, J. Klafter, R. Nolte, F. de Schryver, *Angewandte Chemie International Edition* **2005**, 44(4), 560–564, doi: 10.1002/anie.200460625.

[2] H. Rigler, Rudolf; Vogel (editor), *Single Molecules and Nanotechnology*, volume XIV, Springer, **2008**, ISBN 9783540739234.

[3] N. Boens, W. Qin, N. Basarić, A. Orte, E. M. Talavera, J. M. Alvarez-Pez, *The Journal of Physical Chemistry A* **2006**, 110(30), 9334–9343, doi: 10.1021/jp0615712.

[4] D. Loos, Ph.D. thesis, Katholieke Universiteit Leuven, **2005**, ISBN 9789090259260.

[5] X. S. Xie, H. P. Lu, *Journal of Biological Chemistry* **1999**, 274(23), 15967–15970, doi: 10.1074/jbc.274.23.15967.

[6] *BCECF and BCPCF - Product Information*, Molecular Probes, MP 14440, **2001**.

[7] P. Trodler, J. Nieveler, M. Rusnak, R. D. Schmid, J. Pleiss, *Journal of Chromatography A* **2008**, 1179(2), 161–167, doi: 10.1016/j.chroma.2007.11.108.

[8] L. P. Watkins, H. Yang, *The Journal of Physical Chemistry B* **2005**, 109(1), 617–628, doi: 10.1021/jp0467548.

[9] P. Lu, L. Xun, S. Xie, *Science* **1998**, 282(5395), 1877–1882, doi: 10.1126/science.282.5395.1877.

[10] O. Flomenbom, J. Hofkens, K. Velonia, F. Deschryver, A. Rowan, R. Nolte, J. Klafter, R. Silbey, *Chemical Physics Letters* **2006**, 432(1–3), 371–374, doi: 10.1002/prot.20893.

[11] G. De Cremer, M. B. J. Roeffaers, M. Baruah, M. Sliwa, B. F. Sels, J. Hofkens, D. E. De Vos, *Journal of the American Chemical Society* **2007**, 129(50), 15458–15459, doi: 10.1021/ja077621d.

[12] H.-P. Lerch, A. S. Mikhailov, R. Rigler, *Chemical Physics* **2007**, 331(2–3), 304–308, doi: 10.1016/j.chemphys.2006.10.025.

[13] T. G. Terentyeva, H. Engelkamp, A. E. Rowan, T. Komatsuzaki, J. Hofkens, C.-B. Li, K. Blank, *ACS Nano* **2012**, 6(1), 346–354, doi: 10.1021/nn203669r.

[14] M. van Teeseling: Master's thesis, Radboud University Nijmegen, **2010**.

[15] B. C. Koops, E. Papadimou, H. M. Verheij, A. J. Slotboom, M. R. Egmond, *Applied Microbiology and Biotechnology* **1999**, 52, 791–796, doi: 10.1007/s002530051593.

[16] U. Hanefeld, L. Gardossi, E. Magner, *Chem. Soc. Rev.* **2009**, 38, 453–468, doi: 10.1039/B711564B.

[17] A. Basso, P. Braiuca, S. Cantone, C. Ebert, P. Linda, P. Spizzo, P. Caimi, U. Hanefeld, G. Degrassi, L. Gardossi, *Advanced Synthesis & Catalysis* **2007**, 349(6), 877–886, doi: 10.1002/adsc.200600337.

[18] T. G. Terentyeva, W. Van Rossom, M. Van der Auweraer, K. Blank, J. Hofkens, *Bioconjugate Chemistry* **2011**, 22(10), 1932–1938, doi: 10.1021/bc2001038.

[19] D. L. McClain, H. L. Woods, M. G. Oakley, *Journal of the American Chemical Society* **2001**, 123(13), 3151–3152, doi: 10.1021/ja004099l.

[20] J. C. Lagarias, J. A. Reeds, M. H. Wright, P. E. Wright, *SIAM Journal on Optimization* **1998**, 9(1), 112–147, doi: 10.1137/S1052623496303470.

[21] M. Lambermon: Personal communication.

Chapter 5

A nanoreactor

CCMV virions containing HRP molecules

5.1 Introduction

5.1.1 The concept

Confinement in a container as a method of immobilisation for single enzyme experiments is fundamentally different from surface attachment. In nature, most enzymes are present in cells. Needless to say, cells present a confined environment, but also a highly crowded one [2, 3].

There are several advantages to situating enzymes in a small space: The surroundings more closely mimic the natural environment, there is no danger of the denaturing effect of surfaces, and the enzyme can be efficiently shielded from proteases. Confinement in a container is a generic approach, which is suitable for most enzymes, and does not require chemical modification of the molecule. For example, any labelling for facilitating detection or purification can be done on the container, rather than on the enzyme, giving a 'plug and play' assembly method. In this chapter, the concept of confinement is explored by studying an enzyme immobilised in the empty shell of a plant virus.

Some of this work was published in Nature Nanotechnology [1].

5.1.2 The container

The CCMV (Cowpea chlorotic mottle virus) capsid is the devoid shell of a plant virus, which has been described in greater detail in the introduction to Chapter 3. The reader should recall that CCMV can be evacuated by reversible disassembly of its protein shell into individual subunits [4] and used as a container for a range of molecules. It is possible to encapsulate a protein inside the empty CCMV capsid, either by statistical encapsulation [1] or by linking it to the protein shell [5].

There is yet a third state of the virus: besides the intact virus (at pH 5 and 0.1 M NaCl) and the disassembled state *i.e.* the free protein dimers (at pH 7.5 and 1 M NaCl), there is a 'swollen' state: The virus is known from cryo-EM measurements to grow by roughly ten percent when the acidity is lowered to pH 7 while keeping the NaCl concentration at 0.1 M. The swollen state is shown in Figure 5.1C. In addition, the pores in the protein shell are known to grow to over 2 nm. This is thought to be an intermediate step in the disassembly process leading to RNA release *in vivo* [6].

5.1.3 The payload

As the enzyme, we chose HRP (Horseradish Peroxidase, Figure 5.2) because it is relatively pH insensitive between pH 5 and pH 7.5 and because it accepts many different substrate molecules. HRP is a peroxidase enzyme—nomen est omen—extracted from the plant Horseradish, which is a plant of which the root has been used in cooking since antiquity. HRP is a 35 kDa enzyme (usually found in a glycosilated state of 44 kDa) [7] that is widely used in molecular biology because it accepts a wide range of organic and inorganic substrates. In nature, the enzyme is active in many processes, among others in the metabolism of hormones and in building constituents of the cell wall [8]. In molecular biology, its uses include those of reporter enzyme and as an enzyme for activity assays. The enzyme uses an electron donor to reduce hydrogen peroxide to water, and the by-product of the reaction is the oxidised form of the electron donor. In our experiment the donor is dihydrorhodamine 6G. This compound loses two electrons and a hydrogen to form an imine-conjugated system. Due to the symmetry in the molecule, the conjugated system can resonate to include the second nitrogen atom, making it a fluorophore. This reaction, shown in Figure 5.2,

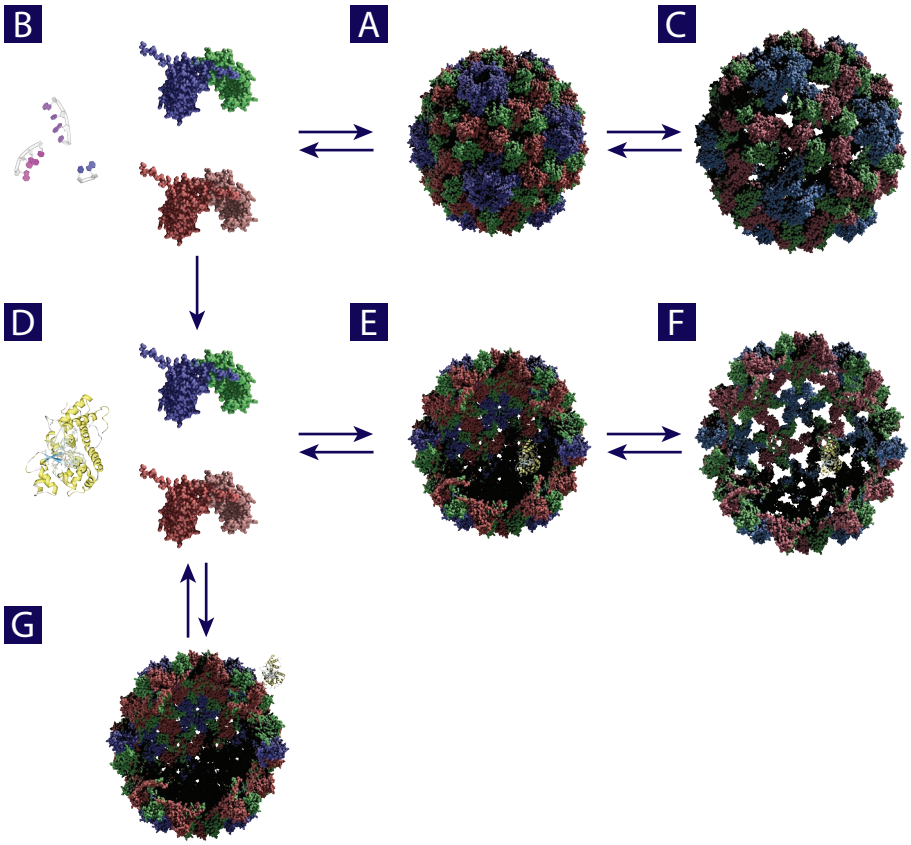

Figure 5.1: Assembly of the CCMV nanoreactor. A) The virus reversibly disassembles—depending on pH and ionic strength—into B) its components RNA and dimers of the coat protein and C) can swell into a form with more and larger pores. The RNA can be precipitated to leave just the coat protein dimers. D) The enzyme HRP is added to build the nanoreactor. E) A capsid containing HRP is obtained if the capsid is reassembled in the presence of HRP. F) Faster diffusion of the product indicates that, as with the virus, this nanoreactor swells at higher pH. G) If the enzyme HRP is added after assembly, it is thought to non-specifically absorb to the outside of the capsid.

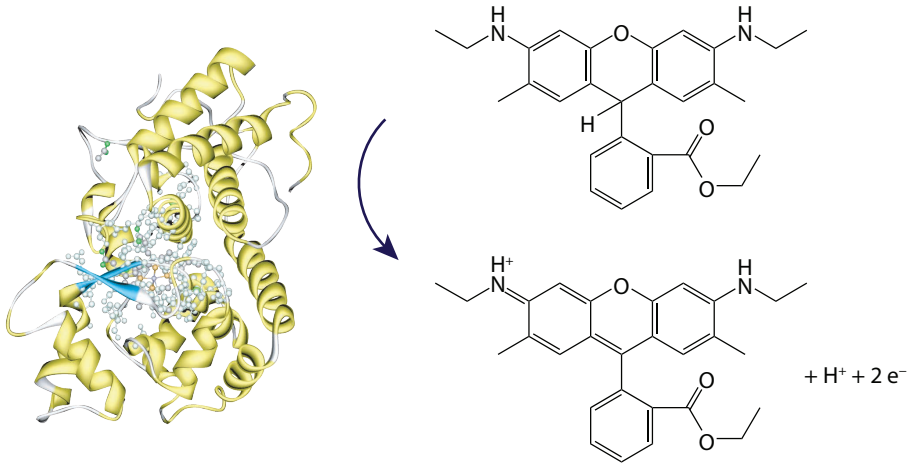

Figure 5.2: Secondary structure of the enzyme horseradish peroxidase, and the oxidation reaction of dihydrorhodamine to rhodamine 6G

yields a strongly fluorescent molecule with a quantum yield of 0.95 [9] named rhodamine 6G, and it is this molecule that is used as the reporter molecule for the activity of the enzyme.

5.2 Results and discussion

5.2.1 Encapsulation of enzyme in the virus cage

Table 5.1: Distribution table for inclusion number 0.37.

No.	Frequency
0	69.1%
1	25.5%
2	4.7%
3+	0.7%

The encapsulation of the HRP payload in the CCMV container is performed by assembling the CCMV capsid in a solution containing HRP molecules. During the formation of the hollow sphere, HRP molecules can be statistically trapped inside. The number of HRP molecules included per capsid depends solely on the concentration of the enzyme as there is no driving force for the encapsulation, the HRP molecules do not interact with one another, and the inclusion process is governed by Poisson statistics. The average number of molecules per CCMV capsid λ is only dependent on the enzyme concentration in the solution [10]. It can be calculated by:

$$\lambda = [HRP]V_{capsid}N_A \tag{5.1}$$

where $[HRP]$ is the enzyme concentration, V_{capsid} is the internal volume of a capsid ($3.05{\cdot}10^{-21}$ L) and N_A is Avogadro's constant. The probability that k enzyme molecules are present in a capsid is:

$$p(k,\lambda) = \frac{\lambda^k e^{-\lambda}}{k!} \tag{5.2}$$

The ratio between the probabilities that a capsid contains 1 or 2 enzyme molecules is [11]:

$$\frac{p(1,\lambda)}{p(2,\lambda)} = \frac{\lambda e^{-\lambda}}{\lambda^2 e^{-\lambda}/2} = \frac{2}{\lambda} \tag{5.3}$$

Since it is our goal to study single enzyme kinetics, it is therefore necessary to use a low average inclusion number to avoid a lot of double filled capsids. Unfortunately, the ratio between empty capsids and capsids with exactly one enzyme molecule scales with λ. The experiment is thus left with a large number of empty capsids that do not contribute to the actual experiment. It may be interesting for future research to try to devise a method of separating the filled from the empty capsids, since the latter may be distinguished from loaded capsids by the absence of a fluorescent label. A procedure analogous to Fluorescence-Activated Cell Sorting, but on a smaller scale as is already shown for polymersomes [12]; conceivably carried out in microchannels [13]. The practical feasibility would be limited mostly by the small amount of fluorescence emanating from the capsid. In our experiment, we calculated the average inclusion number λ to be 0.37 from the chosen HRP concentration. The statistical distribution of the enzyme in the capsid for λ=0.37 is shown in Ta-

ble 5.1. There is a fivefold excess of single loaded over double loaded capsids, with nearly 70% having no included enzyme molecule at all.

5.2.2 Detecting the activity of a single nanoreactor

The CCMV capsids containing HRP were spin-coated on the surface of a microscope cover slip glass. As a control, different samples—containing only empty CCMV capsids, only HRP, or empty CCMV capsids and free HRP—were included in the experiments. A buffer containing the substrate dihydrorhodamine 6G and hydrogen peroxide was added onto each sample. In the sample containing CCMV with HRP included, bright diffraction-limited fluorescent spots were observed after ten minutes while scanning the surface with the confocal microscope. These images are presented in Figure 5.3.

These fluorescent spots are attributed to enzyme containing capsids. The emission is a result of product accumulation on the inside of the capsids due to the enzyme converting substrate molecules that have diffused in. The product molecules inside of the capsid could be only partially bleached with laser light, but never fully bleached to give a fluorescence intensity similar to the (background) level of the surrounding areas (see Figure 5.4).

From this bleaching behaviour it could be ascertained that the spots did not represent single product molecules but numerous molecules. After a few minutes, the spots had regained in intensity because of the continued production of fluorescent product molecules. During the experiment, it was noted that the background level rose slowly because fluorescent molecules leached out of the capsids into the solution. In the control sample where no HRP was present, there was only a very slow rise of background fluorescence, probably due to substrate autoxidation. The bright spots were not found in any of the control samples, indicating that the fluorescent molecules are indeed formed inside the capsids, rather than being created on the outside and subsequently selectively diffusing inwards. AFM images showed that the total number of capsids on the surface greatly exceeded the number of capsids where product accumulation occurred, which (*vide supra*) is to be expected according to the statistics. It is also likely that not all enzyme molecules are active, further increasing the fraction of capsids that are only observable by means of AFM. In fact, when we compare the number of bright spots per area observed by fluorescence microscopy to the number of

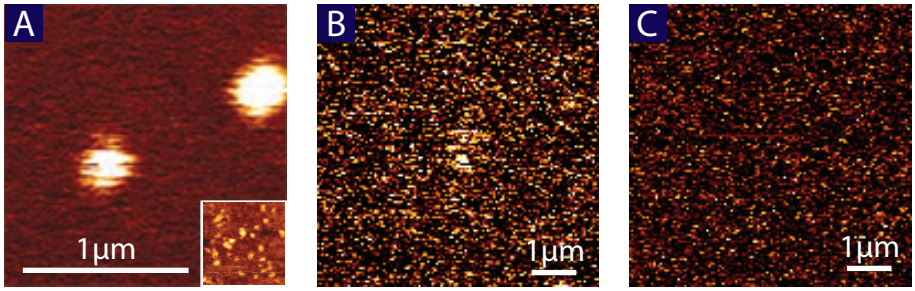

Figure 5.3: A) Confocal fluorescence image of 1.7 × 1.7 µm^2 showing capsids with accumulated fluorescent product molecules inside. The inset shows an AFM image of part of the same region (to scale) revealing that only a few molecules have an active HRP enzyme enclosed. B) Confocal fluorescence image of 6.4 × 6.4 µm^2 of the control sample containing a mixture of empty CCMV capsids and free HRP. A weak spot can be observed in the centre, which is probably caused by fluorescent molecules produced by HRP during the scanning of the image. C) Confocal fluorescence image of 6.4 × 6.4 µm^2 of the control sample containing only empty CCMV capsids.

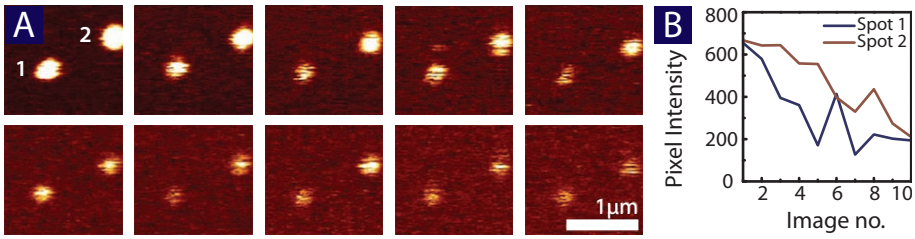

Figure 5.4: A) Confocal fluorescence images of 1.7 × 1.7 µm^2 of CCMV capsids with HRP inside after the addition of the fluorogenic substrate showing accumulation in the first image. The laser was used to photobleach the entrapped product molecules, and in the following images—left to right—the fluorescence diminished until a constant level was reached where the rate of bleaching equals the rate of product formation. Meanwhile, the background fluorescence increased as fluorescent product molecules leached into solution. B) Plot of the fluorescence intensity in each image, corrected for the increasing background level. Both spots bleached under laser illumination. Spot 1 was left to recover in image 6, while spot 2 was being bleached. Spot 2 recovers its fluorescence in image 8. Prolonged illumination could not bleach the spots further than in image 10.

capsids seen by AFM in the same region, it seems that only 1 in every 130 capsids has an active enzyme in it. From a statistical point of view, we expect 30% of the molecules to contain an enzyme. It follows therefore that 97.5% of the enzymes is inactivated.

In the control sample with empty CCMV capsids and free HRP, weak fluorescent spots were found that showed activity (*vide infra*) but no product accumulation. In the control sample with only free HRP, no localised activity was recorded though the background did increase. Our explanation is that in the first case HRP molecules absorb non-specifically to the outside of the capsids (see Figure 5.1G), and become partially protected from the denaturing properties of the glass surface and retain their catalytic activity. It is also known [14,15] that free HRP binds only weakly to glass surfaces and that it binds even less strongly in the presence of hydrogen peroxide, *i.e.* in its oxidised form [16], so it may very well be that most of the HRP molecules have desorbed.

5.2.3 Distinguishing *intra*-capsid and *extra*-capsid activity

In order to learn more about the enzyme's activity, fluorescence intensity timetraces of the fluorescent spots in the sample with HRP encapsulated in CCMV were recorded. These traces are shown in Figure 5.5A. As a control, timetraces of the spots in the sample containing the mixture of empty CCMV and free HRP were also taken, see Figure 5.5B. As noted earlier, the intensity of the fluorescence in the encapsulated HRP sample could never be reduced completely to the background level by bleaching the product molecules, due to the continual turnover of substrate. This meant that it was impossible to use the threshold method to extract the individual turnovers from the trace. The goal of direct analysis of the enzyme kinetics using this turnover data was therefore unattainable. The alternative method of fluorescence autocorrelation was applied to the data in an attempt to extract enzymatic data. This method is much more sensitive to small changes in intensity, but this comes at the cost of losing some temporal information. The advantage was that it enabled us to compare the traces from the encapsulated samples and the samples with HRP absorbed on the surface. The autocorrelation curves of both samples are shown in Figure 5.6.

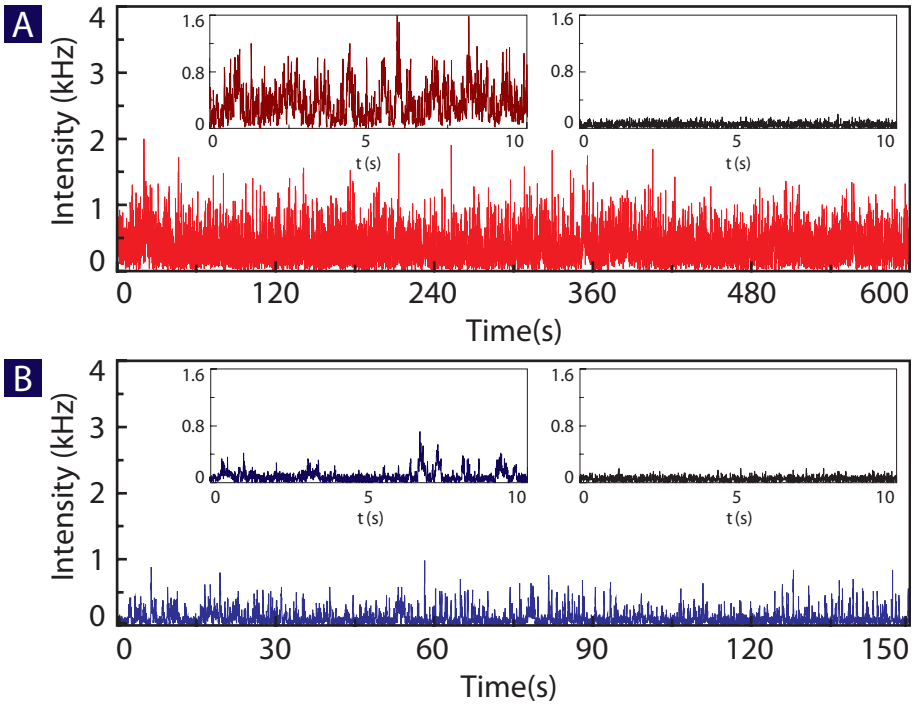

Figure 5.5: Fluorescence intensity timetraces of A) capsids with HRP encapsulated and B) capsids with HRP absorbed to its surface. In each case, the left inset is an enlargement of 10 s of the main trace. The right inset shows a timetrace of the fluorescence intensity of the background, taken at a dark spot in each sample. The Figure shows that individual turnovers can be observed if the enzyme is on the outside of the capsid. In the case of the encapsulated enzyme, however, the signal seldom returns to the background level.

The autocorrelation function of the timetrace from encapsulated HRP fits best to a simple diffusion model

$$G(t) = \frac{1}{(1+t/\tau)} \tag{5.4}$$

which describes the autocorrelation as a function of the diffusion time τ of the molecules in the observed volume. Strictly speaking, this is a 2D diffusion model, where the only route of escape available to the molecule is diffusion perpendicular to the optical axis. The con-

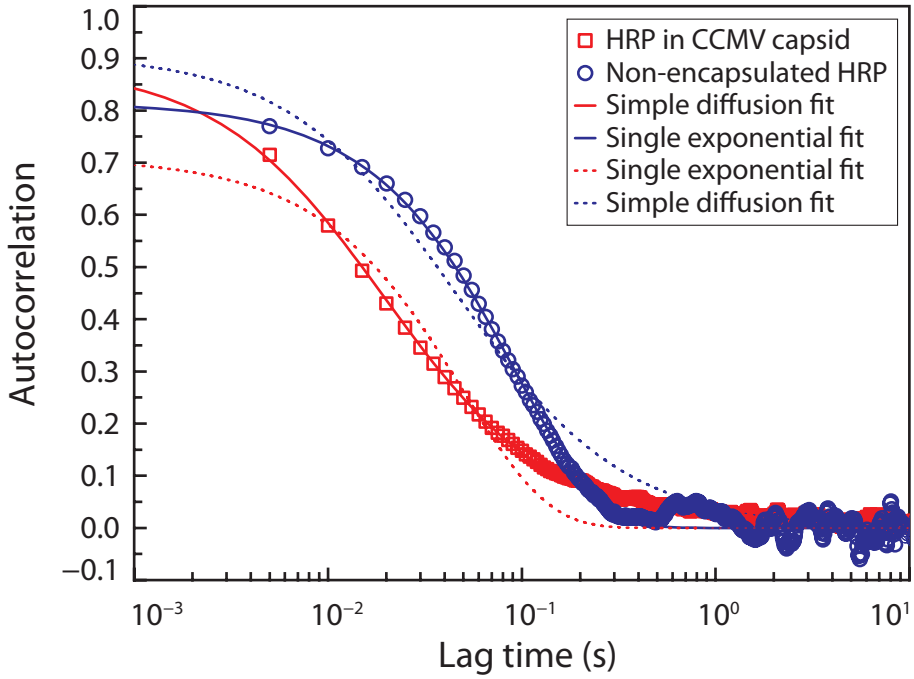

Figure 5.6: Fluorescence autocorrelation curves of the traces shown in Figure 5.5. The red squares represent the normalised autocorrelation curve of the CCMV with encapsulated HRP during catalysis. The solid red line is the best fit using the simple diffusion model. The blue circles represent the autocorrelation curve of the CCMV with HRP bound to its surface. The solid blue line is the best fit using the single exponential function. To emphasize the disparity between the models each curve is also fitted with the opposite model, indicated by the dashed lines, yielding very poor fits.

tribution of the third dimension is modest, and depends on the aspect ratio of the ellipsoid that constitutes the focal volume. An increasing aspect ratio introduces more exit paths, but each with a lesser probability. The autocorrelation from an ellipsoid with an aspect ratio of 1:4 is *de facto* indiscernible from 2D diffusion [17, p.811]. In our microscope setup, the aspect ratio of the ellipsoidal focal volume is even greater, *viz.* 5, therefore this simple model suffices. The apparent diffusion time obtained from the fit is 20 ms. This is 500 times slower

than the value of 40 μs which is known for the diffusion of rhodamine in water [18]. This is likely caused by the protein shell of the capsid acting as barrier and allowing diffusion only through its pores. In contrast, the autocorrelation function calculated for the experiment with HRP bound to the surface of the capsid does not fit to the diffusion model. It fits best to a model that describes the switching between a bright and a dark state, which can be correlated to a reaction scheme representing respectively the presence or absence of a fluorescent product molecule [19]. The equilibrium reaction between the bright state and the dark state has reaction rates k^1 and k^{-1}. The autocorrelation function is best fitted by the single exponential function

$$G(t) = Ae^{(t/\tau)} \tag{5.5}$$

in which A is a constant and τ is the reciprocal of the sum of k^1 and k^{-1}. The observed average turnover time τ of 90 ms can be mainly attributed to the amount of time that the product molecule spends bound to the enzyme, as the subsequent diffusion out of the focal volume is about a thousand times faster, *i.e.* the diffusion time is 40 μs.

5.2.4 pH dependent permeability

As mentioned in the introduction, the virus swells at neutral pH and low ionic strength. Figure 5.8 offers stereo images of the opening of the pores in the capsid. While this swelling has been demonstrated by cryo-EM and FPLC [20] for the virus, it has never been possible to demonstrate this for the empty capsid, likely because of the decreased stability of the capsid compared to the complete virus in conjunction with the harsh conditions experienced in cryo-EM. It was therefore interesting to investigate the influence of the pH, *i.e.* the pore size, on the nanoreactor. To this end, the activity of a single CCMV capsid with HRP encapsulated inside was recorded while changing the pH in small steps from pH 5 to pH 7.5 by the stepwise addition of a NaOH solution. The capsid was first located in the focal volume. The apparent diffusion time of the product of the enzymatic reaction (rhodamine 6G molecules) was then monitored by FCS at each pH point. Each two minute timetrace was autocorrelated and the resulting functions were all found to fit well to the diffusion model. Starting from pH 5, the apparent diffusion time decreased with increasing pH, then exhibited a jump at around pH 5.7 (see Figure 5.7) after which a sort of plateau was reached

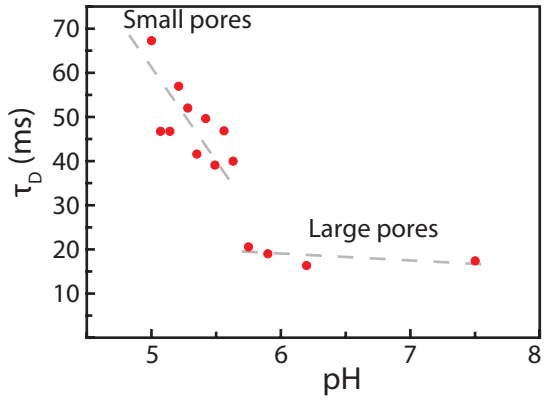

Figure 5.7: Diffusion times for rhodamine 6G generated by HRP encapsulated in CCMV as a function of pH. At pH 5.8 the diffusion time suddenly drops as a result of the opening of the pores in the capsid.

and the measured time remained constant. Since this time is determined by the slowest reaction step, specifically the egress of the fluorescent molecule from the capsid, it follows that this step is facilitated by raising the pH. It is therefore likely that the capsid exhibits a swelling effect with an associated growing of the pores, similar to that which is known to occur in the virus. The shift in apparent diffusion time cannot be explained by a change in catalytic rate of the enzyme at the different pH, because that effect is both moderate and antagonistic as HRP has its maximum turnover rate between pH 6–6.5, and at pH 7.5 its turnover rate merely decreases to 84% [21].

5.2.5 Comparison of autocorrelation algorithms

So far, we have used an autocorrelation algorithm that correlates the bins of a time histogram. The photon data stream is divided into discrete segments, and the number of photons in each time segment is counted, so one ends up with a histogram with bins that hold the photon arrival frequency for that each segment. The autocorrelation function is then obtained by shifting the bins over semi-logarithmically increasing lag times, and calculating

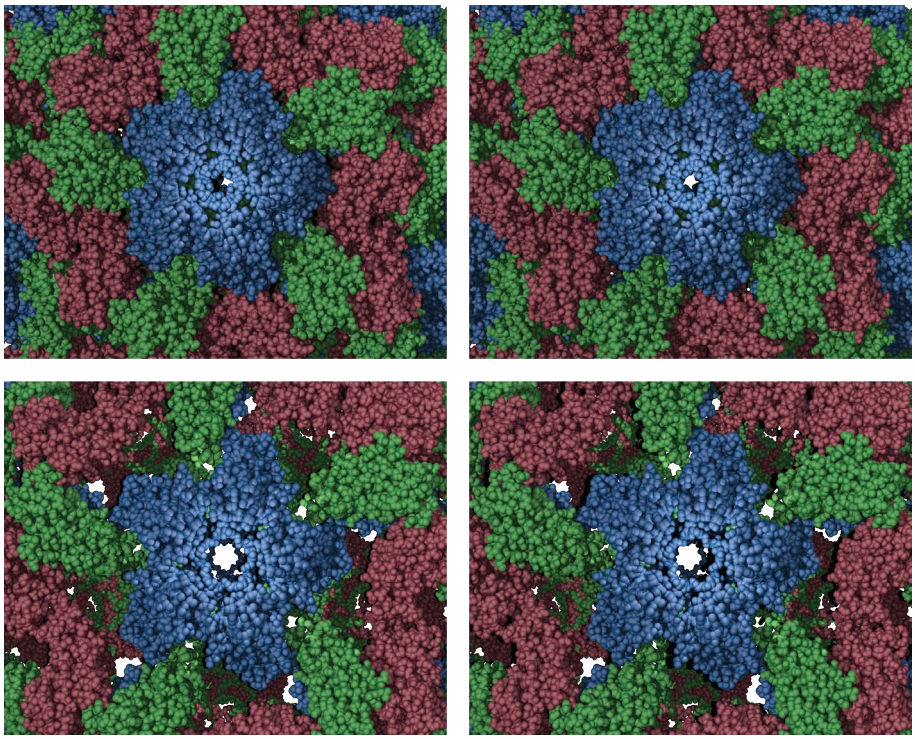

Figure 5.8: Cross-type stereo images of the structure of the CCMV shell. The view is centred on a pentagonal face and one looks straight down the middle of the capsid. *top* Normal virus at pH 5. *bottom* Swollen virus at pH 7.5. Note that while the pore in the pentagonal face grows, as do the pores in the hexagonal faces, it is the opening of the trigonal vertices that seems to account for most of the porosity.

the autocorrelation for each lag time. The main problem with this method is the amount of memory required, as will become obvious. Single molecule experiments are typically performed at count rates of 1–10 kHz, *i.e.* 1000–10000 photons per second, with a inclination towards the lower side of that range. Photons are recorded with a typical resolution of 1 ns to 100 ns—and down to 1 ps for fluorescence lifetime measurements. In our system the resolution was 50 ns. For diffusion and enzyme kinetics, we are most interested at processes

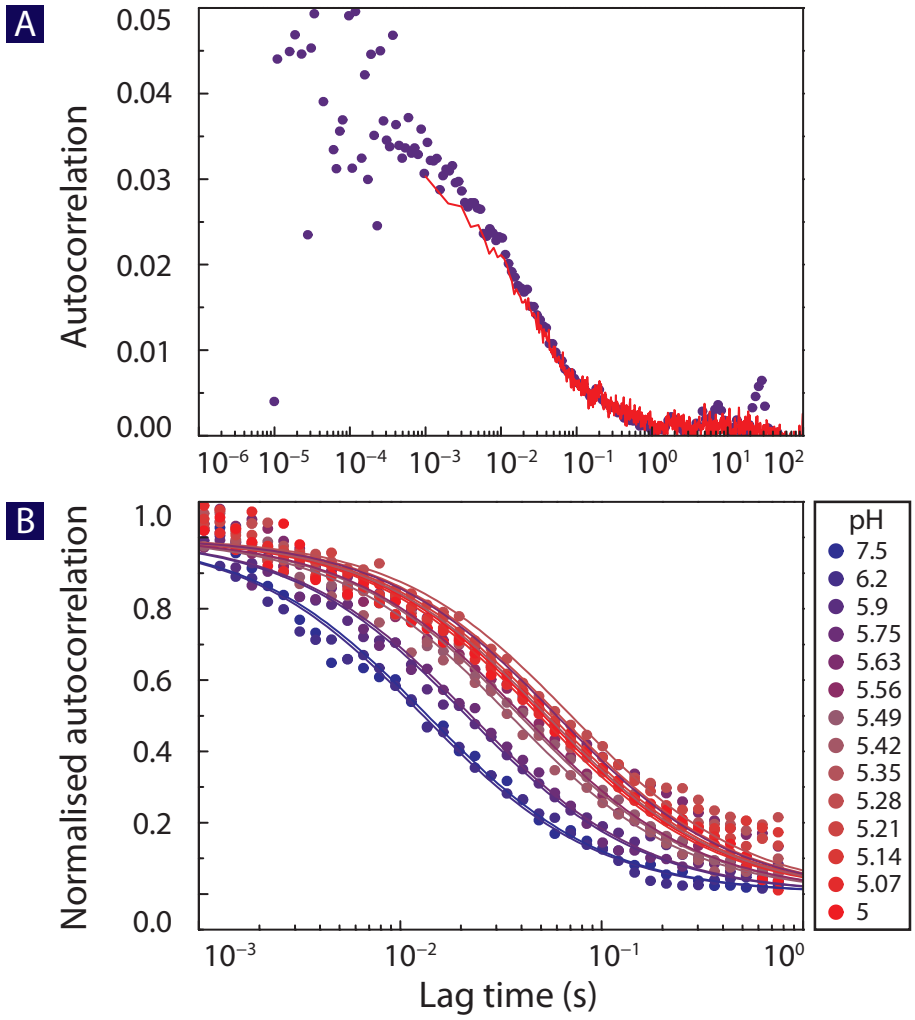

Figure 5.9: A) Autocorrelation curves of the CCMV capsid with HRP inside at pH 5.9 using the bin method (red line) and inter-photon distance algorithm (blue dots). B) Autocorrelation functions (dots), calculated with the inter-photon distance method, of the CCMV capsid with encapsulated HRP measured at increasing pH. The data has been fitted with a simple diffusion model (lines).

happening at time scales varying between 1 µs and 1 s. If we bin our 1 kHz traces at 1 µs, we are left with one million bins every second, of which 99.9% will be empty—assuming for the moment that photons arrive equally spaced, which is the worst case, and photons usually arrive in bursts. To store the bins as 32-bit integers, we now need 4 Mb per second, so the memory requirements of an experiment running little over 13 minutes will trump the memory of a typical desktop computer. Long experiments, therefore, require an unreasonably large amount of memory to calculate the autocorrelation in this way. And most of the bins that are to be correlated are empty and thus do not contribute to the correlation.

There is specialized hardware in the form of a correlator card that uses a method that calculates the autocorrelation in real time by means of the multiple tau algorithm [22, 23]. Since the original photon stream is not saved in this application, it is impossible to further analyse and segment the data afterwards, which for long experiments is impractical.

Recently, a new method for calculating autocorrelation of a photon stream was introduced [24], in which no binning is required and which can be performed offline, *i.e.* after the experiment. This method, which we will refer to as the inter-photon distance algorithm, calculates the correlation as follows. For every photon pair in the data stream, calculate the time that elapsed between the arrival of two photons, and record this time. The autocorrelation is then obtained by making a histogram of these inter-photon times, with any bin spacing desired, followed by a normalisation. In this way, the autocorrelation can be calculated in theory right down to the resolution of the photon stream. In reality, there will be few counts in the lowest bins and therefore the signal becomes more noisy at short lag times.

The traces from the permeability experiment were also processed using the inter-photon distance algorithm to compare the two different methods. In Figure 5.9A, the curves from applying both methods, *i.e.* the bin algorithm and the inter-photon distance algorithm, are plotted. The curves match well at time time scales between 1 ms and 10 s. The curves that were correlated with the inter-photon distance algorithm are separately plotted in Figure 5.9B, and from this graph it is clear that the apparent diffusion time of the product molecules decreases with increasing pH, as was also seen from the bin-correlated data. At times shorter than 1 ms the data gets too noisy to see fast processes, *e.g.* the free diffusion of rhodamine 6G in solution.

A comparison of algorithms is not complete without a word on the calculation time required to arrive at the result. For both algorithms the fluorescence intensity *viz.* the photon count rate is important, but for different reasons. The bin algorithm scales with the number of bins; for a timetrace of a given length, it scales with the bin size. The count rate is only important for the lower limit of the bin size, *i.e.* if the bin size is chosen too small, there will be many empty bins. The number of photons in each bin, however, is irrelevant for the calculation time. The inter-photon distance algorithm, on the other hand, scales quadratically with the number of photons. This becomes an issue when working with measurements containing many photons. As an example, we correlate the data file for the measurement of the CCMV capsid with HRP encapsulated at pH 5.9, for which the autocorrelation curves are shown in Figure 5.9A. The results are summarised in Table 5.2. A computer that could calculate the autocorrelation function in two seconds using the bin correlation method in Labview took nearly fourteen minutes when the inter-photon distance algorithm was used. Some time could be won by implementing the inter-photon distance algorithm in C and subsequent compiling, but real progress was made by reducing the maximum inter-photon arrival time to be correlated. In this example: the entire trace could be correlated in one minute—provided that a maximum lag time of one second was observed—but to calculate the autocorrelation without any limit on the maximum lag time required seventeen minutes.

5.3 Conclusions

The enzyme HRP was encapsulated in CCMV capsids by assembling the capsid in a solution of the enzyme. A fluorogenic substrate was added which resulted in accumulation of product molecules inside of the capsid; this made them visible as bright spots in a confocal fluorescence microscope. In a control experiment where HRP was added after the formation of the capsids, this accumulation was not observed. *Intra*-capsid activity and the activity of an enzyme absorbed to the capsid surface could be distinguished from an autocorrelation analysis of the fluorescence intensity timetraces on the spots. The capsid imposes a diffusion barrier for the product molecules. Considering the fact that substrate and product molecules have a similar size, it seems plausible that the substrate molecules

experience a barrier as well. This limits the practical use of this method for investigating enzyme kinetics to enzymes that are intrinsically slower than the limit imposed by the diffusion barrier. Bin correlation and inter-photon distance correlation methods were compared, and both produced identical results over the interval of 1 ms to 10 s, which is the region of most interest for this experiment. The bin correlation method cannot correlate time lags smaller than the bin size, but is superior to the inter-photon distance algorithm with regard to speed for the longer measurements and traces with high count rates. The inter-photon distance correlation method can provide information at shorter time scales, but the calculation time is significantly longer.

5.4 Experimental

5.4.1 Confocal microscope and atomic force microscope setup

Laser light of 488 nm (Spectra-Physics [Mountain View, CA, USA] 2080 argon ion laser) was coupled into a single-mode optical fibre (Thorlabs [Newton, NJ, USA] P1-460-FC-5), reflected by a dichroic beam splitter (Chroma [Bellows Falls, VT, USA] 505dcxr) and focused onto the sample by an oil immersion 100x objective (Carl Zeiss [Jena, DE], NA=1.30), which was mounted on an inverted microscope (Carl Zeiss Axiovert 200). Fluorescent light coming from the focal volume was collected by the same objective, passed through the dichroic beam splitter, focused through a 50 µm pinhole and subsequently focused onto an avalanche photodiode (PerkinElmer [Waltham, MA, USA] SPCM-AQR-14). The photon count signals were recorded as inter-photon arrival times with a resolution on 50 ns using a data acquisition card (National Instruments [Austin, TX, USA] PCI-6036E). An atomic force microscope (JPK [Berlin, DE] Nanowizard I) with a 100×100 µm XY scanner and a TAO (tip-assisted optics) module was fitted on top of the optical microscope. Experiments were carried out with 125 µm long silicon tips (Nanoworld [Neuchatêl, CH] NCH 20 POINTPROBE) with average nominal resonant frequencies of 320 kHz and average nominal force constants of 42 $\mathrm{N \cdot m^{-1}}$. Scanning was performed in tapping mode at a speed of 1 line per second with amplitude setpoints of 0.7 V. JPK SPM software (3.0.23-1) was used to control the AFM and to process (linear levelling) the data. The sample was prepared by spin coating a solution of CCMV capsid with enclosed enzyme onto a cleaned objective

glass cover slip followed by rinsing with millipore water after which the measurements were carried out.

5.4.2 Encapsulation of enzyme in the virus cage

The encapsulation of HRP in CCMV has been described extensively elsewhere [1, 20]. In the following the process is briefly illustrated. The CCMV virions were obtained from the infected host plant by first blending and filtering the leaf tissue, followed by extensive filtration, centrifugation and finally dialysis. The coat protein was obtained by disassembly of the virion and removal of the RNA by precipitation with calcium ions followed by centrifugation and dialysis. The actual encapsulation of HRP was performed by mixing an HRP solution with the coat protein dimers and lowering the pH to make the dimers assemble into the capsid around the enzyme.

Buffers used: Capsid buffer pH 5.0: 0.5 M NaCl, 0.05 M $NaCH_3COOH$, 0.01 M $CaCl_2$ and 0.001 M EDTA, the pH is set with HCl. Capsid buffer pH 7.5: 0.5 M NaCl, 0.05 M Tris-HCl, 0.01 M $CaCl_2$ and 0.001 M EDTA, the pH is set with HCl.

5.4.3 Confocal microscope and atomic force microscope sample preparation

Glass cover slips of 24 mm diameter (Gerhard Menzel [Braunschweig, DE] #1.5) were cleaned according to the following procedure: they were rinsed with acetone, sonicated [Branson [Danbury, CT, USA] B-1210-MT) for 5 minutes in an aqueous 1 M NaOH solution, rinsed to pH 7 with MilliQ water and then stored in methanol. Immediately prior to use, the cover slips were put in a UV ozone cleaner (UVP [Upland, CA, USA] PR-100 Photoreactor) for 30 minutes. This cleaned glass was spin-coated (Specialty Coating Systems [Indianapolis, IN, USA] Model P6700 series) with 10 µl of the capsid buffer pH 5.0 containing 3 $\mu g \cdot ml^{-1}$ HRP encapsulated CCMV. The coverslips were immediately rinsed four times with 1 ml of MilliQ to avoid excessive salt crystals forming. The samples were mounted onto the confocal microscope and 200 µl of the capsid buffer pH 5.0 containing 120 µM H_2O_2 and 0.5 µM dihydrorhodamine 6G was added on top.

5.4.4 Detecting the activity of a single nanoreactor

The sample was scanned to locate the fluorescence from the HRP-CCMV capsids. The fluorescent molecules were then bleached by parking the laser on an individual capsid until its fluorescence had diminished. After a few minutes, the area was then scanned again to monitor the recovery of the fluorescence.

5.4.5 pH dependent permeability

In the permeability experiment, the diffusion of fluorescent product molecules from individual capsids was monitored. The pH was varied by adding 2 µl aliquots of an aqueous 0.1 M NaOH solution. The pH was checked with pH paper (Schleicher & Schuell [Dassel, DE] PANPEHA) on the confocal microscope, and separately confirmed by repeating the procedure on a larger scale with a pH meter. After each addition, a scan was made to confirm the continued presence of the capsid, and subsequently a two minute timetrace was recorded. The timetraces were autocorrelated with Labview (National Instruments [Austin, TX, USA] 7.1), Matlab (The MathWorks [Natick, MA, USA] 2010b) scripts or GNU C scripts developed in-house and fitted with Matlab using the simplex search method from Lagarias *et al.* [25] to extract the correlation time. Images of the virus capsid and HRP were created from the crystal structures found in the VIPERdb [26] (Scripps Research Institute [La Jolla, CA, USA]), converted using Discovery Studio Visualizer (Accelrys [San Diego, CA, USA] 2.5.5), and rendered using the Persistence of Vision Raytracer (Persistence of Vision Pty. Ltd. [Williamstown, VIC, Australia] 3.7 beta 40).

5.4.6 Comparison of autocorrelation algorithm speed

5.5 References and notes

[1] M. C. Aragonés, H. Engelkamp, V. I. Claessen, N. A. J. M. Sommerdijk, A. E. Rowan, P. C. M. Christianen, J. C. Maan, B.J.M. Verduin, J. J. L. M. Cornelissen, R. J. M. Nolte, *Nature Nanotechnology* **2007**, 2(10), 635–639, doi: 10.1038/nnano.2007.299.

[2] O. Medalia, I. Weber, A. S. Frangakis, D. Nicastro, G. Gerisch, W. Baumeister, *Science* **2002**, 298(5596), 1209–1213, doi: 10.1126/science.1076184.

[3] D. S. Goodsell, *Trends in Biochemical Sciences* **1991**, 16, 203–206, doi: 10.1016/0968-0004(91)90083-8.

[4] B. J. M. Verduin, *FEBS Letters* **1974**, 45(1–2), 50–54, doi: 10.1016/0014-5793(74)80808-2.

[5] I. J. Minten, L. J. A. Hendriks, R. J. M. Nolte, J. J. L. M. Cornelissen, *Journal of the American Chemical Society* **2009**, 131(49), 17771–17773, doi: 10.1021/ja907843s.

[6] J. A. Speir, M. Sanjeev, G. Wang, T. S. Baker, J. E. Johnson, *Structure* **1995**, 3(1), 63–78, doi: 10.1016/S0969-2126(01)00135-6.

[7] R. W. Noble, Q. H. Gibson, *Journal of Biological Chemistry* **1970**, 245(9), 2409–2413.

[8] M. Filizola, G. H. Loew, *Journal of the American Chemical Society* **2000**, 122(1), 18–25, doi: 10.1021/ja992793z.

[9] R. F. Kubin, A. N. Fletcher, *Journal of Luminescence* **1983**, 27(4), 455–462, doi: 10.1016/0022-2313(82)90045-X.

[10] U. Brinker, J. Mieusset, *Molecular Encapsulation: Organic Reactions in Constrained Systems*, 1st edition, John Wiley & Sons, Ltd, **2010**, ISBN 9780470998076.

[11] F. J. Edd, D. D. Carlo, K. J. Humphry, S. Koster, D. Irimia, D. A. Weitz, M. Toner, *Lab on a Chip* **2008**, 8, 1262–1264, doi: 10.1039/B805456H.

[12] M. Nallani, R. Woestenenk, H.-P. de Hoog, S. van Dongen, J. Boezeman, J. Cornelissen, R. Nolte, J. van Hest, *Small* **2009**, 5, 1138–1143, doi: 10.1002/smll.200801204.

Table 5.2: Comparison of algorithm speeds

Method	Photons	Max ΔT (s)	Code	CPU	Time (s)
bin	553186	N.A.	Labview	1	2
photon	553186	1	Labview	1	816
photon	100000	1	Matlab	1	238
photon	553186	1	C	2	60
photon	553186	10	C	2	203
photon	553186	100	C	2	1001
photon	553186	N.A.	C	2	1026

Comparison of the time required to calculate the autocorrelation function of a typical dataset resulting from a measurement of 120 seconds with an average count rate of 4.6 kHz and containing 553186 photons. Method *bin* is the bin correlation algorithm, *photon* is the inter-photon distance algorithm. Max ΔT is the maximum lag time for photons to be correlated. CPU *1* is an AMD Athlon 64™X2 4400+, CPU *2* is an Intel Core™ 2 Q9550.

[13] M. M. Wang, E. Tu, D. E. Raymond, J. M. Yang, H. C. Zhang, N. Hagen, B. Dees, E. M. Mercer, A. H. Forster, I. Kariv, P. J. Marchand, W. F. Butler, *Nature Biotechnology* **2005**, 23(1), 83–87, doi: 10.1038/nbt1050.

[14] M. Takaharu, A. Ayako, *Chemical & Pharmaceutical Bulletin* **1984**, 32(6), 2395–2400.

[15] T. Mizutani, *Journal of Colloid and Interface Science* **1981**, 79(1), 284–286, doi: 10.1016/0021-9797(81)90073-4.

[16] E. S. Kirkor, A. Scheeline, *The Journal of Physical Chemistry B* **2001**, 105(27), 6278–6280, doi: 10.1021/jp011148n.

[17] J. Lakowicz, *Principles of Fluorescence Spectroscopy*, 2nd edition, Kluwer Academic/Plenum Publishers, **1999**, ISBN 0387312781.

[18] M. Kinjo, R. Rigler, *Nucleic Acids Research* **1995**, 23(10), 1795–1799, doi: 10.1093/nar/23.10.1795.

[19] S. Wennmalm, L. Edman, R. Rigler, *Proceedings of the National Academy of Sciences of the United States of America* **1997**, 94(20), 10641–10646.

[20] M. C. Aragonés, Ph.D. thesis, Radboud Universiteit Nijmegen, **2010**, ISBN 9789090249339.

[21] D. Schomberg, M. Salzmann, , D. Stephan, *Springer Handbook of Enzymes 1.11.1.7*, volume 25, 2nd edition, Springer-Verlag, **1993**.

[22] K. Schätzel: in *Inst. Phys. Conf. Ser.*, volume 77, **1985** pages 175–185.

[23] M. J. Culbertson, D. L. Burden, *Review of Scientific Instruments* **2007**, 78(4), 044102, doi: 10.1063/1.2721116.

[24] T. Laurence, S. Fore, T. Huser, *Optics Letters* **2006**, 31(6), 829–831, doi: 10.1364/OL.31.000829.

[25] J. C. Lagarias, J. A. Reeds, M. H. Wright, P. E. Wright, *SIAM Journal on Optimization* **1998**, 9(1), 112–147, doi: 10.1137/S1052623496303470.

[26] M. Carrillo-Tripp, C. M. Shepherd, I. A. Borelli, S. Venkataraman, G. Lander, P. Natarajan, J. E. Johnson, C. L. Brooks, V. S. Reddy, *Nucleic Acids Research* **2009**, 37(suppl 1), D436–D442, doi: 10.1093/nar/gkn840.

Chapter 6

A matrix

sol-gel entrapment for single molecule experiments on enzymes

6.1 Introduction

6.1.1 Why are sol-gels good matrices for single molecule experiments?

A generic method for enzyme immobilisation would make a great tool in the single enzyme researchers's toolkit; its development would facilitate the study of the single enzyme kinetics of different enzymes. In this context, containers seemed to be especially promising and in the previous chapter we explored a virus as a container, which turned out to limit substrate diffusion. We would like, therefore, to employ a matrix that is more porous and this is where gels come in. Gels are highly porous structures that can be used to entrap the large enzyme molecules while allowing the smaller substrate and product molecules to diffuse in more freely. Agarose gels have been used in the past to anchor enzyme molecules and to study their single molecule behaviour, *e.g.* cholesterol oxidase [1], but previous attempts to examine PalB in agarose and polyacrylamide gels have been unsuccessful [2]. Furthermore, although providing mild chemical conditions, agarose gels do not easily allow for pore size tuning or introduction of functional groups, and require elevated temperatures for processing.

In this chapter, we explore the suitability of two types of sol-gels as enzyme immobilisation media for performing single enzyme experiments.

Sol-gels are promising immobilisation matrices that are advantageous because they have proven to be biocompatible for several enzymes, including lipases [3]. They can be made into thin films consisting of a highly porous network of which the pore size is tunable, which should ensure high substrate mobility. A thin film has intrinsically excellent optical properties because it is highly transparent and displays low Raman scattering. Sol-gels can be made under mild chemical conditions which is needed for the protection of the enzymes. High temperatures are not required, so there is no danger of thermal degradation of the biomolecules. Furthermore, the sol-gel precursors are volatile and hence can be easily purified to a very high degree by distillation, eliminating the contamination with fluorescent compounds. Precursors can be chosen such as to incorporate functional groups into the gel structure.

6.1.2 What are sol-gels?

Sol-gels are made from colloids, which are suspensions of particles with a size of 1–1000 nm in a medium [4]. The particles and the medium can be any phase, except if both gas phases in which case colloid systems cannot be formed since all gasses are miscible. Depending on the phases, colloids have different names, *e.g.* aerosols like fog and smoke (liquid or solid in gas), foams like whipped cream or styrofoam (gas in liquid or solid), emulsions like mayonnaise (liquid in liquid), gels like agar-agar (liquid in solid), or sols like paint (solid in liquid) or ruby (solid in solid).

In the sol-gel process a solid-in-liquid colloid is chemically converted into a liquid-in-solid colloid, or in other words: sol-gels are gels made from sols by means of chemical reactions. It is possible to extract the liquid phase from the sol-gel and thus obtain a dry solid material. Depending on the method of drying (*vide infra*), a porous material—an aerogel—or a dense material—a xerogel—is obtained, as shown in Figure 6.1.

Colloids and the sol-gel process have been known and used for millennia in applications ranging from pigments, via pottery to the manufacture of concrete [5]. The silicon alkoxide sol-gel as we know it today was discovered in the middle of the 19$^{\text{th}}$ century by Jacques-Joseph Ebelmen [6]. Virtually all sol-gel chemists at some point cite the first article by Ebelmen—one of 72 scientists commemorated with an engraving on the Eiffel Tower—as

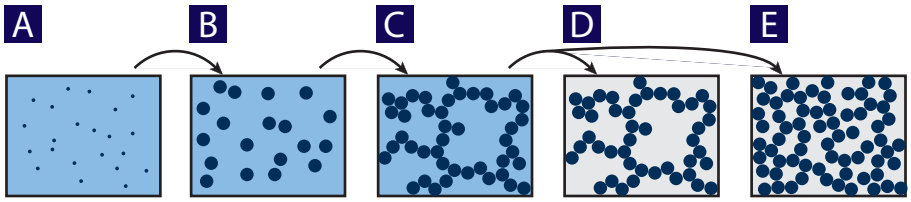

Figure 6.1: In the sol-gel process, A) a solution turns into B) a solid-in-liquid colloid (sol) which then inverts to C) a liquid-in-solid colloid (gel). The liquid can then be removed from the sol-gel to yield either D) a porous solid—an aerogel—or E) a dense solid—a xerogel.

the birth of the sol-gel field, but nearly all place it in the wrong journal, indicating that probably no one actually read it. Ebelmen reacted $SiCl_4$ with ethanol to obtain the compound tetraethoxysilane or tetraethyl orthosilicate (TEOS). He found that the liquid gelled upon exposure to a humid atmosphere [6, 7]. Later research showed that silicon alkoxides polymerise into colloidal particles, the sol. The particles in turn form cross-links and eventually a network, and thereby turn the liquid into the gel.

6.1.3 Chemistry: hydrolysis and condensation

Silicon alkoxides react with water, and in this hydrolysis reaction alkoxide groups are replaced by hydroxyl groups, with alcohols being the byproducts. The hydrolysis can be acid or base catalysed, as is shown in Figure 6.2. The fluoride (F^-) ion is also a good catalyst for the reaction, most likely because it is isoelectronic with and of a similar size as the hydroxyl (OH^-) anion.

Subsequent S_N2-like condensation reactions between the silicon alkoxides produce siloxane bonds (Si-O-Si), alcohol and water. The reaction rate of the condensation step is highest near neutral pH.

The ratio of silicon alkoxide to water is important for the rate of the reactions, and has a profound effect on the evolution of the particle size. Because water is formed in the condensation reaction, a starting molar ratio H_2O:Si of 2 is theoretically sufficient for complete hydrolysis and condensation to SiO_2. In spite of this, the reaction cannot go to completion

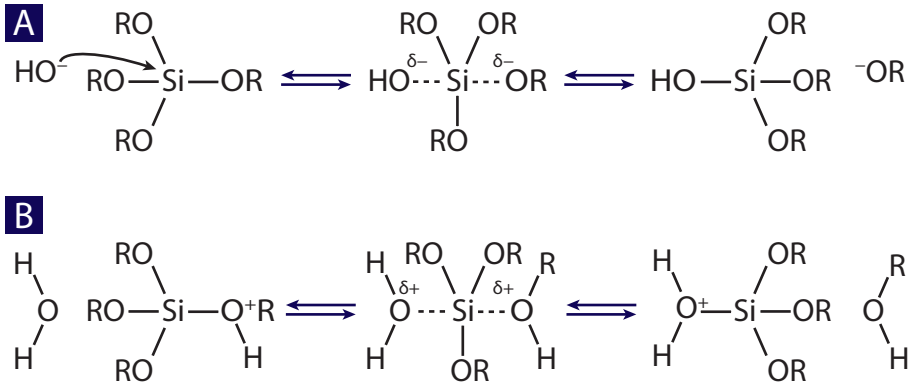

Figure 6.2: A) Base and B) acid catalysed hydrolysis reactions of silicon alkoxides.

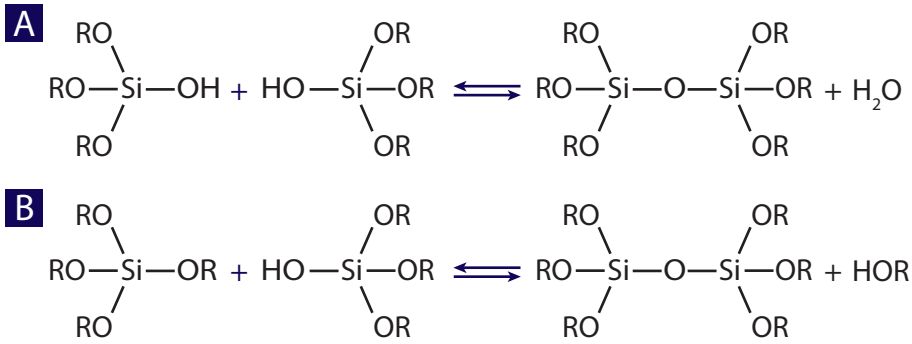

Figure 6.3: A) Water and B) alcohol forming condensation reactions of silicon alkoxides.

even at higher water ratios, since the mobility of the reactants approaches zero as the gel is formed. Furthermore, at the surface of the colloidal particles sites remain available for cross-linking between particles.

6.1.4 Physics: gelation, ageing and drying

The actual gelation is the transition from sol to gel, so from the solid-in-liquid colloidal form to the liquid-in-solid form. The gelation occurs as the colloidal particles form cross-links. During gelation, structural differences in the gel appear as a result of variations in the pH. Hydrolysis and condensation reactions will occur concurrently, but their reaction rates depend divergently on the pH. A different pH will therefore result in a different gel structure. At low pH (<2), hydrolysis is fast but condensation is slow, yielding primarily linear or randomly branched polymers and a network of small colloidal particles. Above pH 7, developing particles are similarly charged and therefore mutually repulsive, thus large and highly branched particles will form that eventually cross-link. Between pH 2 and 7, intermediate structures are formed.

After the transition from liquid to solid, the gel network continues to evolve in a process of dissolution and reprecipitation called ageing, coarsening or ripening [4]. If the gel is allowed to age sufficiently, it builds up mechanical strength—by the continuous formation of more cross-links—and shrinks, forming a xerogel.

If the solvent is allowed to evaporate freely, gels have a tendency to shrink more and crack because of the capillary pressures that build up during the recession of the liquid-vapour interface. Ageing and the associated mechanical strength is important since evaporation can cause the development of large pressure gradients in the liquid phase of the gel. Eventually, the capillary pressure can surmount the mechanical strength of the gel network, with the result of the gel tearing and fracturing. It is also possible to decrease the capillary stress by the addition of surfactants. In order to obtain an aerogel it is necessary to prevent excessive shrinking of the gel, as well as to avoid the damaging stresses caused by the receding liquid-vapour interface. This can be accomplished by avoiding such an interface altogether, *i.e.* by means of supercritical drying. Above the critical point, there is no distinction between liquid and vapour, *ergo* there is no interface, *ergo* there is no cap-

illary pressure. In this way, the liquid phase can be extracted in the absence of forces that would lead to collapse of the pore network. Although we did not have the equipment for supercritical drying, it may be interesting for future single enzyme studies to immobilize the enzyme molecules in aerogels.

6.1.5 Applications

After the original discovery in the 19th century, a profusion of applications (*vide infra*) for silica alkoxide sol-gels arose in the middle of the 20th century. By ageing, drying and a heat treatment, the sol-gel turns into solid silicon dioxide, having the same composition as quartz, which is known for its excellent optical properties. Many applications therefore can be found in optics manufacturing and related fields. Sol-gels are used in the manufacture of optical elements such as optical fibres, lenses, gratings, coatings, doped glasses (filters), and hard contact lenses [4]. Because they can be doped, they are also used to make catalytic materials, as well as chemical sensors [8] and biosensors [9]. Sol-gels are so versatile that it is possible to manufacture micro lenses by inkjet printing of sols [10]. There is even a recent article in which a biosensor is incorporated into a contact lens for the direct measuring of glucose levels in tears [11].

6.2 Results and discussion

The challenge for the present study lies in finding a good procedure that results in a gel with the right distribution of small pores—for entrapping enzymes—and large pores—for fast substrate diffusion—with good optical properties. The extreme pH that is beneficial for silicon alkoxide hydrolysis can be avoided by adding the enzymes later at near-neutral pH—in the stage in which the condensation reactions are dominant.

Silicon alkoxides and water are immiscible and therefore the hydrolysis reaction only takes place at the interface between the liquids. By means of sonication, bubbles can be generated in which water vapour reacts with the alkoxides, increasing the rate of the reaction. Since sonication is often not beneficial to the activity of enzymes [12, 13], we have to sonicate first and add the enzymes later.

To avoid tearing due to gel contraction and surface tension, we made thin films by spincoating and kept the gels wet to avoid evaporation. Furthermore, by adding methyltrimethoxysilane (MTMS), in which the methyl group blocks one site for cross-linking, we aimed to avoid excessive cross-linking so the gel network retains more flexibility and is able to cope better with capillary stress [5].

We used Alexa488-labelled PalB as our enzyme, as in Chapter 3, since lipases are known to retain their activity in sol-gels [3]. We used the same profluorescent substrate (see Figure 6.4) as before in Chapter 4. We have performed control experiments to make sure that neither the silane precursors nor the sol-gel are autofluorescent. Therefore, apart from the labels on the enzyme molecules, the only fluorescent molecules in the experiment are the product molecules. In addition, we made sure that the sol-gels did not speed up the autohydrolysis of the profluorescent substrate.

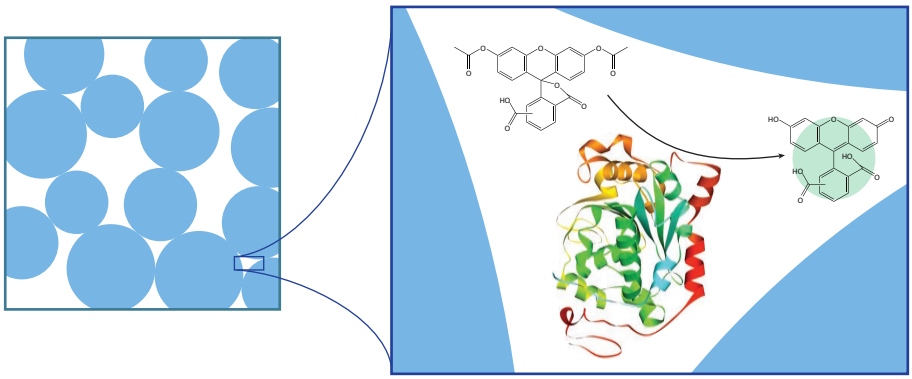

Figure 6.4: Schematic representation of a PalB molecule immobilized in the sol-gel, and the reaction that it catalyses. Nonfluorescent compound (5,6)-carboxyfluoresceindiacetate is converted to the fluorescent molecule (5,6)-carboxyfluorescein.

6.2.1 Preliminary screening of sol-gel recipes

There are many parameters affecting sol-gel formation, the most important being the Si:H_2O ratio, temperature and pH. In search of a compatible gel, we did a preliminary screening of

the parameters using a design-of-experiment (DOE). Since we want to avoid high temperatures, we chose to carry out all experiments at room temperature. We varied the Si:H_2O ratio, the pH (catalyst concentration), and also the TMOS:MTMS ratio. For each parameter we chose three levels, requiring 3^3=27 runs. To keep the amount of runs to a reasonable number, we chose to run with a fractional factorial experimental design and restricted the experiments to a carefully chosen subset of all possible parameter combinations (see Table 6.1). By sacrificing the possibility to determine any interactions between parameters—which are not really expected in this experiment anyway—we can quickly find the main effects.

Table 6.1: Fractional factorial design investigating the effect of various parameters on sol formation.

#	Si	H_2O	H^+	result
1	C	F	Z	sol
2	C	E	X	half sol, half gel
3	C	D	Y	cracked gel pieces
4	B	F	X	sol
5	B	E	Y	sol starting to gel
6	B	D	Z	fractured gel
7	A	F	Y	sol
8	A	E	Z	clear gel
9	A	D	X	clear gel

The composition of each sol-gel mixture is listed, together with the resulting observation on the gel structure. A–C are different molar ratios of the two silane compounds: A) TMOS:MTMS=1:3, B) TMOS:MTMS=1:1, C) TMOS:MTMS=3:1. D–F are different Si:H_2O molar ratios: D) Si:H_2O=1:21, E) Si:H_2O=1:34, F) Si:H_2O=1:75. X–Z are different catalyst concentrations: X) 200 mM HCl, Y) 20 mM HCl, Z) 2 mM HCl. The samples were made in a randomized order to exclude any temporal effects.

From the "statistical analysis", the most important factor was the Si:H_2O ratio. The samples with the least water had all solidified, whereas the ones with most water had not yet gelled. In case of the gelled samples, the ones with the highest concentration of MTMS remained intact—likely because they had cross-linked to a smaller extent and thus had retained more flexibility—whereas the gels with a high concentration of TMOS had all frac-

tured to some degree. The sols that led to intact gels had taken over an hour to mix, and had then quite quickly gelled. Determining the right moment to add the buffered enzyme solution to the sol before it gelled was difficult. In search of a more convenient method, we found in literature [4] that fluoride ions acted as a very fast catalyst. Indeed in a initial test, we noticed that sols can gel in seconds following the addition of sodium fluoride. In addition, the fluoride did not have a strong effect on the pH, unlike the addition of acid or base for instance. We could now rapidly make the sol-gel in the presence of the buffered enzyme solution.

6.2.2 Activity of PalB in a TMOS/MTMS sol-gel

Based on the studies shown in the previous paragraph, we made sol-gels with fluoride as a catalyst, and immediately observed enzyme activity on the microscope in one of those gels. By spincoating sol followed by addition of the fluoride catalyst, we were able to make thin layers of sol-gel on microscope cover slips. Polyvinylalcohol was added to the sol as a macromolecular templating agent. Cracking was avoided by keeping the gels wet.

Samples containing a thin layer of sol-gel immersed in buffer were placed onto the confocal microscope. Confocal images were scanned, as shown in Figure 6.5 to locate the enzyme molecules. To improve image quality, a median filter—which replaces pixels with the median value of the neighbouring pixels [14]—was applied in software to the images in order to eliminate noisy pixels. Additionally, a lowpass filter—which convolves the image with a Gaussian function—was used to soften the sharp artefacts introduced by delays in the signal processing during the scanning of the images. After the image quality was improved in this fashion, fluorescent spots were distinguishable, which we attributed to the fluorescently labelled PalB enzyme molecules.

The successive scans in Figure 6.6 clearly show that nearly none of the fluorescent spots move—though some blink and some are bleached—which points to successful immobilization of the PalB molecules in the sol-gel.

Once located, we added the fluorogenic substrate, and took timetraces of the fluorescent spots. Examples of timetraces taken on a spot and taken on a location in the background are shown in Figure 6.7. The trace taken on a spot shows spikes corresponding to

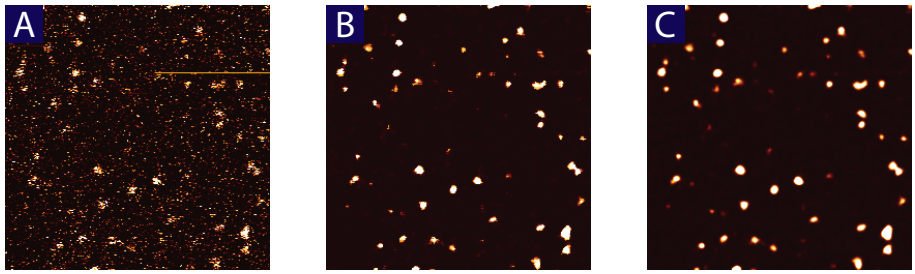

Figure 6.5: A) $10 \times 10\ \mu m^2$ Confocal fluorescence image of Alexa488-labelled PalB enzyme molecules immobilized in the spincoated TMOS/MTMS sol-gel. B) The same image with a square 5×5 pixel median filter. C) The same image with the median filter and an additional 1 pixel lowpass filter.

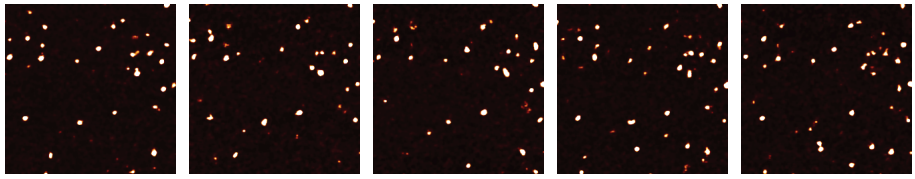

Figure 6.6: $10 \times 10\ \mu m^2$ Confocal fluorescence images of Alexa488-labelled PalB enzyme molecules in the TMOS/MTMS sol-gel, taken sequentially at five minute intervals.

bursts of fluorescence, whereas the trace taken on a location in the background shows only Poisson noise.

The autocorrelation of the time trace in Figure 6.7A was calculated as shown in Figure 6.7C. Lu *et al.* [15] found in their experiment with cholesterol oxidase that the autocorrelation of the fluorescence intensity did not fit to a single exponential function (See Equation 5.5). In the short trace shown in Figure 6.7A, the data does fit to a single exponential function, which is expected for a reaction between two states [16], with a fitted decay time τ of 13.5 ms. The decay time is the reciprocal of the sum of the forward and backward rates, but we do not know the relative contribution of those rates to the decay time. We therefore needed to look at single turnovers.

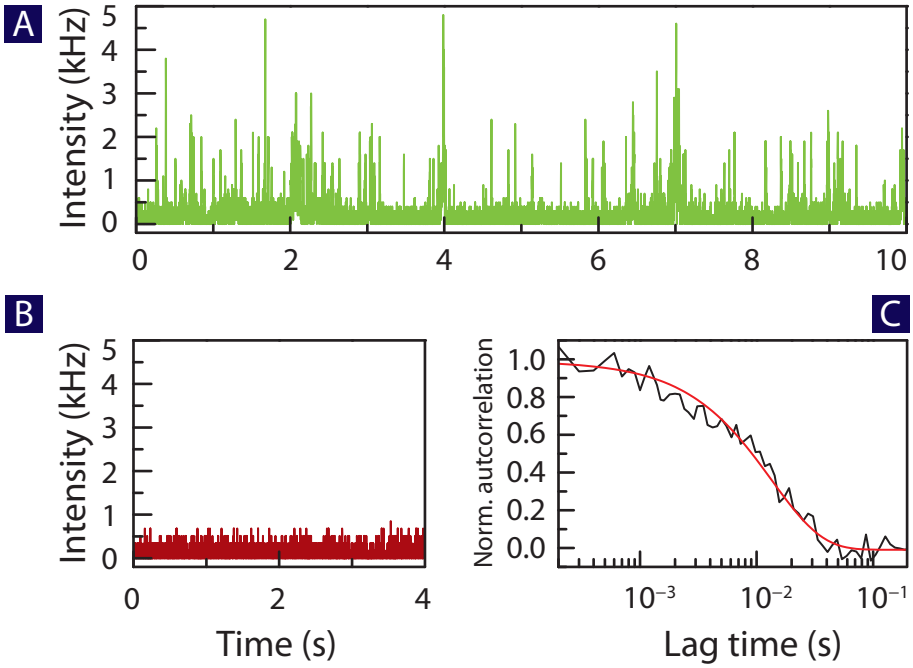

Figure 6.7: Fluorescence intensity time traces of sol-gel immobilized PalB, binned at 1 ms, taken A) on a fluorescent spot and, B) on a location in the background. C) Normalised autocorrelation function of the timetrace in A (black line), with single exponential fit (red line).

We were able to measure the activity of one particular PalB molecule for nearly one hour. Parts of that trace are shown in Figure 6.8. We used a change point algorithm (see Section 4.2.2) to convert the trace into a binary state trajectory, which is shown in the same figure. In the two-state trace of 3388 s, we found 15526 turnovers at an average turnover rate of 4.5 s^{-1} with a mean offtime of 193 ± 251 ms, and a mean ontime of 25 ± 59 ms. Figure 6.9 shows the turnover rate of a single PalB enzyme molecule as a function of time—with a resolution of 1 s—and its histogram and its autocorrelation. The turnover rate is constant over time at these time scales, and there is no sign of stepwise deactivation, as has been observed earlier for the enzyme chymotrypsin [17]. The histogram fits well to a Guassian peak with

an average turnover rate of 3.9 s^{-1}. The autocorrelation of the turnover rates shows a single exponential decay with a τ of 151 s. We suspect that this decay has no biological basis, but may rather be an artefact from the change point analysis, which had to be carried out for each 100 s segments as the complete trace was too lengthy to process in one go.

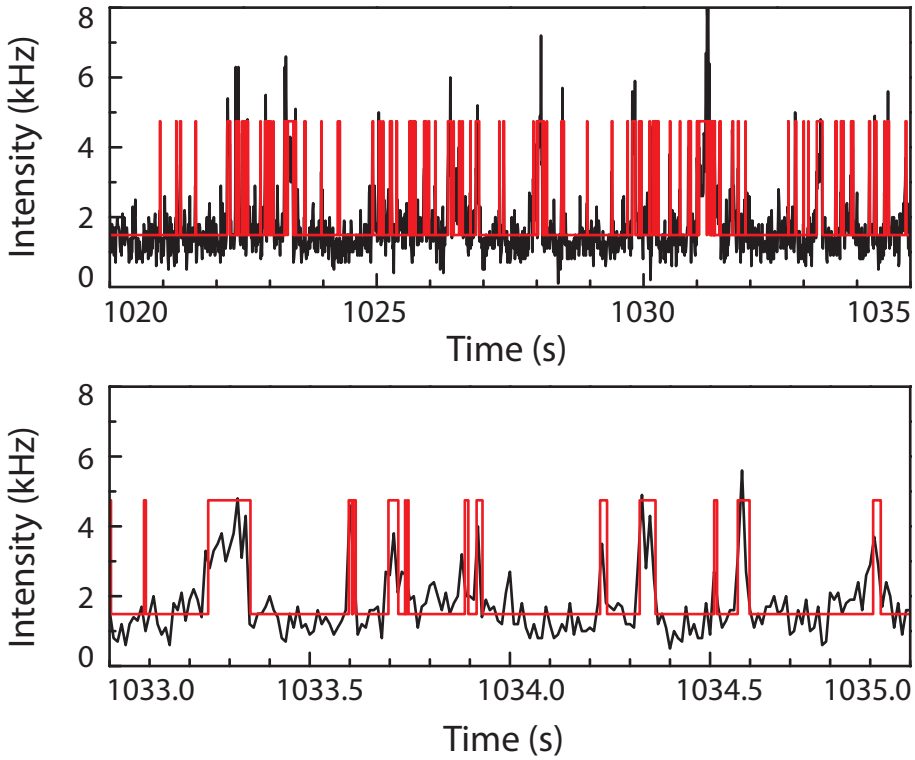

Figure 6.8: Parts of the fluorescence intensity timetrace, taken for a single PalB molecule, binned at 10 ms (black line) with the binary levels generated with the change point algorithm (red line).

The ontimes and offtimes of the binary trace, and a histogram of the ontimes and offtimes are shown in Figure 6.10. Neither histograms fits to a single exponential function at short times (<0.1 s). The long decay component τ is 232 ms for the offtimes and 61 ms

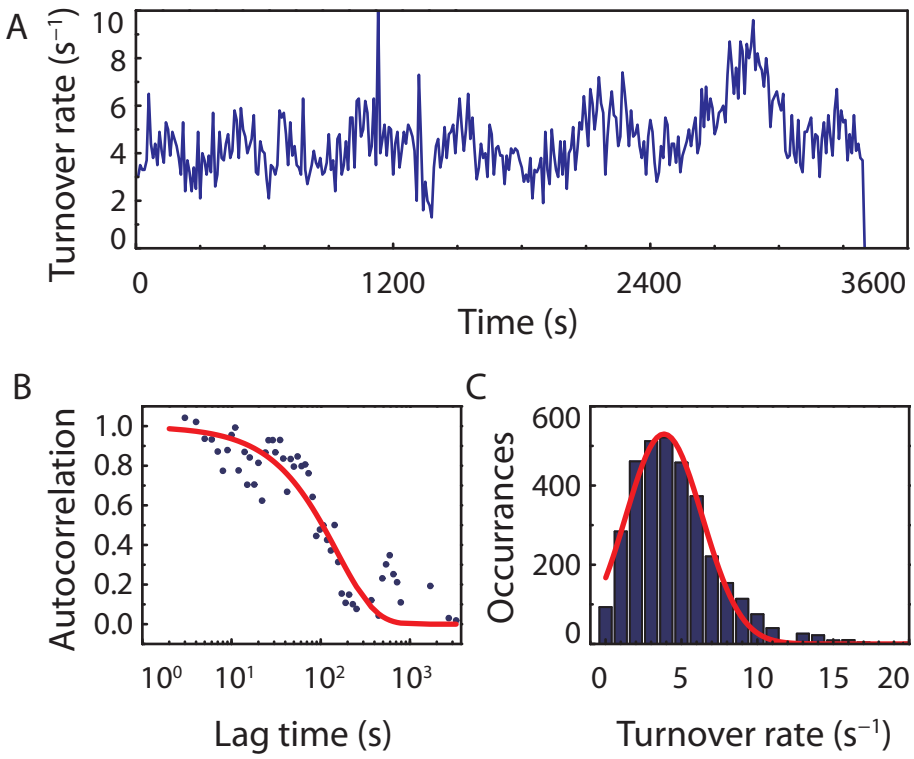

Figure 6.9: A) Turnover rate of a single PalB enzyme plotted over the experiment time. B) Autocorrelation of the turnover rate (blue dots), with single exponential fit (red line). C) Histogram of the turnover rates (blue bars), with gaussian fit (red line).

for the ontimes, which are obviously longer than the mean values found in the two-state trajectories, since the short components are not taken into account. The overabundance of short offtimes brings to mind the memory effect that was used to explain similar results originally by Lu *et al.* [15] for cholesterol oxidase and more recently by Flomenbom *et al.* for PalB [18, 19].

To see if there are trends in the turnover times, we constructed 2D histograms of the time between *n* turnovers (see Figure 6.11). These histograms plot, on logarithmic time scales, the probability distribution *P(t(i),t(i+n))* for the correlation between turnovers spaced *n* turnovers apart, corrected by subtraction of the chance *P(t(i))P(t(i+n))*, yielding the difference distribution of turnover times [17, 20].

The diagonal feature, present in the figure showing the data for n=1, indicates that short turnover times are more often followed by short waiting times, than can be expected from statistics. Conversely, long turnovers are more often followed by long turnovers. This memory effect disappears as the interval separating the turnovers increases.

However, many PalB enzyme molecules were found to be inactive. In many samples there was a dearth of active enzyme molecules. It is currently unknown if they are inactivated by the conditions of the sol-gel or if they are deprived of substrate. Lipases have been immobilized before—in bulk conditions—in sol-gels for catalysis with excellent results [3]. It is possible that PalB does not survive the conditions it is presented with in the current sol-gel system. However, it seems more likely that many enzymes are trapped in pores that are too small for the substrate to diffuse into. In support of this is the fact that we did not find PalB enzyme molecules diffusing through the sol-gel, either by means of FCS or by means of comparing sequential scanned confocal images. They therefore appear particularly tightly secured in the sol-gel network, and this may be the reason that only few enzyme molecules are accessible for substrate molecules.

6.2.3 Ethylene glycol modified silane precursors

TMOS (tetramethoxyorthosilane) and TEOS (tetraethoxyorthosilane) release methanol and ethanol, respectively, upon hydrolysis, which are not necessarily bio-friendly chemicals, especially in the high concentrations that can occur as each silane molecule releases up

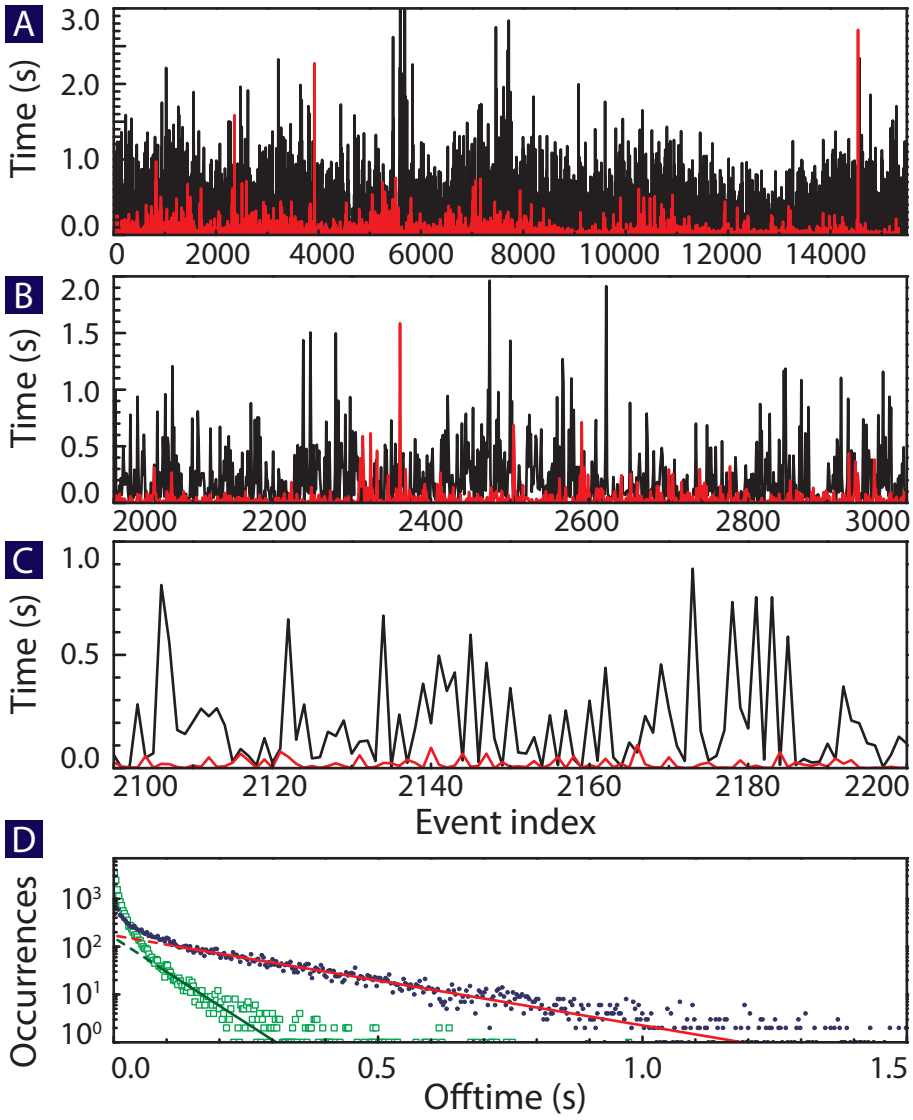

Figure 6.10: A, B and C) Offtimes (black) and ontimes (red) of a single PalB molecule. D) Histogram of the offtimes (blue dots) and ontimes (green squares) of a single PalB molecule. Both histograms deviate from single exponential fits (solid red line for the offtimes, solid green line for the ontimes—the dashed lines are extrapolations) at times shorter than 0.1 s.

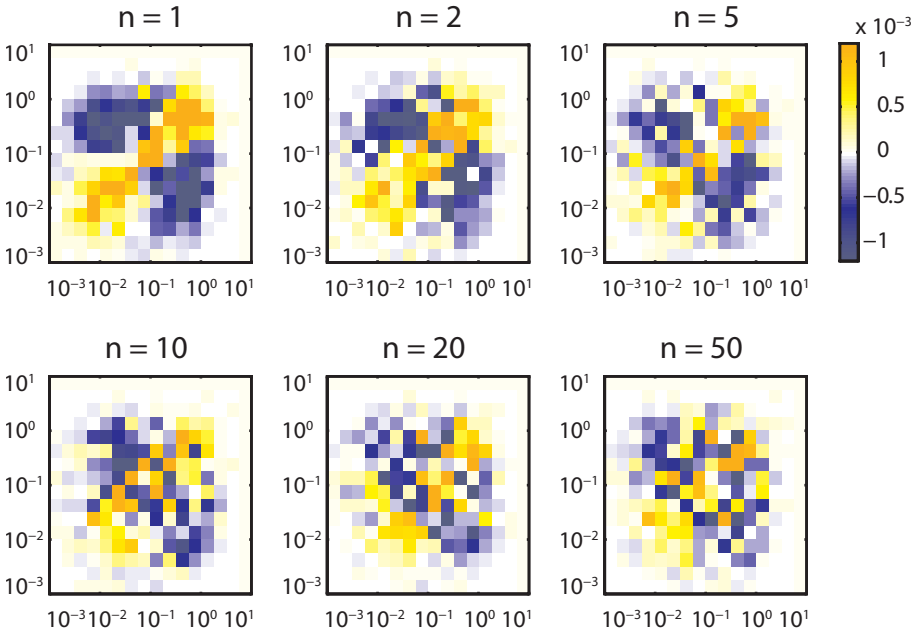

Figure 6.11: 2D histograms of turnovers of a single PalB molecule spaced *n* events apart. The time between turnover events is plotted in seconds on a logarithmic scale. The diagonal feature that is prominent at n=1 disappears as the event lag is increased.

to four alcohol molecules during the condensation reaction. In search of other precursor compounds, we came across the family of ethylene glycol-based silanes [21]. In particular, the compounds ethylene glycol modified silane (EGMS) and methyl ethylene glycol modified silane (MEGMS) seemed suitable. The ethylene glycol released during hydrolysis is considered to be much less denaturating to proteins than methanol. An additional advantage of these precursors is that they are miscible with water due to the presence of the hydroxyl groups at the end of the side chains, making the hydrolysis of EGMS much faster than that of TMOS or TEOS, especially near neutral pH.

To explore the usefulness of EGMS and MEGMS, we set up another screening experiment using a fractional factorial design. As the parameters, we chose the H_2O:Si ratio, the

concentration of the macromolecular additive polyvinylalcohol (PVA), the EGMS:MEGMS ratio, and the pH. The tested combinations are listed in Table 6.3 in the experimental section. Ideally, we would like to find a gel that strongly retains the enzyme molecules that were added before the condensation of the gel, but allows for fast diffusion of substrate and product molecules, so that the kinetics of the immobilized enzyme molecules are not affected. On dry gels, analysis methods such as mercury penetration [22] and nitrogen desorption porosimetry [5, 23] are used to get an indication of the porosity and pore size distribution. However, since we are working with wet gels, this is not possible. We have therefore used electron microscopy and fluorescence correlation spectroscopy to analyse the gels. As a start, we manually scored—on a scale of 1–5—the gels obtained from each parameter combination from the design according to a visual examination as well as an inspection of tomography electron microscopy (TEM) images, where we considered gel structure and pore size distribution. Gels that fractured or were very dense—*i.e.* had no visible pores—received low scores, whereas gels that formed nice thin layers or had visible pores were given higher scores. The results are summarized in Figure 6.12, the full experimental conditions and scores can be found in Table 6.3. Typical TEM images are shown in Figure 6.13.

From the screening results we observed that there is a—weak—correlation between gel score and H_2O:Si ratio. The initial rate of hydrolysis is dependent on H_2O concentration, and a faster reaction may have advanced the state of gel formation. The analysis seems to suggest that the addition of more H_2O would be opportune. The addition of a low concentration of the macromolecular additive PVA has a beneficial effect on the gel structure, as was previously found for TMOS gels [24]. Unlike the TMOS gels however, we found that while the addition of the methylated silane—MEMGS in this case—improved the gel, a surplus of methylated silane provided no extra enhancement. The pH of the aqueous solution did not have any effect in the range of pH 6–8, which is fortunate since it provides some flexibility in the pH of the buffered enzyme solution.

To see which gels were porous enough to allow a good diffusion of small molecules—like enzymatic substrate and product molecules—we checked if we could measure the diffusion of the dye molecule Alexa488 in each sol-gel using our confocal microscope (see Table 6.2). For gels 10,16,21 and 28, we measured the diffusion time of Alexa488, which was

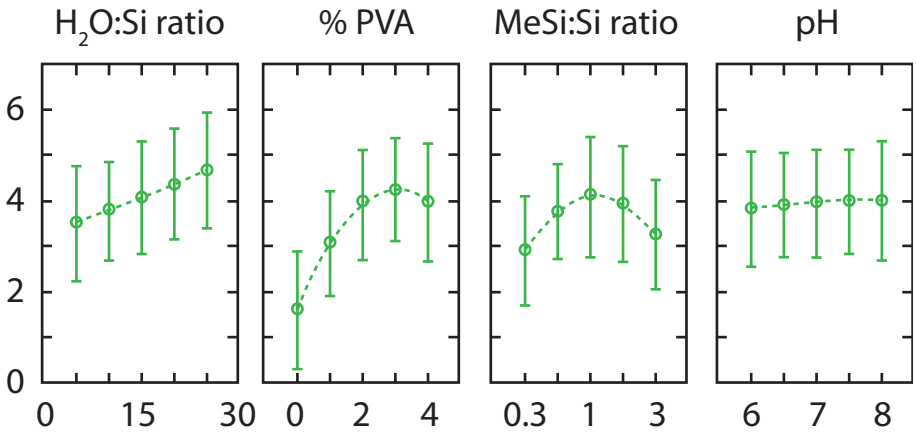

Figure 6.12: Results of screening of experiment parameters. The values of each parameter are given on the x-axis and the score of the gel is indicated on the y-axis. The gels' score increase with increasing H_2O:Si ratio and the addition of PVA. A 1:1 ratio of EGMS and MEGMS is optimal. The pH has no influence within the screened interval.

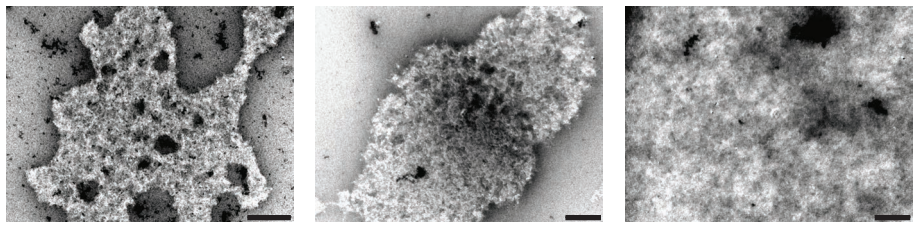

Figure 6.13: Transmission electron microscopy images of EGMS sol-gels 6, 1 and 7 (see Table 6.3) from left to right. The black bar in the lower right corner of each image corresponds to 200 nm.

0.1 ms. This number agrees well with the diffusion time of the similarly sized dye molecule rhodamine 6G in water (0.2 ms) which we measured previously, see Chapter 3. In gels 2,4,13–15 and 24, the diffusion time of the dye molecule was slower that of rhodamine 6G in solution, in some cases by three orders of magnitude. In gels 11,12,18 and 23, the fluorescence intensity data displayed a positive autocorrelation, but the autocorrelation data did not fit a standard diffusion model, see Figure 6.14. In the remainder, we detected neither autocorrelation nor diffusion.

We found four gels in which the diffusion of the small molecule Alexa488 was apparently not decreased by the gel structure. We decided to focus on these gels for further investigations. Interestingly, the gels in which we measured the diffusion of dye molecules did not receive high scores in the preliminary screening. It seems, therefore, that a visual assessment of the porosity of a sol-gel is not a good indicator of diffusion-permissive properties for single-molecule experiments, and fluorescence correlation spectroscopy seems to be the only available alternative. We have previously seen in agarose gels by means of FCS that diffusion was slower at the air–gel interface than in the interior of the gel, and we attributed this to local drying effects of the gel near the air–gel interface. Since we expected a similar process in sol-gels, we did not feel that examination of the sol-gel by means of atomic force microscopy—which is necessarily superficial—would expose significant information about the interior of the gel.

The sequential images in Figure 6.15 show that many—though not all—fluorescently labelled enzyme molecules move between images. By means of FCS we also observed diffusion of the PalB molecules. The many enzyme molecules that are diffusing interfere in the observation of the immobilized enzymes. We were therefore unable to record any activity of PalB molecules in the EGMS based sol-gels.

6.3 Conclusions

Single PalB enzyme molecules were successfully immobilised in a TMOS/MTMS sol-gel. Nearly all enzyme molecules were found to be stationary. A few enzyme molecules showed activity, as observed by the formation of fluorescent product molecules on the addition of a profluorescent substrate. One PalB molecule was observed to be active for nearly one

Table 6.2: Diffusion times of Alexa488 dye molecules in the EGMS-based sol-gels.

#	τ_D (ms)	#	τ_D (ms)	#	τ_D (ms)
1	–	11	*	21	0.1
2	19	12	*	22	–
3	–	13	0.8	23	*
4	12	14	12	24	37
5	–	15	17	25	–
6	–	16	0.1	26	–
7	–	17	–	27	–
8	–	18	*	28	0.1
9	–	19	–	29	–
10	0.1	20	–	30	–

A dash indicates that no autocorrelation was observed. An asterisk indicates autocorrelation data that did not fit the diffusion model. An example of an autocorrelation function that did not fit a diffusion model is given in Figure 6.14 for sample 11.

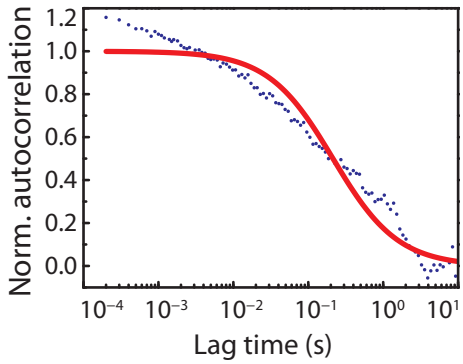

Figure 6.14: An example of an autocorrelation function (sample 11 from Table 6.2, blue dots) that did not fit a diffusion model (red line). The shape of the curve is reminiscent of samples in which objects of various sizes are diffusing through the focus. Alternatively, the dye molecules might reversibly adsorb to the sol-gel, which would also cause fluorescence bursts of various lengths.

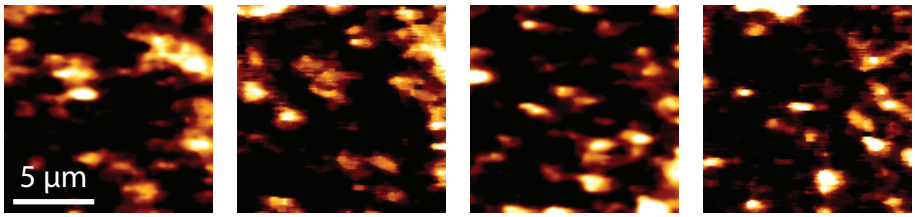

Figure 6.15: 12.8×12.8 µm^2 Confocal fluorescence images of Alexa488-labelled PalB enzyme molecules in sol-gel sample 10 from Table 6.2, taken sequentially at circa one minute intervals.

hour. In many other immobilisation methods, most enzyme molecules are inactive, and the sol-gel is no exception. It is currently unknown if this is the result of enzyme inactivation or of substrate diffusion limitations. We have also investigated ethylene glycol–modified silane–based sol-gels as immobilisation media. As it turns out, the enzyme molecules were found to be mobile in the gels of our parameter screening experiment. As a result, no enzyme activity could be observed in EGMS gels.

6.4 Experimental

6.4.1 Confocal microscope and atomic force microscope setup

Laser light of 488 nm (Spectra-Physics [Mountain View, CA, USA] 2080 argon ion laser) was coupled into a single-mode optical fibre (Thorlabs [Newton, NJ, USA] P1-460-FC-5), reflected by a dichroic beam splitter (Chroma [Bellows Falls, VT, USA] 505dcxr) and focused onto the sample by an oil immersion 100x objective (Carl Zeiss [Jena, DE], NA=1.30), which was mounted on an inverted microscope (Carl Zeiss Axiovert 200). Fluorescent light coming from the focal volume was collected by the same objective, passed through the dichroic beam splitter, focused through a 50 µm pinhole and subsequently focused onto an avalanche photodiode (PerkinElmer [Waltham, MA, USA] SPCM-AQR-14). The photon count signals were recorded as inter-photon arrival times with a resolution on 50 ns using a data acquisition card (National Instruments [Austin, TX, USA] PCI-6036E).

6.4.2 Preliminary screening of sol-gel recipes

Mixtures A, B and C were prepared by mixing tetramethoxyorthosilane (TMOS) and methyltrimethoxysilane (MTMS) in ratios of 1:3,1:1 and 3:1, respectively, to a final volume of 1 ml in an Eppendorf vial. A volume of 100 µl of the silane mixture was then mixed with the following amount of water, D (23 µl), E (40 µl) or F (90 µl). The samples were sonicated for 90 minutes.

6.4.3 Activity of PalB in a TMOS/MTMS sol-gel

The sol was prepared by mixing 50 µl TMOS with 50 µl MTMS and 10 µl 4% PVA, and then sonicating the mixture for 10 minutes. Subsequently, 10 µl 1 ppm Alexa488-labelled PalB was added and the mixture was gently shaken. 10 µl of the sol was spincoated onto a coverslip glass at low speed, followed by 2 µl 1M NaF solution at high speed. The samples were rinsed profusely with MilliQ water (>20 ml) and kept wet. The coverslip was mounted onto the microscope, and subsequently 100 µl of 0.1 M pH 7.5 buffer followed by 5 µl of a freshly prepared 1 mM aqueous solution of the substrate carboxyfluorescein diacetate (CFDA) was added.

The fluorescence intensity timetraces were cut into 100 s segments and processed with the change point algorithm as implemented in C by the Haw Yang group [25] [version 1.11, parameters: type-I error 5%, 95% selection confidence interval]. The change points of all the segments thus obtained were recombined to obtain complete binary traces. The binary traces were processed using Labview (National Instruments [Austin, TX, USA] 7.1), Matlab (The MathWorks [Natick, MA, USA] 2010b) scripts or GNU C scripts developed in-house and fitted with Matlab fitted using the simplex search method from Lagarias *et al.* [26] to extract correlation times, 'on' times and 'off' times.

6.4.4 Ethylene glycol modified silane precursors

Confocal microscopy samples were prepared by depositing a volume of 5 µl of each sample (as formulated in Table 6.3) on a clean coverslip glass and spinning for 20 s at 3000 RPM.

Transmission Electron Microscopy (TEM) images of the gels were taken as follows. A droplet of the sample was put on a C-grid that had been made hydrophilic by the stan-

Table 6.3: Fractional factorial design investigating the effect of various parameters on sol formation.

Exp. num.	Block	Si:H_2O	% PVA	MEGMS:EGMS	pH	Score
1	2	2.0	2	1.0	8	4
2	2	2.0	2	1.0	6	5
3	2	1.0	0	0.3	7	1
4	2	0.5	2	1.0	8	3
5	2	1.0	4	3.0	7	4
6	2	1.0	2	1.0	7	2
7	2	1.0	4	0.3	7	2
8	2	0.5	2	1.0	6	4
9	2	1.0	2	1.0	7	5
10	2	1.0	0	3.0	7	1
11	3	1.0	2	1.0	7	4
12	3	1.0	0	1.0	6	1
13	3	2.0	2	0.3	7	4
14	3	0.5	2	0.3	7	2
15	3	1.0	0	1.0	8	2
16	3	0.5	2	3.0	7	3
17	3	2.0	2	3.0	7	5
18	3	1.0	4	1.0	8	3
19	3	1.0	4	1.0	6	5
20	3	1.0	2	1.0	7	4
21	1	2.0	4	1.0	7	4
22	1	1.0	2	3.0	6	2
23	1	0.5	4	1.0	7	3
24	1	1.0	2	3.0	8	2
25	1	1.0	2	0.3	6	1
26	1	0.5	0	1.0	7	1
27	1	1.0	2	0.3	8	5
28	1	2.0	0	1.0	7	1
29	1	1.0	2	1.0	7	2
30	1	1.0	2	1.0	7	5

The composition of each sol-gel mixture is listed, as determined by Si:H_2O ratio, percentage of the macromolecular additive polyvinylalcohol (PVA), the ratio between methylated and unmethylated silane, and the pH. On the right, the score as judged from TEM images is given. The samples were made in randomized order, so to exclude any temporal effects.

dard "glow-charge" method. Each sample was then stained using a 0.02 (v/v)% solution of uranylacetate in MilliQ. The TEM-measurements were carried out the following day.

6.5 References and notes

[1] X. S. Xie, H. P. Lu, *The Journal of Biological Chemistry* **1999**, 274(23), 15967–15970, doi: 10.1074/jbc.274.23.15967.

[2] K. Velonia, O. Flomenbom, D. Loos, S. Masuo, M. Cotlet, Y. Engelborghs, J. Hofkens, A. Rowan, J. Klafter, R. Nolte, F. de Schryver, *Angewandte Chemie International Edition* **2005**, 44(4), 560–564, doi: 10.1002/anie.200460625.

[3] M. T. Reetz, A. Zonta, J. Simpelkamp, *Biotechnology and Bioengineering* **1996**, 49(5), 527–534, doi: 10.1002/(SICI)1097-0290(19960305)49:5<527::AID-BIT5>3.0.CO;2-L.

[4] C. J. Brinker, G. W. Scherer, *Sol-Gel Science: The physics and chemistry of sol-gel processing*, Academic Press, **1990**, ISBN 9780121349707.

[5] J. D. Wright, N. A. J. M. Sommerdijk, *Sol-gel materials: chemistry and applications*, CRC press, **2003**, ISBN 9789056993269.

[6] J.-J. Ebelmen, *Comptes Rendus de l'Académie des Sciences* **1845**, 21, 502–505.

[7] J.-J. Ebelmen, *Annales de chimie et de physique* **1846**, 16, 129–166.

[8] B. Mac Craith, C. Mc Donagh, A. McEvoy, T. Butler, G. O'Keeffe, V. Murphy, *Journal of Sol-Gel Science and Technology* **1997**, 8, 1053–1061, doi: 10.1023/A:1018338426081.

[9] J. Jia, B. Wang, A. Wu, G. Cheng, Z. Li, S. Dong, *Analytical Chemistry* **2002**, 74(9), 2217–2223, doi: 10.1021/ac011116w.

[10] A. Voigt, U. Ostrzinski, K. Pfeiffer, J. Kim, V. Fakhfouri, J. Brugger, G. Gruetzner, *Microelectronic Engineering* **2011**, 88(8), 2174–2179, doi: 10.1016/j.mee.2010.12.004.

[11] H. Yao, A. J. Shum, M. Cowan, I. Lähdesmäki, B. A. Parviz, *Biosensors and Bioelectronics* **2011**, 26(7), 3290–3296, doi: 10.1016/j.bios.2010.12.042.

[12] W. T. Coakley, R. C. Brown, C. J. James, R. K. Gould, *Archives of Biochemistry and Biophysics* **1973**, 159(2), 722–729, doi: 10.1016/0003-9861(73)90512-2.

[13] B. Özbek, K. O. Ülgen, *Process Biochemistry* **2000**, 35(9), 1037–1043, doi: 10.1016/S0032-9592(00)00141-2.

[14] JPK Instruments AG: *JPK Data Processing Manual*, 4.0 edition, **2011**.

[15] P. Lu, L. Xun, S. Xie, *Science* **1998**, 282(5395), 1877–1882, doi: 10.1126/science.282.5395.1877.

[16] J. Wang, P. Wolynes, *Phys. Rev. Lett.* **1995**, 74, 4317–4320, doi: 10.1103/PhysRevLett.74.4317.

[17] G. De Cremer, M. B. J. Roeffaers, M. Baruah, M. Sliwa, B. F. Sels, J. Hofkens, D. E. De Vos, *Journal of the American Chemical Society* **2007**, 129(50), 15458–15459, doi: 10.1021/ja077621d.

[18] O. Flomenbom, J. Hofkens, K. Velonia, F. Deschryver, A. Rowan, R. Nolte, J. Klafter, R. Silbey, *Chemical Physics Letters* **2006**, 432(1–3), 371–374, doi: 10.1002/prot.20893.

[19] H. Rigler, Rudolf; Vogel (editor), *Single Molecules and Nanotechnology*, volume XIV, Springer, **2008**, ISBN 9783540739234.

[20] H.-P. Lerch, A. S. Mikhailov, R. Rigler, *Chemical Physics* **2007**, 331(2–3), 304–308, doi: 10.1016/j.chemphys.2006.10.025.

[21] S. Hartmann, D. Brandhuber, N. Hüesing, *Accounts of Chemical Research* **2007**, 40(9), 885–894, doi: 10.1021/ar6000318.

[22] H. Giesche, *Particle & Particle Systems Characterization* **2006**, 23(1), 9–19, doi: 10.1002/ppsc.200601009.

[23] S. Brunauer, P. H. Emmett, E. Teller, *Journal of the American Chemical Society* **1938**, 60(2), 309–319, doi: 10.1021/ja01269a023.

[24] M. T. Reetz, A. Zonta, J. Simpelkamp, *Angewandte Chemie International Edition in English* **1995**, 34(3), 301–303, doi: 10.1002/anie.199503011.

[25] L. P. Watkins, H. Yang, *The Journal of Physical Chemistry B* **2005**, 109(1), 617–628, doi: 10.1021/jp0467548.

[26] J. C. Lagarias, J. A. Reeds, M. H. Wright, P. E. Wright, *SIAM Journal on Optimization* **1998**, 9(1), 112–147, doi: 10.1137/S1052623496303470.

Summary

The cel is nature's factory and enzymes are its machines. We have come to rely on these machines for many processes, from the making of beer to washing our laundry. Much has been published on the kinetics of enzymes starting almost one century ago with the work of Michaelis and Menten, and it is generally thought to be a well understood subject. However, with a single exception, all of this work has focussed on enzyme kinetics at an ensemble level, *i.e.* by observing many molecules at the same time. Advances in optical microscopy have made it possible to look at single molecules and early single enzyme experiments have indicated that perhaps we do not yet know everything there is about the way enzymes work; single enzyme molecules may or may not work intermittently and at fluctating rates.

To study single enzyme molecules, certain practical preconditions must be met: apart from keeping background noise to a minimum—which is a challenge in all single molecule experiments—there has to be a way of detecting enzyme turnovers, and there should be some method of observing an enzyme molecule for a long period of time to study the turnover rate in time. The solution to the first challenge is to use substrates that are converted by the enzyme into brightly fluorescent molecules, which are observed with a highly sensitive detector. The second issue has become the focus of this very thesis. Due to Brownian motion, the enzyme molecules that we have studied in solution move around much too fast to observe enzymatic turnovers. Several strategies have been explored to address this issue.

Larger objects experience less Brownian motion and therefore we encapsulated *Pseudozyma antarctica* lipase B (PalB) enzyme molecules in a large container, *viz.* the empty protein shell of a plant virus named cowpea chlorotic mottle virus (CCMV). As it turned out, the diffusion of the virus container was still faster than the rate of the enzyme molecule and therefore no enzymatic activity could be observed. Attempts to investigate the assem-

bly and disassembly behaviour of the virus container using fluorescence correlation spectroscopy (FCS) proved unsuccesful. For future research it would be interesting to examine cascade reactions in containers, and therefore—as a start—we showed by means of dual-colour FCS that a PalB enzyme molecule can be co-encapsulated with the green fluorescent protein (GFP) in a CCMV container.

Direct absorption onto a hydrophobic glass surface yielded a few active PalB molecules, which we were able to follow up to several hours. Individual enzymatic turnover events were extraced from the fluctuating fluorescence data with a change-point algorithm. Analysis of the distribution of the times between turnovers provided further evidence for a memory effect that was earlier found for PalB. However, the large number of molecules that appeared to move on the surface indicated weak binding, and also the majority of the enzyme molecules did not appear to be active. Therefore this method was found to be too unreliable for further experiments.

The combination of the previous two strategies of encapsulation and surface immobilisaiton led to studies in which enzyme-filled virus particles are observed on a surface. Virus containers with another enzyme, horseradish peroxidase (HRP), were absorbed onto a glass surface. The fluorescent product molecules that were generated by the enzyme accumulated on the inside of the container which made them appear as bright spots in our microscope images. The activity of enzyme molecules on the inside of the container could be distinguished from the activity of enzyme molecules that were accidentally absorbed on the outside of the container by differences in the autocorrelation functions of the fluorescence signals. Advances in autocorrelation analysis methods allowed us to observe correlations at short times down to a microsecond. Individual turnovers of the enzyme could not be seen, however, because they were lost in the large signal of the accumulated product molecules. The diffusion barrier imposed by the virus container likely also restricts the substrate concentration available to the encapsulated enzyme molecule.

Finally, single PalB enzyme molecules were immobilised in various sol-gels. In a preliminary screening of new ethylene glycol-modified silane-based sol-gels the enzyme molecules were found to be mobile. In a so-called TMOS-MTMS sol-gel, nearly all enzyme molecules were found to be stationary, but only a few of them showed activity. One PalB molecule was observed to be active for nearly one hour, but this was not enough to be statistically significant. In many other matrices for immobilisation most enzyme molecules are inactive, and the sol-gel matrix is no exception. It is currently unknown if this is the result of enzyme inactivation or of substrate diffusion limitations.

Samenvatting

De cel is de fabriek van de natuur en enzymen zijn haar machines. We maken gebruik van deze machines voor vele processen, van het brouwen van bier tot het reinigen van ons wasgoed. Sinds Michaelis en Menten er bijna een eeuw geleden over schreven is er veel gepubliceerd over enzymkinetiek, en men gaat er in het algemeen van uit dat het bekende stof is. Desalniettemin is dit onderzoek op een enkele uitzondering na altijd uitgevoerd op ensembleniveau, dat wil zeggen met grote hoeveelheden enzymen tegelijk. Door de technologische vooruitgang in optische microscopie is het tegenwoordig mogelijk om naar individuele moleculen te kijken en voorlopig onderzoek heeft aanwijzingen opgeleverd dat we misschien toch nog niet alles weten over de manier waarop enzymen werken; enkelvoudige enzymmoleculen werken misschien slechts af en toe en dan ook nog in een wisselend tempo.

Voordat men enkelvoudige enzymmoleculen kan bestuderen moeten aan bepaalde voorwaarden worden voldaan: naast het zo veel mogelijk elimineren van achtergrondlicht—hetgeen in alle experimenten met enkelvoudige moleculen een uitdaging is—is er een manier nodig om individuele omzettingsstappen te kunnen detecteren en daarnaast is het noodzakelijk om het enzym gedurende een langere periode te kunnen observeren om fluctuaties in de omzettingsfrequentie te kunnen meten. Aan de eerste conditie is te voldoen door substraten te gebruiken die door het enzym worden omgezet in sterk fluorescerende moleculen die vervolgens met een zeer gevoelige detector waargenomen kunnen worden. De tweede uitdaging is eigenlijk het hoofdonderwerp van dit proefschrift geworden. Door de Brownse beweging verplaatsen enzymmoleculen in oplossing zich veel te snel om enzymatische omzettingen te kunnen detecteren. Een aantal strategiën is gevolgd om deze uitdaging aan te gaan.

Grote objecten ondergaan minder Brownse beweging en daarom hebben we als eerste het enzym *Pseudozyma antarctica* lipase B (PalB) gestopt in een soort grote verpakking, namelijk in het lege eiwitomhulsel van het plantenvirus cowpea chlorotic mottle virus (CCMV). Het bleek echter dat de diffusie van die virusmantel dan nog steeds sneller is dan

de omzettingssnelheid van het enzym en we konden daarom geen activiteit waarnemen. Het lukte ook niet om het uit elkaar vallen of de wederopbouw van de virusmantel met fluorescentiecorrelatiespectroscopie (FCS) te volgen. Voor toekomstig onderzoek zou het wel interessant kunnen zijn om cascadereacties van enzymen in een soort nanoverpakking te bekijken en daarom hebben we in een initieel onderzoek met tweekleuren-FCS aangetoond dat het enzym PalB tezamen met een ander eiwit groen-fluorescerend eiwit (GFP) kan worden ingepakt in een CCMV-mantel.

Door PalB moleculen direct op een hydrofoob glasoppervlak te zetten konden we een aantal actieve enzymmoleculen vinden, die we vervolgens enkele uren lang konden bestuderen. Individuele omzettingen konden worden getraceerd in het fluctuerende fluorescentiesignaal. Analyse van de tijd tussen de omzettingen gaf extra aanwijzingen voor het geheugeneffect dat eerder bij PalB waargenomen was. Het was echter zo dat veel moleculen maar zwak aan het oppervlak gebonden waren en dus voortdurend bewogen. Tevens was de meerderheid van de enzymmoleculen niet actief en daarom vonden we deze methode niet goed genoeg voor verdere experimenten.

Het combineren van de bovenstaande strategiën van inpakken en op een oppervlak plaatsen stimuleerde ons ertoe virusmantels gevuld met een enkelvoudig mierikswortelperoxidase (HRP) enzymmolecuul op een oppervlak te zetten. De fluorescente productmoleculen die het enzym maakte hoopten zich op aan de binnenkant van de mantel en daardoor verschenen die als felle stippen op de microscoopplaatjes. Het bleek mogelijk om de activiteit van enzymmoleculen binnenin of juist geabsorbeerd aan de buitenkant van de virusmantel van elkaar te onderscheiden doordat ze verschillende autocorrelogrammen van het fluorescentiesignaal opleverden. Individuele omzettingen waren echter niet zichbaar omdat deze niet uitkwamen boven het sterke achtergrondsignaal van de opgehoopte productmoleculen. De virusmantel is waarschijnlijk ook een barrière voor de diffusie van substraatmoleculen naar het ingesloten enzymmolecuul.

Als laatste werden enkele PalB moleculen in verschillende sol-gels gezet. In een experiment met nieuwe sol-gels gebaseerd op ethyleengylcol-gemodificeerde silaanverbindingen bleken de enzymmoleculen niet vast genoeg te zitten. In een zogeheten TMOS-MTMS sol-gel daarentegen waren vrijwel alle enzymmoleculen goed vastgezet, maar bleken slechts enkele moleculen actief te zijn. Een PalB molecuul was een uur lang actief, maar dat was niet voldoende om statistisch significant te zijn. Het lijkt erop dat net zoals bij de andere immobilisatiemethodes die in het verleden uitgeprobeerd zijn ook bij immobilisatie in deze sol-gels de meeste enzymmoleculen niet actief aangetroffen kunnen worden; of dat komt door inactivatie van het enzym of doordat de substraatmoleculen het enzym niet kunnen bereiken blijft voorlopig nog onbekend.

Acknowledgements

Looking back on the whole thing now, it seems like a million years ago that I got the call from TuHa informing me that there was an opening for a PhD student in prof. Nolte's and prof. Rowan's group in Nijmegen. A few days later I had the 'job', and the adventure began. And what an adventure it has been: It took me to places near and far, gave me new insights, and new colleagues who often became good friends. True friendship does not depend on the listing of names, so I will limit myself to acknowledging the ones who contributed directly to this thesis, in the understanding that those I omit will know that I still value our time together.

Hans, whatever I would write here on how important your contribution to this thesis was, it would be an understatement. For your help and guidance, I am greatly indebted. And from now on, I will also pause to think about the advantages. Alan, our meetings were infrequent but always good for new schemes and dreams. Roeland, your thorough reading has benefited this thesis immensely, and I thank you for it. Peter C., I came to appreciate you playing the role of devil's advocate, which often led me to a deeper understanding of the science. Jan-Kees, thanks for offering me refuge from the cubicles, and sorry about the seminars. Kerstin, your enzymes proved very valuable and I appreciated your fine-tuning of my review.

To say that I spent **all** the time *alone in the dark* would be doing great injustice to a few of my fellow researchers. Nikos, since you left, focussing the laser has become a lot less fun. Alexandros, during your brief stay you gathered some valuable data for Chapter 4. I hope you're doing well in Greece. Inge, thanks for the virus samples, which allowed me to test and validate the two colour setup in Chapter 3. I keep thinking about the catalysis results we might have had if it hadn't been for that ash cloud. Mark and Sanne, thank you

for the work you did on the PalB-leucine zipper experiment in Chapter 4. Marta, I enjoyed cooperating with you on Chapter 5, and I thank you for your part in it. I'm sorry that we had to start at 6 AM every day and I sincerely hope I didn't drive you insane with all the autocorrelations before you had your coffee. Mahsa, I hope you liked your internship as much as I did; we only had a brief time for doing experiments, but I think you've spent that time well and Chapter 6 benefits greatly from your efforts. Thanks go out to Nicola Huësing from the Universität Ulm for inviting me to give a talk in her group. Dominique, I appreciate that you took the time to give me some pointers on the synthesis of sol-gels.

Janneke, you've given new depth to the term *vortex of improductivity* with all the Friday afternoon projects and then some, while this somehow hardly seemed to affect your own projects. Thanks for helping out in the lab and for sharing the magnet research–experience. To my fellow AFM-confocallist and paranymph Arend go many thanks for helping keeping the machine running, and for co-designing many of the improvements, as well as for our ping-pong sessions. I was very lucky to chance upon someone like Frans who was always willing to help me out with any optics problems, like the time when I completely ruined the Argon laser's alignment; I guess he couldn't bear to see me set myself on fire *again*. He also always made tea during the coffee break, something which should not be undervalued. Speaking of laser-fixing tea drinkers: Peter A., recht schönen Dank for fixing the dye laser several times, I hope someday you will get the stains out. Last but not least as far as the optical room is concerned is Lijnis who fabricated many important parts of the microscope setup: thanks also for thinking *about* the box in this case, as now we can keep most of the photons *outside* of the box.

Anyone should consider himself lucky if he can call on the support of no less than four secretaries: Ine, Desiree, Jacky and Paula, whether I needed a temporary place to live, a box of pens, some form signed, or an appointment made; I'm grateful that I could always count on you. Peter van Dijk, thanks for guiding my orders safely through the bureaucracy. Recognition goes out to Geert-Jan Janssen from the department of General Instruments for his help with the electron microscopy. Special mention must go out to Stijn, Luiz and Erik, who made certain conferences a lot more entertaining. Stijn, thanks for enduring French library bureaucracy. Olivier, my other paranymph, I thank for reminding me that there is life beyond the thesis, and for introducing me to Guinness.

In closing I'd like to thank my parents, Els and Marcel, for their tremendous support. The final thought goes out to TuHa, without whom I would not have started writing this thesis in the first place and without whom I certainly would not have finished it: Thanks for being there, babe.

Biography

Victor I. Claessen was born on the 29th of September 1981 in Amsterdam. He graduated from Johan de Witt-gymnasium in Dordrecht before starting a study in Chemical Engineering at Delft University of Technology. Because of mixed feelings on the relevance of learning how best to stir reaction vessels, he switched to Chemistry at Leiden University. He spent the last two years of that study doing two research internships and a course in Science Based Business. During his major internship, which he undertook at the Bio-Inorganic Chemistry department, he investigated new platinum-ruthenium complexes. His minor internship at the Biochemistry department comprised research on the copper proteome of *S. lividans*.

He started his PhD research in 2006 at the Radboud University Nijmegen in the groups of prof. dr. Roeland Nolte and prof. dr. Alan Rowan, under the direct supervision of dr. Hans Engelkamp at the high field magnet laboratory. Some of that research is presented in this thesis.

In addition, Victor is a freelance IT consultant, website designer/hoster and (co)author of a children's book on programming. He likes to dedicate his free time to scuba diving, (underwater) photography and tinkering with technology.

Publications

[1] M. C. Aragonés, H. Engelkamp, V. I. Claessen, N. A. J. M. Sommerdijk, A. E. Rowan, P. C. M. Christianen, J. C. Maan, B. J. M. Verduin, J. J. L. M. Cornelissen, R. J. M. Nolte, *Nature Nanotechnology* **2007**, 2(10), 635–639, doi: 10.1038/nnano.2007.299.

[2] V. I. Claessen, H. Engelkamp, P. C. M. Christianen, J. C. Maan, R. J. M. Nolte, K. Blank, A. E. Rowan, *Annual Review of Analytical Chemistry* **2010**, 3(1), 319–340, doi: 10.1146/annurev.anchem.111808.073638.

[3] J. H. Blokland, V. I. Claessen, F. J. P. Wijnen, E. Groeneveld, C. de Mello Donegá, D. Vanmaekelbergh, A. Meijerink, J. C. Maan, P. C. M. Christianen, *Physical Review B* **2011**, 83(3), 035304, doi: 10.1103/PhysRevB.83.035304.

[4] I. J. Minten, V. I. Claessen, K. Blank, A. E. Rowan, R. J. M. Nolte, J. J. L. M. Cornelissen, *Chemical Science* **2011**, 2, 358–362, doi: 10.1039/C0SC00407C.

Propositions

belonging to the PhD thesis

Alone in the dark: Time-resolved single-molecule fluorescence spectroscopy on biomolecules.

1. It is remarkable that the seminal paper in the field of single enzyme studies by Rotman is not cited by Lee and Brody, especially as they use the same technique for individualisation.
   A.I. Lee, J.P. Brody, *Biophysical journal* **2005**, 88, 4303–4311,
   doi:10.1529/biophysj.104.055053

2. Craig and Nichols have failed to notice or to mention that two units in a β-galactosidase tetramer—more specifically: both units in one of the dimers in the tetramer—are deactivated concurrently.
   D.B. Craig, E.R. Nichols, *Electrophoresis* **2008**, 29, 4298–4303,
   doi:10.1002/elps.200800482

3. It is amusing that while pretty much all sol-gel chemists cite the first article by Jean-Jacques Ebelmen—one of 72 scientists commemorated on the Eiffel Tower—as the birth of the sol-gel field, nearly all place it in the wrong journal, indicating that probably no one actually read it. This is the treatise that conceived the sol-gel field:
   M. Ebelmen, C.R. Acad. Sci. Fr. **1845**, 21, 502.
   This is the article that is invariably cited, but does not actually exist:
   M. Ebelmen, Ann. Chim. Phys. **1845**, 15, 319.

4. Scientific writing could benefit from the introduction of evidentiality—as it exists in the grammar of certain amazonian languages—into English.

5. STROOPWAFEL (Synchrotron Terahertz Radiaton from Oscillating Operating Principle Wigler Array Free Electron Laser) instead of FLARE would have been more appropriate as an acronym for the new Nijmegen free electron laser, and wittier too.

6. The Institute for Molecules and Materials would be well served by hiring a dedicated graphical artist for the illustrations in its scientific publications.

7. It is terrific being knowledgeable about computers, provided no one else finds out.

8. Doing your PhD project is a lot like scuba diving.

9. In single molecule studies, two is a crowd.

Stellingen

behorende bij het proefschrift

Alone in the dark: Time-resolved single-molecule fluorescence spectroscopy on biomolecules.

1. Het is opvallend dat het eerste artikel in het onderzoek naar enkelvoudige enzymmoleculen niet wordt geciteerd door Lee en Brody, als men in aanmerking neemt dat zij dezelfde techniek gebruiken voor het onderling afzonderen van die moleculen.
   A.I. Lee, J.P. Brody, *Biophysical journal* **2005**, 88, 4303–4311,
   doi:10.1529/biophysj.104.055053

2. Craig en Nichols hebben niet opgemerkt of niet opgeschreven dat twee eenheden in een tetrameer van β-galactosidase—of preciezer: de beide eenheden van één van de dimeren in het tetrameer—tegelijkertijd inactief worden.
   D.B. Craig, E.R. Nichols, *Electrophoresis* **2008**, 29, 4298–4303,
   doi:10.1002/elps.200800482

3. Het is amusant dat, hoewel het eerste artikel van Jean-Jacques Ebelmen—een van de 72 wetenschappers die herdacht worden met een plakkaat op de Eiffeltoren—door sol-gelchemici vrijwel altijd geciteerd wordt als de bakermat van het sol-gelonderzoeksveld, dit artikel vrijwel altijd in het verkeerde tijdschrift geplaatst wordt. Dit geeft aan dat waarschijnlijk geen van die onderzoekers de tekst ooit gelezen heeft.
   Dit artikel markeert het begin van het onderzoek naar sol-gels:
   M. Ebelmen, C.R. Acad. Sci. Fr. **1845**, 21, 502.
   Aan het volgende artikel wordt vaak gerefereerd, ondanks het feit dat het niet bestaat:
   M. Ebelmen, Ann. Chim. Phys. **1845**, 15, 319.

4. De geschreven wetenschap zou haar voordeel kunnen doen met de introductie van evidentialiteit—zoals die bestaat in de grammatica van bepaalde talen uit het Amazonegebied—in het Engels.

5. STROOPWAFEL (Synchrotron Terahertz Radiaton from Oscillating Operating Principle Wigler Array Free Electron Laser) in plaats van FLARE zou passender zijn geweest als acronym voor de nieuwe vrije elektronenlaser in Nijmegen, en tevens amusanter.

6. Het Instituut voor Moleculen and Materialen zou gebaat zijn bij het aannemen van een grafisch artiest voor het maken van illustraties bij wetenschappelijke pubicaties.

7. Het is geweldig om veel van computers te weten, zolang niemand erachter komt.

8. Het werken aan een promotieproject heeft veel weg van scubaduiken.

9. Bij het onderzoeken van enkelvoudige moleculen is twee te veel.